Fabrication of Al-CNTs MMC by induction melting with improved dispersion and wetting of CNTs in Al matrix using a multifunctional flux

By

Muhammad Mansoor

Supervisor: Dr. Muhammad Shahid

School of Chemical and Materials Engineering (SCME)

National University of Sciences and Technology (NUST)

2015

Fabrication of Al-CNTs MMC by induction melting with improved dispersion and wetting of CNTs in Al matrix using a multifunctional flux

Muhammad Mansoor

Reg. No:

2012-NUST-DirPhD-MS-E-10

This work is submitted as a PhD thesis in partial fulfillment of the requirements for the degree of

PhD in Materials and Surface Engineering

Supervisor: Dr. Muhammad Shahid

School of Chemical and Materials Engineering (SCME)

National University of Sciences and Technology (NUST), H-12

Islamabad, Pakistan

2015

Certificate

This is to certify that work in this thesis has been carried out by **Mr. Muhammad Mansoor** and completed under my supervision in Department of Materials Engineering, School of Chemical and Materials Engineering, National University of Sciences and Technology, H-12, Islamabad, Pakistan.

Supervisor**:** _____

Prof. Dr. Muhammad Shahid

Department of Materials Engineering,

School of Chemical & Materials Engineering,

National University of Sciences and Technology, Islamabad

Submitted through

Principal/Dean,

Department of Materials Engineering,

School of Chemical & Materials Engineering,

National University of Sciences and Technology, Islamabad

Dedication

I dedicate this work to my family, whose affectionate support was a continuous supply of motivation.

Acknowledgements

All thanks to Almighty Allah who gave me the ability to complete the project successfully.

There I wish to acknowledge, with humble gratitude, to my supervisor Dr Muhammad Shahid, who made priceless contribution to the project in the form of information, guidance and practical experience.

I also express most cordially thanks to my co-supervisor Dr Amir Habib and GEC members: Dr Muhammad Mujahid, Dr Ahmed Nawaz and Dr Iftikhar us Salam for their excellent advice and selfless succor.

Last but not the least, I pay my salutations and recognitions to Mr Shahid Shah, Mr Muhammad Altaf, Mr Muhammad Irfan, Mr Muhammad Imran Baig, Mr Abdul Ghafoor, and Mr Muhammad Bashir whose incessant and sincere support made this work an agreeable memory.

Abstract

Aluminum/carbon nanotubes (Al-CNTs) composite is an encouraging candidate material for aerospace applications due to its expected high strength-to-weight ratio. Carbon nanotubes (CNTs) offer remarkable reinforcements owing to their high specific strength and specific modulus. However, uniform dispersion and wetting of the CNTs is extremely difficult in molten aluminum, due to large difference in surface tension forces of the two components.

In present work, the dispersion issue was improved using induction melting technique, where innate stirring action of induction melting dispersed the nanotubes in molten aluminum. The wetting was improved using a multifunction flux (titanate of potassium), which, when was incorporated in molten mixture of aluminum and CNTs having, instigated in-situ reactions to form titanium carbides on the surface of the nanotubes causing increased wetting of CNTs by molten aluminum.

The composites were characterized using scanning electron microscopy, x-ray diffraction, transmission electron microscopy and mechanical testing. Refinement in crystallite size was achieved down to ~150 nm and a corresponding increase in lattice strain up to ~3.46×10^{-3} was observed in the composites. A simultaneous increase in yield strength ~208 %, tensile strength ~218 %, and hardness ~100 % was observed. However, the decrease in the ductility of the composite associated with the strengthening of the matrix was <25 %. Additionally, stress relaxation behavior of the annealed composite was improved by ~30 % compared with pure aluminum. Consequently, the stress relaxation rate of the composite was decreased even beyond the yield strength of the annealed pure aluminum. Therefore, induction melting and usage of the flux for improvement in the dispersion and wetting of the nanotubes, respectively, appeared to be a potential method to fabricate Al-CNTs composites.

Contents

List of Figures

List of Tables

List of Abbreviations

µm	Micron
A/cm^2	Ampere per centimeter square
AFM	Atomic force microscope
CFs	Carbon fibers
CMCs	Ceramics matrix composites
CNTs	Carbon nanotubes
CVD	Chemical vapor deposition
DC	Direct current
emu/g	Electro-magnetic unit per gram
FCCVD	Floating catalyst chemical vapor deposition
GPa	Giga Pascal
HVOF	high velocity oxy-fuel
J/kg. K	Joules per kilogram per Kelvin
MM-CNT	Metal matrix carbon nanotubes
MMCs	Metal matrix composites
$mN.m^{-1}$	Milli Newton per meter
MPa	Mega Pascal
MWCNTs	Multi walled carbon nanotubes
NIC mode	Nomarski interference contrast mode
PM	Powder metallurgy
PMCs	Polymeric matrix composites

PVD	Physical vapor deposition
rpm	Revolution per minute
RPS	relative ratio of particle size
S/cm	Semen’s per centimeter
sccm	Standard cubic centimeter per minute
SEM	Scanning electron microscope
SPS	Spark plasma sintering
SWCNTs	Single walled carbon nanotubes
TEM	Transmission electron microscope
TGA	Thermogravimetric analysis
TPa	Tera Pascal
W/m. K	Watts per meter Kelvin

Chapter No: 1

Introduction

1.1 Background

Contemporary engineering applications, deeming for special combinations of mechanical and physical properties, instigated the era of composite materials. A composite material is a combination of constituent materials realizing distinct set of properties, which otherwise is not possible for the constituent materials in their monolithic forms. Emergence of automobile and aerospace industries, the demand for stronger and lighter, yet economical, materials increased the interest of material engineers in the development of MMCs, which are a class of composite materials comprising a metallic matrix (i.e. more than 50% constituent of the composite) and strengthening materials could be metal, organic compound or ceramics[1]. MMCs bring in numerous potentials for development of custom-made composites fulfilling conceptual desires of the designer. However, a realistic benefit can only be realized when a justified performance-to-cost relationship could be achieved.

The properties of the MMCs are essentially dependent on their constituent materials. These constituents could be metallic, ceramics or non-metals, which provide enormous possibilities of their combinations for specific properties. For instance: increased mechanical strengths while maintaining toughness, increased fatigue and creep strengths especially at higher temperatures, improvement in thermal shock resistance, reduction in thermal coefficients or better corrosion resistance, etc.

Although, various classifications of MMCs are available in literature but generally they are classified on the type of reinforcement material used. These types are penetration-, layer-, fiber- and particle composite materials. Fiber composites are further divided into short-fiber and continuous-fiber composites.

The reinforcement materials for MMC applications are very crucial and their demands are manifold. For example, low density, chemical stability, thermal stability, high mechanical strengths and high Young's modulus[2]. Besides other reinforcement

materials, carbon nanotubes (CNTs), after their discovery by Iijma[3] in 1991, became promising reinforcement material owing to excellent mechanical and physical properties fulfilling exhaustive list of required characteristics.

1.2 Statement of the Problem

The recent trends to strengthen the matrix using filler materials are rapidly transforming from macro- or micro- scale fillers to nano-scale fillers. Carbon nanotubes (CNTs), being one of the candidate materials, hold a strong promise to augment not only localized but also global physical and mechanical properties of the composite. During last decade, numerous researchers have quoted their work encompassing amelioration in mechanical and physical properties of CNT-Aluminum composites, however, in each case major limiting factors remained same i.e., dispersion and wettability of CNTs.

The structure of CNTs consists of rolled-up, concentric layers of graphene having diameter ranging from few to several nanometers, while their lengths vary between nanometer to millimeters. The large differences between their dimensions result in high aspect ratios[4]. CNTs have strong tendency to tangle forming agglomerate due to attractive Van der Waal forces, which make nano-ropes or bundles having wider diameters than individual nanotube. Another factor which contributes towards the agglomeration of CNTs is their synthesis method. Once the nanotubes get tangled, whether during or after their synthesis, it becomes very difficult to untangle them without scarifying their aspect ratio. There are certain methods available to disperse CNTs but usually they result in surface imperfections, end-cap opening and reduction in lengths of the nanotubes. These characteristics of CNTs make them very difficult to disperse in metal matrix. In situations where CNTs are to be dispersed in liquid/molten matrix; the nanotubes move to the liquid surface under the buoyancy generated by the density difference of the nanotubes and liquid matrix.

As described earlier that the walls of CNTs are rolled-up graphene sheets, which have sp^2-hybridization, where each atom joined to three neighbors in a trigonal planar arrangement forming sheets of hexagonal rings, which make CNTs extremely inert and difficult to get wetting with most of the solvents and liquid metals[5]. For instance, surface tension forces of MWCNTs and molten aluminum are 45 and 860 mN/m,

respectively, reducing the probability of their wetting to negligible under normal circumstances.

1.3 Definition of Terms

Following are major terms, which would be the prime focus of the present research:

Dispersion:

Scattering and spreading the nanotubes (i.e. MWCNTs) in aluminum matrix during melt-cast fabrication route.

Wetting:

Reducing the difference of surface tension forces between the nanotubes (i.e. MWCNTs) by introducing a second phase (i.e. titanium carbide) on the walls of the nanotubes during fabrication of Al-CNTs composite.

1.4 Objective of the Study

The prime objective of the proposed research is to fabricate Al-CNTs composite featuring:

- easy dispersion of MWCNTs in molten aluminum
- convenient rout of increased wetting of CNTs with molten aluminum

Various theoretical and conceptual models have proven the fact that better dispersion and increased wettability of CNTs, not only strengthens the matrix but also render unique physical properties. However, for the present research, strengths of the composites will be the main focus for amelioration.

1.5 Contributions of the Study

1.5.1 CNTs Synthesis with Optimization of Parameters

For alleviated dispersion of the nanotubes, an approach of CNTs synthesis using CVD process would be adopted, which may yield mono-strands of CNTs with larger aspect ratios and lesser extent of entanglement. The operational parameters of the synthesis

process will be optimized to produce mono-strands of the CNTs. This activity will provide capabilities to tailor CNTs during synthesis besides mass production of MWCNTs for their subsequent used for Al-CNTs composite fabrication.

1.5.2 Using Induction Melting for the Dispersion

Further, induction melting technique would be utilized to disperse the mono-strands of CNTs in molten aluminum. It is a novel idea to produce Al-CNTs composites. It is expected that innate stirring action of induction melting will assist to disperse the nanotubes in molten aluminum besides ease of fabrication and scale-up capabilities.

1.5.3 Wetting of CNTs with Molten Al

To increase wetting characteristic of the nanotubes with molten aluminum, an in-situ reaction will be incorporated during fabrication process, which will be assisted by exchange reaction(s) of potassium hexafluorotitanate forming titanium carbides on the walls of the nanotubes. Presence of titanium carbides on the walls of CNTs will effectuate reduction in difference between surface tension forces of the nanotubes and molten aluminum; hence CNTs would get coated with aluminum. It is novel idea and could not found in available literature till date.

1.6 Organization of the Study

In the succession of present chapter (Introduction), an extensive literature review is presented in chapter-2. CNTs have been discussed in the first part of the chapter covering their history, structure, properties, synthesis routes and potentials. In next part, various popular methods for the synthesis of CNTs have been discussed, including electric arc discharge method, laser ablation method and chemical deposition method along with their merits and demerits. However, major focus is kept on chemical deposition method. In last part of the chapter, various aspects of Al-CNTs composites are discussed. Solid phase and liquid phase processing for Al-CNTs composite fabrication routes have been discussed separately; however major emphasize is given to liquid phase processing.

In chapter-3, motivation for the present research is presented along with proposed approach to instigate the experimental work. The chapter comprises four main stages i.e. synthesis of MWCNTs, dispersion of CNTs in aluminum, coating of CNTs with aluminum and fabrication of Al-CNT nanocomposite.

In chapter-4, experimental procedures with materials and equipment for various synthesis and fabrication stages have been discussed. In the first part of the chapter, synthesis of MWCNTs is described. In second part, dispersion of MWCNTs in molten aluminum is described, where induction melting technique is introduced. In third stage, coating of CNTs with aluminum is described separately and finally (fourth stage) the fabrication of Al-CNTs composite is presented for dispersion of CNTs assisted by induction melting and wetting of CNTs by potassium hexafluorotitanate.

In chapter-5, all the experimental results have been presented and discussed. The sequence of the results is the same as used during chapter-4. Finally, the conclusions are presented, which are drawn from the experimental results and concurrent discussions, in chapter-6.

Chapter No: 2

Carbon Nanotube Reinforced Aluminum Nanocomposites – Literature Survey

2.1 Background

In the domain of engineering materials, metallic materials exhibit a variety of controllable properties through composition, mechanical, thermo-mechanical and/or surface treatments. The primary reasons for the use of metallic materials, besides strength, are their ease of fabrication, low cost, and wide choice of processing routes. The quest of materials engineers to develop metallic materials with special combinations of properties lead to the development of MMCs, which otherwise not possible for monolithic metals and alloys. Consequently, reinforced MMCs may provide: improved mechanical properties including fatigue and wear coupled with reduced thermal expansion. MMCs require special processing procedures hence have increased cost; however, the cost is justified by the combination of special properties for particular applications. During recent years, the use of MMCs has progressively increased in automobile and aerospace industries due to their remarkable specific modulus, strength, and thermal stability.

Generally, large fractions of various types of fillers (e.g. fibers, whiskers, or particles) are used to reinforce MMCs, where ceramics particles raise the strength at the expense of a decrease in toughness. Further improvement in strengths could be achieved by the incorporation of nanoparticles. Along with strength enhancement, lighter MMCs are required to meet increasing fuel costs and environmental regulations. Therefore, advancement in composites for functional and characteristic features is ever rising in industrial sectors[1].

The breakthrough of Ijima[3] about CNTs which have excellent properties like mechanical, electrical, thermal, high aspect ratio, low density and large surface area, attracted the global interest of scientific and technological community. The excellent set of properties made researchers to consider CNTs as a candidate reinforcement

material for PMC, CMC and MMC, specifically encompassing enhanced mechanical properties with lighter weight structures[6].

The term “nanocomposite” emerged from the size of at least one of the constituents being less than 100 nm. CNTs having 10-40 nm diameters with length up to several microns are incorporated in various matrixes, with very low loading levels, resulted in excellent improvement in mechanical and physical properties[6,7].

2.2 Carbon Nanotubes

CNTs possess a wide range of physical and mechanical properties including exceptional surface area, high aspect ratio, high thermal conductivity, low thermal expansion, ultra high specific modulus, outstanding tensile strength and many other electronic and physical characteristics. However, in the forthcoming section only those properties will be reviewed which have direct relationship with the application of CNTs as filler material for MMCs i.e. aluminum matrix.

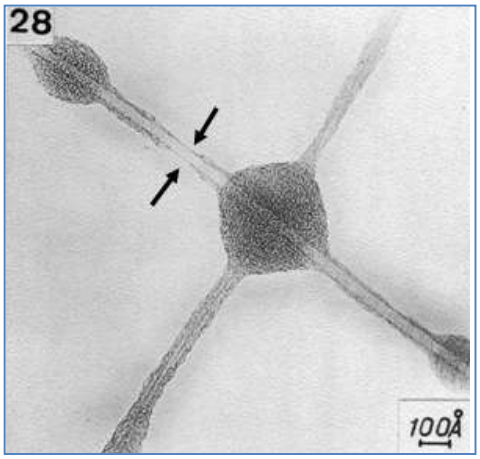

Figure – 2.1 Bright-field image of branched inhomogeneous fibers[8].

2.2.1 History

The discovery of CNTs has been long debated besides Ijima[3] as many other researchers have reported their work on the synthesis of carbon structures similar to CNTs. A compilation of early work on the topic by Monthioux et al[9] appeared in a guest editorial of the journal “Carbon”, where the distinguishable contributions included synthesis of filamentous tubes by Radushkevich et al[10] in 1952, Bacon in 1960[11], and Oberlin et al[8] in 1976. Oberlin et al reported the synthesis of hollow tubes

of 2-50 nm in diameter by decomposing a mixture of benzene and hydrogen and elucidated the structure as "turbostratic stacks of carbon layers, parallel to the fiber axis and arranged in concentric sheets like the annular rings of a tree." Figure-2.1 represents the early work of Oberlin[8].

Despite the fact that MWCNTs have been synthesized previously, it was Ijima who comprehended the MWCNTs as multiple seamless concentric tubes[3] and subsequent to his findings SWCNTs were reported separately by Ijima[12] and Bethune[13] in 1993.

2.2.2 Types of Carbon Nanotubes

The sp-, sp^2- and sp^3- hybridization of carbon orbital generates various allotropic structures as shown in Figure-2.2[14]. The sp-hybridization corresponds to a linear chain-like arrangement of atomic orbital i.e. carbyne. Graphite has sp^2-hybridization, where each atom joined to three neighbors in a trigonal planar arrangement forming sheets of hexagonal rings, which are bonded with each other through Van der Waals forces. These Van der Waals forces are week; making graphite a good electrical conductor and lubricant. Diamond, another form of carbon, has a sp^3-type tetrahedral covalent bonding, where each carbon atom is linked to four others at the corners of a tetrahedron through covalent bonding, which is the prime reason for its extremely high hardness and density.

All other carbon forms are classified into intermediate or transitional forms in which the degree of hybridization of carbon atoms can be expressed as sp^n ($1<n<3$, $n\neq2$). These include fullerenes, carbon onions and carbon nanotubes[14,15]. Fullerene is made up of 60 carbon atoms arranged in a spherical net with 20 hexagonal and 12 pentagonal faces, forming truncated icosahedra[16].

Simplistically, carbon nanotubes are rolled sheets of graphene, where SWCNTs consist of a single graphene layer while MWCNTs comprises 2-50 layers with a spacing of 0.34 nm. A SWCNT and MWCNT may have a diameter in the range of 0.4-3 nm and 4-100 nm, respectively, with a length up to several hundred micrometers which attributes a very high aspect ratio to them[17].

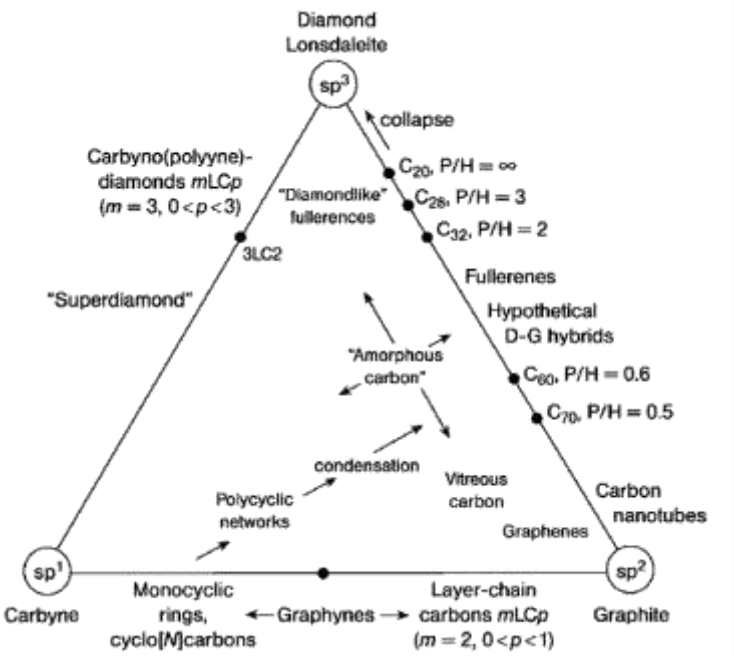

Figure – 2.2 Proposed carbon allotropy diagram based on valence bond hybridization. P/H corresponds to the ratio of pentagonal/hexagonal rings[14].

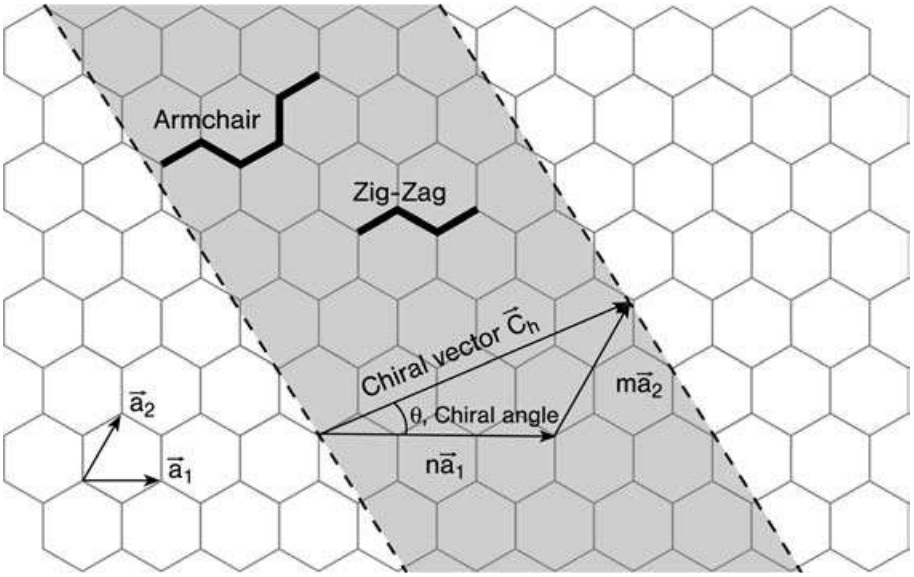

Figure – 2.3 Schematic diagram showing chiral vector and chiral angle in a rolled graphite sheet with a periodic hexagonal structure[18].

Conceptually, graphene sheets can be rolled into various structures i.e. zigzag, armchair and chiral. Therefore, the carbon nanotube structure can be illustrated by a chiral vector (C_h) defined by the following equation[19]:

$$C_h = na_1 + ma_2 \quad (2.1)$$

where a_1 and a_2 are unit vectors in a two-dimensional hexagonal lattice, and 'n' and 'm' are integers. Thus, the structure of any carbon nanotube can be expressed by the two integers (i.e. n, m) and chiral angle "θ" (Figure-2.3). Possible combinations of the chiral angle and integer values resulting in various structures of CNTs are given in Table-2.1[18,19].

Table-2.1 Various types of CNTs with different structural parameters

Structure	**Chiral angle (θ)**	**The integers (m & n)**
Armchair carbon nanotubes	30°	m=n
Zigzag carbon nanotubes	0°	m or n=0
Chiral carbon nanotubes	0° - 30°	m & n other than 0 or equality

Mathematically, the nanotube diameter can be written as[20]:

$$d = (a \times \sqrt{m^2 + n^2 + nm}) \div \pi \quad (2.2)$$

where;

'a' is the lattice constant of the graphene sheet and is equal to $\sqrt{3}\, a_{c\text{-}c}$,

'$a_{c\text{-}c}$' is the carbon–carbon distance and is equal to 1.421 Å.

The chiral angle "θ" is given by:

$$\tan\theta = \frac{\sqrt{3}m}{2n+m} \quad (2.3)$$

The electrical properties of CNTs vary from metallic to semiconducting, depending on the chirality and diameter of the nanotubes e.g. if $n - m = 3k$ (k is any integer), the nanotubes will have metallic nature, otherwise, semiconducting[4].

2.2.3 Properties of Carbon Nanotubes

A single rolled graphene layer forms SWCNTs which have a diameter range of 0.4-3.0 nm and a length of 20-1000 nm. MWCNTs are consisting of several layers of rolled graphene therefore they have larger diameter (4-100 nm) with lengths up to several microns[4], or millimeters[21]. Due to attractive Van der Waals forces, CNTs have strong tendency to bundle-up together in ropes (nano-ropes) which could be considerably wider and longer than their native nanotubes[19]. These bundles of SWCNTs or MWCNTs may have a diameter up to 500 nm or 3 µm, respectively. Consequently, the bundles or nano-ropes can form agglomerates, generating even wider regime of particle size in micrometer range[22]. The type and extent of MWCNTs bundles or nano-ropes is led by: i) the rigidity of nanotubes and ii) their thin enough diameters to allow buckling. Another aspect which may contribute to the type of bundles or nano-ropes is the production method of the CNTs. Thus, depending on above mentioned parameters there could be an appreciable difference between bundles or nano-ropes of thin and thick-walled MWCNTs[23].

Generically, very high surface areas are associated with CNTs. Theoretical calculations have shown that SWCNTs may have surface areas up to 1300 m^2/g, while MWCNTs usually have few hundreds of m^2/g surface areas, owing to the fact that CNTs have strong tendency to form bundles and get tangled, their surface areas reduce significantly i.e., ~300 m^2/g [24]. Additionally, CNTs are renowned for exceptionally high mechanical strength, and electrical and thermal conductivity. As prepared, non-functionalized (pristine) CNTs are inherently hydrophobic. Modification of the surface with various functional groups can make them more hydrophilic, which also decreases bundling or aggregation[4].

2.2.3.1 Physical Properties

The physical properties of carbon materials including carbon nanotubes are listed in Table-2.2. Due to ballistic nature of electron conduction, SWCNTs have excellent electrical and thermal conductivities making them able to conduct exceptional amounts of current densities without lose i.e. heating. As mentioned in Table-2.2,

mono-strands of nanotubes have higher thermal conductivities than, for example copper ($400 Wm^{-1}K^{-1}$), but their bulk specimens have substantially reduced values [25].

Table-2.2 Physical properties of carbon materials.

Property	**Graphite**	**Diamond**	**SWNTs**	**MWCNTs**
Electrical Conductivity, (S/cm)	900–1700 [26]	Insulator	10000 with current density of 10^9 A/sq.cm [27]	1850 with current density of 10^7 A/sq.cm [27]
Magnetic susceptibility, (emu/g)	-30×10^{-6} when magnetic field is parallel to c-axis [28]	-4.9×10^{-7} [25]	-10.65×10^{-629}	1.1 [30]
Specific heat capacity at RT, (J/kg. K)	710 [31]	486 [31]	~650 [32]	~480 [33]
Thermal conductivity at RT, (W/m. K)	165 [34]	3320 [25]	6600 for single SWNT [35] 37 for disordered mat [36], 200 for aligned mats [37]	3000 for single MWCNT [38] 2.5 for bulk sample [39]

2.2.3.2 Mechanical Properties

The exceptional mechanical properties of carbon nanotubes are attributed to the covalently bonded carbon atoms in a fullerene lattice[40]. Carbon nanotubes are much lighter than steel yet possess up to several times more strength. According to the experimental findings, "they are the strongest known fibers to mankind" [41].

The stability of CNTs against deformation is accredited to the shorter bond length of sp^2 hybridization of the atomic orbital, which is 0.142 Å vs. 0.154 Å for graphene and diamond, respectively. Though theoretical studies have claimed twenty times more tensile strength of CNTs to that of steel, only ~45 GPa could effectively be measured[42,43]. However, very high tensile strength could be expected for concentric defect-free MWCNTs, such a case is quoted in literature for MWCNTs synthesized using arc discharge method, have tensile strength of 150 GPa[44].

In 1996, Treacy et al first demonstrated the measurement of Young's modulus of MWCNTs using thermal vibrations in TEM, where the nanotubes were heated to 800 °C and being clamped cantilevers they thermally vibrated and blurred the image. The Young's modulus was determined from the slope of mean square vibration versus temperature, which resulted in an average value of 1.8 TPa[45].

The following year, Wong et al used AFM to measure elastic modulus of MWCNTs which were pinned at one end to molybdenum sulfide surface. They measured the bending force against the displacement along the unpinned tube length. By correlating experimental data and mathematical models, the stiffness was determined to be 1.28 TPa[46].

Clamping the both ends of the nanotubes, Salvetat et al used AFM to measure the stiffness of MWCNTs grown by arc and CVD methods. They found that arc grown nanotubes were stiffer than CVD one's, attributing to their defect densities[47].

"Sword-in-sheath" morphology of MWCNTs failure was demonstrated by Yu et al[43] when they performed in situ tensile testing of single strand of the nanotubes using SEM. The morphology was featured by outer layer breaking of the nanotubes. They found that the arc grown MWCNTs had stiffness in the range of 270 to 950 GPa.

Apart from single strand of nanotubes, Xie et al[48] used same technique, as described by Yu et al, to measure the stiffness of nanotube bundles. They found a rational

increase in stiffness of nanotube-bundles. The results of experimental findings for mechanical properties of MWCNTs are shown in Table-2.3.

2.2.4 The Potentials

From the preceding discussion it could be inferred that carbon nanotubes has excellent mechanical properties. For instance MWCNTs have far higher tensile strength than SEA 4340 steel in annealed form (745MPa), which is frequently used to manufacture high strength structural parts. The large variations in the experimental results could be attributed to the variations in experimental conditions, method of synthesis, structural homogeneity and aspect ratios of the nanotubes.

Due to their unique structural properties, CNTs have immense potential in various fields including electronics, chemistry, medicine, and materials science. However, their application is mainly restricted by their:

- Inertness
- Tendency to agglomerate
- Structural heterogeneity
- Structural defects
- Size inconsistency
- Cost

Furthermore, advanced engineering applications of CNTs require the ability to control and tailor their properties. Fundamental understanding of structure to properties relationship can play a vital role for any pragmatic applications.

Table-2.3 Experimental Young's modulus and tensile strength of MWCNTs synthesized from various techniques.

Investigator	Young's modulus (TPa)	Tensile strength (GPa)	Synthesis process	Test method
Demczyk et al[44]	0.9	150	Electric arc	TEM
Treacy et al[45]	1.8	-	Electric arc	TEM
Wong et al[46]	1.28	-	Electric arc	AFM
Salvetat et al[47]	0.81	-	Electric arc	AFM
	0.027	-	CVD	
Yu et al[43]	0.27-0.95	11-63	Electric arc	SEM
Xie et al[48]	0.45	3.6	CVD	SEM

2.3 Synthesis of Carbon Nanotubes

Although CNTs and their related structures (i.e. SWCNTs, MWCNTs, fullerenes, nano-onions, nano-rods and nano-particles) can be synthesized by a variety of methods, this literature survey will be focused on the synthesis of MWCNTs using CVD methods. MWCNTs can be synthesized using three basic methods: (1) electric arc discharge method, (2) laser ablation and (3) chemical vapor deposition, each of the methods has its own merits and limitations.

2.3.1 Electric Arc Discharge Method

It is the earliest method to synthesize CNTs. Principally, a DC arc is struck between two graphite electrodes under inert conditions. At anode, evaporated carbon plasma is generated due to the high temperature of the arc (typically 2800 °C). The evaporated carbon then condenses on the cathode forming cylindrical deposits of CNTs and related structures. The outer shell of the cylinder consists of hard fused carbon while inner shell consists of soft and fibrous materials containing CNTs and by-products. One of the prime features of the process is "higher degree of crystallinity" which is due to higher reaction temperature[49].

The mechanism of MWCNTs growth (catalyst-free) is not exactly known, however, Ijima proposed the "open-end" growth mechanism. According to which formation and incorporation of primary graphene structure occurs by carbon precursor at nucleation stage, subsequently, carbon atoms are added at the open ends of the tube while the ends remain open during growth. Meanwhile, the thickness of the tubes increases by the formation of graphite basal planes on their surfaces[50,51].

The processing conditions play a vital role towards the quality and yield of nanotubes, which include pressure of reaction chamber, uniformity of plasma, cathode cooling rate, inter-electrodes gap[52].

Inert gas environments (for example argon and helium) are widely used for the process. Ebbesen et al[52] first time produced large quantities of MWCNTs using this method. They employed catalytic (Fe, Ni, Co) carbon source at a partial pressure of 600 mbar. Vaporization of the carbon occurred in the discharge region and nanotubes deposited on the surface of cathode and chamber walls.

The generic problems of unstable plasma in the process induce heterogeneity in the growth. Lee et al[53] introduced rotating electrode modification, where the anode rotates at high speed (~10000 rpm). The schematic of their apparatus used is shown in Figure-2.4. Rotating anode causes centrifugal forces which accelerate the carbon vapors perpendicular to the anode surface. Yield of nanotubes can be varied with rotation of the anode. Additionally, the rotating anode causes uniform plasma with higher temperature, which increases vaporization resulting in higher CNTs yield.

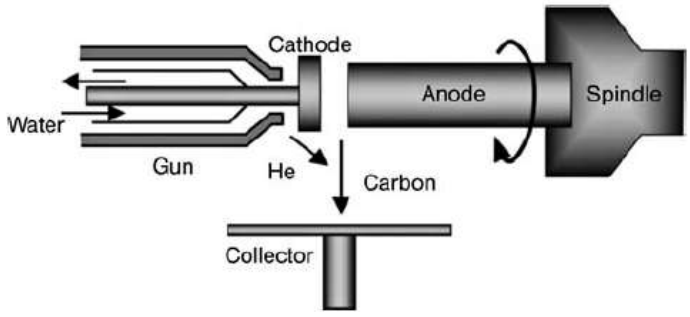

Figure-2.4 Schematic diagram of plasma rotating electrode process system[54].

Another approach used to produce better nanotubes at higher yield is electric arc discharge in liquid environment. In 1991, Hsin et al[54] first time used water as liquid

environment to produce CNTs by electric discharge, eliminating requirements like high quality glass, high temperature furnace and vacuum chamber. Since then, many researchers have used liquid nitrogen[55], benzene[56] and water[57] for the purpose. As de-ionized water is insulator and causes turbulence in arc generation, therefore, brine solution was used as environment for better electrical conductivity.

2.3.2 Laser Ablation Method

In this method carbon vapors are generated from graphite with high energy laser beam, which are subsequently collected by condensation. The process is featured with ease of operation and high quality product. The method followed the discovery of C_{60} in 1985, which was further extended to the synthesis of CNTs. However, the process is limited to the synthesis of SWCNTs because the length of MWCNTs produced by the method is too short with poor yield[58,59]. A schematic of the process is shown in Figure-2.5.

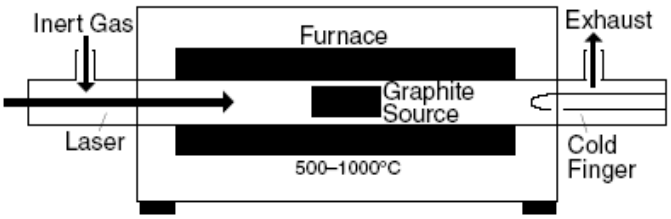

Figure-2.5 Schematic of Laser ablation furnace [59].

Due to coherency and intensity, laser beams are able to vaporize target material rapidly. During process, cobalt impregnated graphite source is placed in a quartz tube surrounded by a furnace at 1000 °C with inert conditions. The laser beam irradiates the target and carbon vapors are formed, which are swept by the flowing inert gas from the furnace to collection cold finger at the furnace end[60]. A yield of SWCNTs up to 80% could be achieved by the process.

Electric arc discharge and laser ablation methods have similarities: for SWCNTs both use catalyst impregnated graphite anode (or target) and for MWCNTs both use pure graphite. Laser ablation can produce very fine SWCNTs having 1 to 1.6 nm diameter. The SWCNTs produced by laser process are widely used for physical properties measurements.

2.3.3 Chemical Vapor Deposition Method

Principally, a CVD process is based upon high temperature chemical reactions of gaseous phases yielding solid products on the substrate, while a PVD process is different owning the fact that no chemical reactions occur. CVD is a popular process in industry due to its simplicity, flexibility and low cost. Furthermore, it is capable to produce high purity films and coatings of various materials i.e. metals, semiconductors and ceramics.

CVD equally supports the synthesis of CNTs as it facilitates a variety of carbonaceous feedstock (e.g. solid, liquid and gas phase hydrocarbons) and allows numerous choices to deposit CNTs, for example: thick film, thin film, powder, randomly oriented and aligned nanotubes[61].

The decomposition of hydrocarbons is catalytic assisted and occurs at temperature far lower than that of electric arc discharge and laser ablation methods. Type of CNTs is controllable by tailoring the process conditions like temperature, catalyst size and precursor. Usually, MWCNTs are produced at lower temperatures (600-900 °C) than SWCNTs (900-1200 °C). There are "various steps" during CVD process[62]:

(a) Transport of reacting gases from the inlet to the reaction zone

(b) Chemical reactions in the gas phase to form new reactive species

(c) Transport and adsorption of species on the substrate's surface

(d) Surface diffusion of the species to growth sites

(e) Nucleation and growth

(f) Desorption of volatile surface reaction products and transport of the reaction by-products away from the surface

Mainly, the CVD process is categorized according to the type of heating source used to activate the chemical reaction, which includes thermal, laser assisted and plasma assisted heating sources. The heat source helps to decompose reactant hydrocarbon precursor in to reactive atoms of carbon, which then diffuses on the surface of catalyst coated substrate. The size of the catalyst is in nanometers and is deposited on the substrate by evaporation or sputtering of metals like iron, nickel or cobalt[63]. Alternatively, catalytic particles can be distributed more evenly by spin coating[64].

Besides deposition conditions, size and type of catalytic particles play a vital role to control structure, growth rate, morphology, and diameter of the nanotubes[65]. Choi et al[66] found that finer catalytic particle of nickel resulted in better growth rate of MWCNTs in plasma enhanced CVD i.e. the carbon atoms' diffusion time to reach at the nucleation sites decreased for finer catalytic particles, hence increase in growth rate and density occurred.

Another important aspect for the CVD synthesis of CNTs is "substrate material", i.e. a catalyst may perform differently on different types of substrates. Commonly used substrate materials for the synthesis of CNTs are silicon, silica, alumina, quartz, zeolite and graphite. If substrate material has some chemical activity at process temperature, catalyst particle will not or least available for the growth of CNTs hence reducing the yield and quality of the product[67].

Due to moderate process conditions i.e. low temperature and low partial pressure, CVD method is relatively simple and less expensive when compared with previously discussed methods. However, MWCNTs grown by CVD are inferior in crystallinity than arc discharge and laser ablation ones, whereas, in case of SWCNTs it is comparable. In terms of yield and purity, CVD process is unbeatable by any other process. Similarly, for structural and architecture controls, CVD is the obvious choice. Versatility of the process is increased by[61–67]:

- Variety of the hydrocarbon (solid, liquid, gas)
- Variety of the substrate materials (silica, alumina, quartz etc.)
- Variety of the CNTs products (powder, thin films, thick films)
- Variety of the architecture (aligned, vertical, coiled)

2.3.3.1 Synthesis Process

The CVD reactor used for the synthesis of CNT consists of a tube furnace with a quartz tube, which is attached to an inlet for reactant and process gases. The catalyst coated substrate is placed in the quartz tube and flue gases are exhausted from the outlet, usually, through a water bubbler. Hydrocarbon gas is passed at a controlled rate (typically 10 to 100 sccm) through the heated tube (600 to 1200 °C) where catalyst coated substrate is placed. The hydrocarbon decomposes at the catalyst and CNTs are grown on the substrate. A simplest schematic is shown in Figure-2.6.

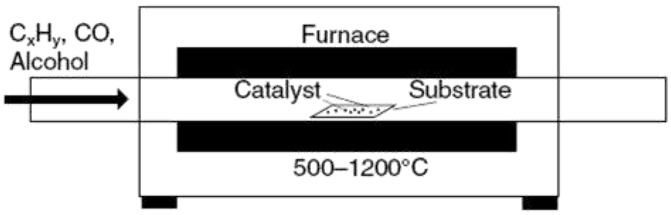

Figure-2.6 A schematic of CVD reactor[68].

For liquid phase hydrocarbons (alcohol, benzene etc.), a heating flask is used to heat up the liquid hydrocarbon and an inert gas is bubbled through it, which further transports the hydrocarbon vapors into the reaction chamber. If hydrocarbons to be used are solid (camphor, paraffin wax etc.), they could be directly place in the reactor chamber at such a location where temperature meets the sublimation temperature of the solid hydrocarbon, subsequently, the sublimated vapors are transported across the tube for decomposition and CNT growth[68].

2.3.3.2 Growth Mechanism

Exact growth mechanism of CNTs is unclear, though several researchers have proposed various approaches towards the growth mechanisms considering reactants, process conditions and catalyst characteristics but are often opposing each other. Consequently, there exists no established growth mechanism. However, generally accepted mechanism is as follows:

When vapors of hydrocarbon interact with the heated catalytic particles they decompose into atomic hydrogen and carbon; carbon is absorbed in the catalyst while hydrogen is escaped out of the reactor. When solubility limit of carbon in catalyst, at process temperature reaches, the excess carbon precipitates out and crystallizes into stable cylindrical network. At the first stage, where hydrocarbon decomposes, exothermic reaction releases heat at the catalyst, while at the second stage where crystallization occurs, endothermic reaction absorbs the heat. This thermodynamic balance inside the catalytic particle carries on the growth[69].

Besides the initial growth mechanism, the propagation of CNTs may occur in two different manners, as shown in Figure-2.7[70].

The first case is known as "tip-growth model" (Figure-2.7a), where the weak bond exists between catalyst and substrate; hydrocarbon decomposition occurs at the catalyst surface and atomic carbon diffuses through catalyst, precipitating CNT below the catalyst particle's bottom, lifting it out the substrate surface. As long as the catalyst particle is exposed to hydrocarbons the growth continues. The CNT growth retards once the catalyst particle is fully covered with the amorphous carbon accounting for its reduced catalytic activity[71].

In second case (Figure-2.7b), where the catalyst–substrate bond is strong, precipitation of carbon fails to push out the particle and emerge out on its surface forming initially a dome which further converts into tube as growth continues. Subsequent hydrocarbon decomposition continues at the root of the growing nanotube, where actually catalytic particle resides. It is known as "base-growth model"[72].

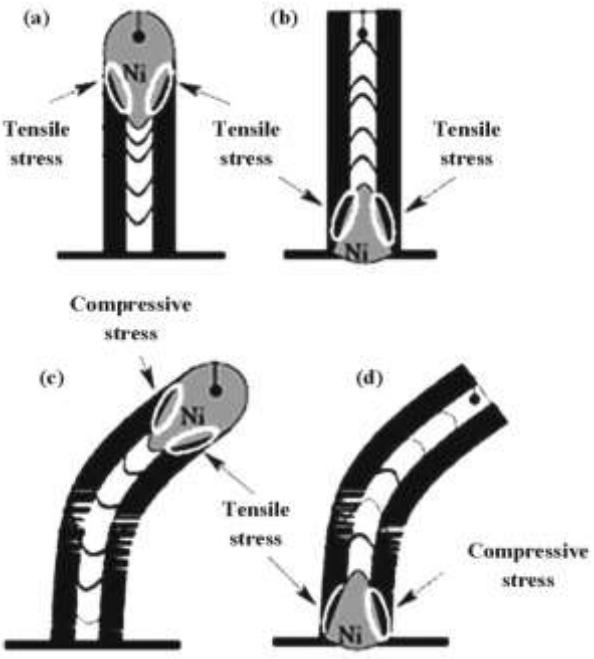

Figure-2.7 Tip (a) and bottom (b) growth mechanisms for CNTs, while (c) and (d) are the alignment mechanisms[70].

Aligned growth of CNTs for either of the models requires uniform precipitation of excess carbon atoms from the catalyst particles. If any kind of spatial fluctuation in

the precipitation occurs it will cause non-uniformity of stresses around the growing nanotubes, which results in their misalignment with more structural defects[73]. The mechanism is elaborated in Figure-2.7 c and d.

2.3.3.3 Precursors

In the absence of shrewd understanding of the CNTs growth mechanism, it is hard to define any particular precursor which dominates others; still there are specific processes where certain precursors perform better than others.

Reactivity of the precursor materials can affect the structure and morphology of the CNTs grown, and could be an obvious choice. The reactivity of methane, ethylene and acetylene are in ascending order and hence it is much easier to produce CNTs from acetylene than the rest[74]. Thermodynamics of the reactions are very important consideration, and should be favorable for synthesis parameters i.e. temperature and pressure. The reactivity of a hydrocarbon depends upon its pyrolysis or decomposition Gibb's free energy[75]. A comparison of reactivity, in terms of Gibb's free energy, of various hydrocarbons is shown in Figure-2.8, where it is evident that methane is not reactive below 600 °C, whereas ethylene, acetylene and benzene are reactive even at 200 °C with negative Gibb's free energies.

Complexity of the molecular structure of the precursor is also harmful for CNTs. Hydrocarbons having linear structures, normally decompose into linear dimers or trimers and produce straight CNTs with good internal to external diameter ratio. While the hydrocarbons with complex structures i.e. cyclic hydrocarbons like benzene or xylene, produce CNTs having structural defects e.g. curved or bamboo like structures[76].

Generally, the hydrocarbons used as precursors for the CNT synthesis include methane[77], ethylene[78], benzene[79], acetylene[80], and xylene[81]. In early works, Endo et al[79] and Jose-Yacaman et al[80] used high temperatures (1100 °C and 700 °C) for the pyrolysis of benzene and acetylene, respectively, to synthesize a variety of carbon nanostructures e.g. SWCNTs, MWCNTs, nano-ribbons and nano-cones. During latter years choice of precursor materials increased.

Maruyama et al[82] introduced alcohol based precursors for CVD synthesis of high purity SWCNTs in 2002. The process featuring alcohol has characteristic of

amorphous carbon free growth of CNTs due to the etching effect of hydroxyl ions[83]. In their later work they have enhanced and facilitated the growth of SWCNTs by introducing acetylene intermittently during the alcohol process. The variation additionally improved the catalytic activity resulting in longer CNTs and increased catalyst's capabilities[84]. The use of alcohol as precursor materials for the growth of MWCNTs is equally promising, as Mendoza et al[85] used ethanol over silica supported iron nanoparticles to synthesized MWCNTs at 700 °C, obtaining better results than many other liquid precursors.

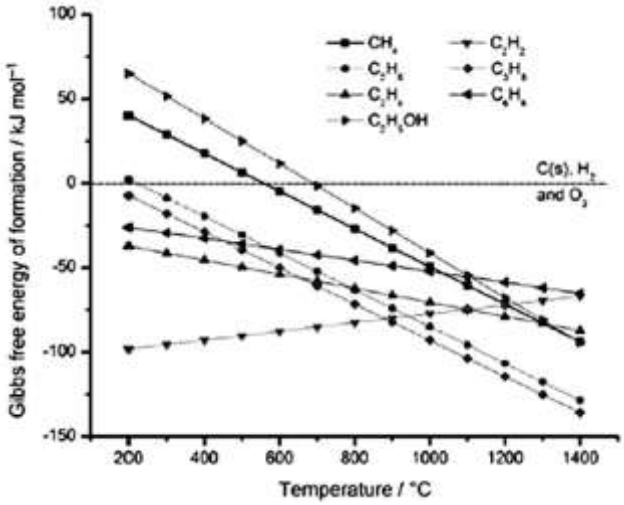

Figure-2.8 Gibbs free energies of formation for various hydrocarbon precursors. The energies are normalized to the number of carbon atoms in the precursor and correspond to its pyrolysis[75].

2.3.3.4 Catalysts Materials

Catalyst plays a vital role to decompose precursor at substantially lower temperatures and to produce less defective CNTs. To promote CNT synthesis, the catalyst should have high carbon diffusion rate and high carbon solubility. Additionally, the catalyst must be compelling the requirements of high melting point and low equilibrium pressure so that it can withstand precursor decomposition temperatures. Transition metals nanoparticles (e.g. iron, nickel and cobalt) are commonly used as catalyst for CVD synthesis of CNTs[86]. These transition metals have strong adhesion with CNTs during growth process; hence effectively support high curvature growth resulting in SWCNTs or low diametric MWCNTs[87].

An essential factor to synthesize pure CNTs is to decompose precursor at the catalyst while avoiding its decomposition in the surroundings. Substrate coated with thin films of the catalyst nanoparticles serve the purpose. In this way one may have aligned growth of CNTs with minimum unwanted amorphous carbon[78].

Another approach of using catalysis is to liberate in-situ catalytic nanoparticles within the CVD reactor to achieve effective pyrolysis of the precursor. Various kinds of organometallocenes[88] (e.g. ferrocene, cobaltocene, nickelocene) are reported periodically in literature having excellent catalysis for CNTs synthesis.

Although, noble metals like gold, silver, platinum, palladium etc. have extremely low carbon solubility limits, however, their nanoparticles (<5 nm) manage to dissolve enough carbon to grow CNTs[89].

2.3.3.5 Catalyst Support Materials

The catalyst support material has many important aspects during CVD synthesis of CNTs[75]:

- It restricts narrow size distributions of the catalyst
- Nanoparticles are dispersed on the substrate's surface, hence excessive agglomeration of the particles is avoided during sintering or growth temperatures
- It permits ease of catalyst handling
- Definite shape of CNT product could be achieved e.g. aligned growth

There are several materials, reported in literature, used as catalyst support including quartz, silicon, silica, silicon carbide, alumina, zeolite, magnesium oxide, etc. Type of support material has significant effect on the CNT growth; same type of catalyst behaves differently on different substrates. Therefore, the interaction between catalyst and substrate is very important i.e. occurrence of any reaction between catalyst and substrate can distort catalytic activity for CNT growth. Moreover, surface characteristics (morphology and roughness) of the substrate have significant effect on the CNT growth[90,91].

2.3.4 Rationale

Though CNTs have remarkable and extraordinary applications but their homogeneous and uniform synthesis is the main “bottle-neck” for their engineering developments. The major challenge is the knowledge of exact mechanism of CNTs growth, which is yet unclear after more than two decades of their discovery. The growth mechanism becomes even more complicated when small structural variations transform the nanotubes’ structures completely i.e. chirality.

CVD synthesis of CNTs holds the promises to:

- Obtain homogeneity in size (diameter and length),
- Reduced structural defects, and
- Minimized entanglement.

Appropriate choice of precursor and catalyst materials, besides other operational parameters, may help to achieve the above listed benefits of the technique.

2.4 CNT Based Aluminum Matrix Composites

Due to the depleting recourses of fossil fuels, augmented fuel prices and environmental regulations, the research focus on materials having high strength to mass ratios i.e. MMCs, is increased, particularly, for automotive and aerospace applications. Primarily, strengthening is carried out in traditional MMCs through ceramic particulates (~25%), which not only increase their weight but also degrade their mechanical properties due to complex processing[61,92]. Relatively larger size of ceramics particles leads towards their fracture, assisted by deformation; when propagating cracks are perpendicular or parallel during tensile or compressive loadings, respectively. Hence, MMCs with micro-particulate reinforcements are attributed to low tensile properties. Alternatively, smaller particulates resist to their fracture during deformations, therefore, rendering more strength to the composite[93]. Many researchers have demonstrated the improvement in mechanical properties of MMCs having nanoparticles because reduced size of the particles prevented their cracking effectively[94–96].

Previous work related to the incorporation of ceramic nanoparticles in MMCs, strongly support the beneficial effects of CNTs, which have even superior flexibility, higher aspect ratio, and enhanced mechanical properties. Additionally, comparing CNTs with carbon fibers (CFs) for MMC applications, CFs have considerably high tensile strength but their fracture strains are quite low. Therefore, remarkable reduction in fracture strains of the MMC may occur due to the incorporation of larger quantities of CFs in the matrix. Here again CNTs have the edge of having significantly more flexibility besides their stiffness and strength[59] . Hansang et al[97] reported enhancement in tensile strengths of CNT reinforced MMC while not compromising upon its ductility.

Though CNTs are quite promising filler material for MMCs, extensive work on their fabrication and intrinsic properties is hindered due to:

- suitable and reproducible processing
- CNTs' dispersion in matrix
- development of CNT-metal interface (i.e. wetting)
- type of matrix metal

During processing, CNTs tend to cluster in the matrix, which are characteristics of their high aspect ratio and strong Van der Waals forces. For example, Kuzumaki et al[98] reported feeble increase in tensile properties of 5 and 10 volume percent CNT-Al nanocomposites, which were prepared by conventional powder metallurgy. The processing resulted in segregation of CNTs in the matrix which caused ineffective load transfer from matrix to the nanotubes during testing.

Besides dispersion, the role of reinforcement's interface with the matrix is quite vital during plastic deformation and crack propagation. A strong interface between CNTs and matrix supports load transfer effectively. Processing conditions may generate or influence the structural properties of the CNT-metal interface. The interfacial reaction between CNTs and matrix (aluminum) was investigated by Ci et al[99]. They coated the CNTs by sputtering aluminum followed by thermal treatments at 400 to 950 °C. During TEM investigations it was found that at the interfacial regions aluminum carbide was formed after annealing, consequently, increasing the interfacial strength of the MMC. Another compatibility issue of CNTs with metallic matrix is wettability. Modifications of CNTs' surface and/or processing techniques are required to overcome the wetting problem[100,101].

An additional vital consideration in preparing CNTs based MMCs is the type of CNTs. The first option may include SWCNTs or MWCNTs. To attain maximum strengthening one may opt for SWCNTs, however, these are more expensive and difficult to handle within matrix because of very high aspect ratios which makes them easy to tangle. Alternatively, MWCNTs are less difficult to manage but they have intrinsic characteristics of sliding the outer graphene layers under shear loading (outer layer sliding phenomenon is more prone to the CNT with larger diameters), which make them less fortifying than SWCNTs. Secondly, the CNTs to be used in the matrix should have close diameter range i.e. a mixture of CNTs having various diameter ranges will behave differently when experiencing loadings, hence unexpected and premature failures may occur[102].

In non-ferrous engineering materials, aluminum alloys are the most popular being light in weight, good in strength and compatible for processing, which made them the choice of many researchers to use for MM-CNTs nanocomposite fabrication. In fact it has been investigated as matrix material more than any other class of material for MM-CNTs nanocomposites. There are two major processing routes to fabricate Al-

CNTs nanocomposites; one is solid phase processing and other is liquid phase processing.

2.4.1 Solid Phase Processing

Solid phase processing or powder metallurgy route is an easy way to obtain good dispersion of the constituent elements; therefore many researchers have used it for the fabrication of Al-CNTs nanocomposites. However, processing of Al-CNTs nanocomposites through the route usually cause CNTs' clustering and porosity, which act as stress raisers and cause deterioration of the mechanical properties. Any deformation process after sintering (e.g. extrusion or rolling) can improve the dispersion of the nanotubes along with closure of the pours. Such post sintering deformation processes can disintegrate CNTs clusters and align them in the deformation direction.

In solid phase processing following methods have been used to fabricate Al-CNTs nanocomposites:

- Ball milling
- Blend mixing
- Dispersion by liquid suspension of CNTs
- Nano-scale dispersion
- Roll bonding
- CVD growth of CNTs on aluminum powder
- Thermal spraying

2.4.1.1 Ball Milling & Blend Mixing

Majority of the work done is based upon dispersion of CNTs in aluminum powder by ball milling and blending owing to the fact that it can provide ease of operation and multiple choices of grinding mediums. It was Kuzumaki et al[98] who reported first time on the fabrication of Al-CNTs nanocomposites in 1998. They have dispersed MWCNTs in alcohol and mixed aluminum powder by stirring, which resulted in insufficient dispersion of the nanotubes. Their nanocomposite (having ~10% MWCNTs) had reduced values of tensile strength. The successors[103–108] adapting ball-milling, altered the approach by using mechanical alloying, high energy ball-milling

and directional deformations (i.e. rolling or extrusion) of the nanocomposites after sintering, came up with better dispersion of CNTs along with increased mechanical strength. Especially, any post sintering rolling or extrusion is reported to cause improved dispersion and alignment of the CNTs in the deformation direction.

2.4.1.2 Dispersion by Liquid Suspension of CNTs

Another approach to achieve better dispersion of CNTs in aluminum matrix is first suspending CNTs in a solvent (e.g. ethanol) and then adding aluminum powder during sonication of the solution. Afterwards, the solvent is evaporated and powder mixture is ball-milled and then compacted using conventional or spark plasma sintering. The latter has an added benefit to limit the grain growth during sintering which causes additional increase in the mechanical strength[109–112].

In another similar experiment, Deng et al[113] ultrasonically mixed CNTs and aluminum powder in ethanol and isostatically cold compacted at 300 MPa. Subsequently, the sintered composite was extruded at a ratio of 25 at 460 °C. They found homogeneous dispersion of CNTs along the grain boundaries of the aluminum particles. Due to high temperature and extrusion strains, CNTs at the grain boundaries transformed into aluminum carbides (Al_4C_3) at their interfaces. Appreciable increase in tensile strength and hardness were achieved.

2.4.1.3 Nano-scale Dispersion

Initially, Noguchi et al[114] and later other researchers[97,115] used natural rubber to increase dispersion of CNTs in aluminum powder. They mixed CNTs and aluminum powder in elastomeric natural rubber and filled the mixture in aluminum hollow billets. The billets were vacuum-encapsulated for sintering and then extruded at various extrusion ratios (i.e. 5 to 25). Good dispersion of CNTs was observed during microscopic examinations and about 100% increase in tensile strength was attainable.

Lim et al[116] filled CNTs and Al powder in a groove of aluminum plate and covered it with the same material and welded it with a friction stir tool. The thickness of top plate was one fifth of the bottom plate. The tool was a cylindrical cone of 4 mm diameter and rotated (1500-2500 rpm) anticlockwise which increased the downwards flow of

the material. Microscopic examination revealed that a laminar flow of material occurred with varying hardness bands. It was a process to produce localized Al-CNT nanocomposite with limitation of specimen geometry and depth of nanocomposite.

2.4.1.4 Roll Bonding

The process was introduced by Lahiri et al[117] in 2009. They prepared a suspension of CNTs in acetone and sprayed it on a commercial grade aluminum foil. They used a hand atomizer to spray the CNTs suspension on the foils. After drying, they stacked the foils (four layers) and cold rolled it followed by stress relieving at 250 °C for 60 minutes. Afterwards, they again rolled it to the final thickness of 50 μm. The final rolling reduction was 70%. Their technique resulted the homogeneous dispersion with good bonding at the interfaces of aluminum and CNTs. An increase of 250% in tensile strength was achieved in nanocomposites having 9.5% CNTs.

2.4.1.5 CVD Growth of CNTs on Aluminum Powder

In-situ dispersion of CNTs on aluminum powder was attained by CVD, which additionally provided excellent bonding between CNTs and aluminum. After CNTs' growth on aluminum particles, the powder was compacted and sintered at 640 °C for three hours in vacuum. Then it was further compacted (at 2 GPa) and annealed. Investigation revealed that good dispersion was achieved, while interface was strengthened by the formation of Al_4C_3. A maximum of 150% increase in tensile strength was observed in Al-5% CNTs composites[118].

2.4.1.6 Thermal Spraying

It is generally used to fabricate coatings of Al-CNTs nanocomposites ranging from few microns to 5 mm thickness. The extended coating thicknesses may facilitate near-net-shape fabrication of the bulk nanocomposites. The process has three broad categories: plasma spraying, cold spraying, and high velocity oxy-fuel spraying (HVOF). In plasma spraying, an arc is generated between two electrodes in an inert atmosphere and injected powder (having high temperature and velocity) when sprayed on the substrate form a coating[119]. In cold spraying, as the name suggests, powder is

accelerated using inert gas at relatively lower temperature (200-500 °C). Severe plastic deformation occurs when the high velocity particles hit the substrate's surface, this helps them to stick on each other. Lower processing temperature ensures to restrain oxidation[120]. In HVOF spraying, a mixture of oxygen and fuel gas (e.g. hydrogen, methane, propane) is burnt at high pressure. The processing conditions result in very high temperature and velocities of the powder, consequently producing higher density coatings. A comparison of the results obtained by different researchers in different experimental conditions is shown in Table-2.4.

Table-2.4 Summary of selected work carried out on Al-CNT nanocomposite by thermal spraying

Process	Experimental Conditions	CNTs contents (Vol %)	Change in Elastic Modulus (%)	Change in Tensile Strength (%)	Ref.
Plasma Spraying	Blended powder and spraying on a metallic substrate.	10	>3	78	[121]
	After spraying SPS and hot extrusion.	1	-	200	[122]
Cold spraying	CNTs blended in Al-Si eutectic powder. Nanoindentation was done.	1	<200	-	[123]
HVOF Spraying	Blended and mixed by ball milling (48 h).	1	14	-	[124]

2.4.2 Liquid Phase Processing

Liquid phase processing or casting is an economical method to produce intricate shapes at industrial scale. For MM-CNTs nanocomposite fabrication, it has two major limitations: (1) high melting temperature of matrix metal which may damage CNTs and (2) segregation of CNTs due to the surface tension forces of molten metal. In this regard, aluminum is a promising matrix material having low melting point and ease of subsequent processing, however, high surface tension forces of molten aluminum (i.e.

860 mN/m) remain a problem for the uniform dispersion[125]. To overcome segregation of CNTs in aluminum melt, some additional steps or process (e.g. coating of CNTs and stirring) would be required. Al-CNTs nanocomposites are prepared by following liquid phase processes:

- Casting
- Melt infiltration
- Powder Precursor Casting
- Stir Casting
- Compo-casting
- Ultrasonic Assisted Casting
- Squeeze Casting

2.4.2.1 Casting

In casting process, molten metal is poured in a mold and allowed to solidify. CNTs have very low density which makes them extremely difficult to disperse uniformly within the melt; instead they tend to segregate at the melt's surface. A specialized methodology is required for their dispersion. Another hindrance for the dispersion of CNTs in the melt is non-wetting behavior of CNTs towards most of the molten metals.

Wetting of a liquid and a solid substrate is a balance of surface tension forces between the two, as shown in Figure-2.9. Mathematically, the wetting or contact angle (θ) could be calculated from equation-2.4.

$$\gamma ls - \gamma sv = \gamma lv.Cos\theta \qquad (2.4)$$

Where; γ_{ls}, γ_{sv} and γ_{lv} are the surface energies of liquid-solid, solid-vapor and liquid-vapor interfaces, respectively. To get wetting between solid and liquid the contact angle should be less than 90° and as the angle decreases wetting increases. An optimum value of contact angle is 0° (Cosθ = 1) where complete wetting occurs. Poor wettability is associated with contact angles > 90° [126].

Some metals e.g. cesium and selenium exhibit appreciable wetting with CNTs. In non-wetting conditions, buoyancy is established due to surface tension forces causing the CNTs to form clusters. High surface tension metals do not wet CNTs. Wetting behavior with CNTs and surface tensions of some metals are enlisted in Table-2.5. It

could be seen in the Table that most of the metals are non-wetting with CNTs; therefore certain treatments are required to obtain wetting properties[125].

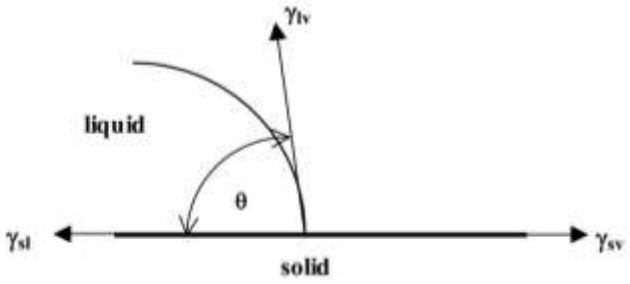

Figure-2.9 Contact angle between liquid on a solid surface[126].

Table-2.5 Surface tension values of some elements and their wettability with CNTs[125].

Element	Surface Tension ($mN.m^{-1}$)	Wetting with CNTs
S	61	Yes
Cs	67	Yes
Rb	77	Yes
Se	97	Yes
Te	190	No
Pb	470	No
Hg	490	No
Ga	710	No
Al	860	No

Fabrication of MM-CNT nanocomposite through casting process is more favorable for low melting point metals matrix e.g. aluminum, magnesium and some metallic glasses. In 2005, Li et al[127] used casting method to fabricate Mg-CNT bulk metallic glass. CNTs were added in the molten Mg (at 700 °C) and stirred. Subsequently casting was carried out in metallic molds. Prior to mixing, CNTs were coated with nickel to attain better wetting with matrix. An addition of 0.67 wt% of CNTs resulted in the increase of 150% in ultimate tensile strength of the nanocomposite. However, any further

increase in CNTs contents in the melt caused their segregation resulting in substantial decrease in mechanical properties.

In the succeeding years, Goh et al[128] presented a technique named "disintegrated melt deposition" improving CNTs dispersion in the melt. They used a ceramic coated steel stirrer to disperse CNTs in the molten magnesium. After stirring, the mixture was atomized using argon jets and collected in a metallic mold, which was further hot extruded (at 350 °C) into Mg-CNT nanocomposite rods. They fabricated Mg-CNTs nanocomposites with varying weight percentages of the CNTs (~2 wt%). A simultaneous increase in tensile strength and ductility was observed, however, a decrease in the endurance limit (fatigue life) was found; a comportment of the increased void density at CNT-matrix interfaces. Same research group used another approach by first dispersing CNTs in liquid polymer. They first dissolved disperbyk-2150 (a block co-polymer) in ethanol and added CNTs during stirring. After the dispersion of CNTs in the mixture they added Mg powder while stirring continued. After the evaporation of ethanol the mixture was melted in inert conditions and melt was stirred before casting. Any refinement in the grain size was not found and hence the increase in the compressive strength was attributed to the CNTs strengthening effects[129].

In 2004, Bian et al[130] reported the fabrication of zirconium based bulk metallic glass-CNTs nanocomposite by induction heating. They mixed CNTs in the powder of $Zr_{52.5}Cu_{17.9}Ni_{14.6}Al_{10}Ti_5$ and compacted into a cylindrical shape, which was then rapidly melted in inert atmosphere. Finally, the molten composite was casted in a metallic mold of 5 mm diameter. They have prepared nanocomposites having up to 10 vol. % CNTs. Rapid heating and solidification helped to avoid clustering of CNTs in the melt and casting. Although increase in hardness and acoustic wave absorption was observed but clustering of CNTs was also present.

The advantages of rapid solidification include less time for CNT segregation and less time to re-crystallize and/or growth. Melt spin casting is another technique which provides rapid solidification of the molten metal forming amorphous ribbons. Li et al[131] prepared amorphous $Fe_{82}P_{18}$-CNTs ribbons using this technique. They mixed CNTs in the melt and poured it on a water-cooled copper wheel rotating at 2500 rpm. Molten metal solidified to amorphous ribbon (40 µm thick) when came in contact with the rotating cold wheel.

Casting is a viable route for the synthesis of MM-CNTs nanocomposites as it provides easy processing at feasible costs along with end-product shape compatibility. However, besides segregation and dispersion issues of CNTs, high reactivity of molten metals could be deleterious for CNTs integrity. As mentioned above the problem could be addressed by using rapid melting, coating of CNTs or both, which may result in better wetting, dispersion and retention of CNTs in the metal matrix.

2.4.2.2 Melt Infiltration

The technique is widely used for the synthesis of MMCs with higher reinforcement loadings. Principally, a porous preformed filler material is prepared by PM or by fibers woven cloth, which is then infiltrated with molten matrix metal to form the composite. Figure-2.10 shows a schematic of pressure-less melt infiltration setup, where a CNT perform is placed in a crucible while an appropriate block of metal/alloy is place at its top. The whole arrangement is placed in a furnace having inert atmosphere. As temperature rises the metal melts and infiltrates into the perform making a nanocomposite[132].

The melt infiltrates into perform due to its low viscosity and gravity, however, for high viscosity melts additional pressure may be required to get complete infiltration. The pressure required for a particular preform and melt can be estimated form Darcy's law[133]:

$$h^2 = \frac{2k_p t}{\mu(1-V_p)}(P - P_0) \qquad (2.5)$$

where h is depth of infiltration, k_p is compact's permeability, μ is melt's viscosity, t is time of infiltration, V_p is the volume fraction of the particulates. P and Po are applied pressure and infiltration threshold pressure, respectively. The law states that large infiltration will occur if the infiltrating liquid metal has low surface tension and viscosity.

Mechanical ball milling is a simple approach to prepare preforms for melt infiltration. Zhou et al[132] reported their work on the technique: they milled aluminum powder and CNTs for several hours at 300 rpm and then compacted to a preform, which was infiltrated using LY12 aluminum alloy at 800 °C in inert atmosphere. They prepared composites up to 20 vol. % of CNTs and found that dispersion of CNTs was limited.

Wear properties were studied and found that wear rate decreased with increasing the nanotubes contents, however, friction coefficient decreased till 15 vol. % of CNTs afterwards it became constant. Maximum hardness was attained in Al-CNT nanocomposite with 10 vol. % CNTs; any further increase in CNTs contents did not increase hardness.

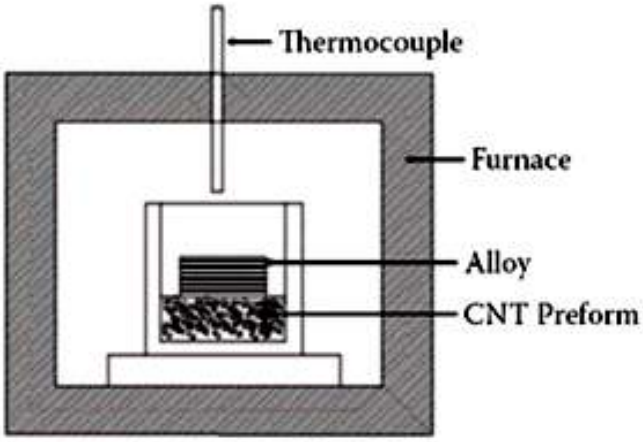

Figure-2.10 Schematic diagram of melt infiltration process[132].

Yang et al[134] used a distinct methodology to prepare the preform. They grew vertical CNTs on alumina fibers and infiltrated with magnesium using pressurized infiltration technique. The Mg-CNT nanocomposite showed increased shear modulus. Similarly, another common technique is mixing CNTs in an organic binder and metallic powder. Subsequent, sintering evaporates the organic binder and a porous network of MM-CNTs is fabricated, which is used as melt infiltration preform. Molten melts like Al, Mg, Al-Mg alloy and Al-Si alloys were pressurized infiltrated. Significant improvement in mechanical properties was observed[135].

Though melt infiltration is a longer route than casting for MM-CNTs fabrication but it is yet economical for high CNTs loadings. The dispersion of CNTs is primarily driven by the efficiency of preform fabrication. In actual, the infiltrating metal or alloy is free from CNTs, as not enough time is given to infiltrate CNTs from preform to molten metal. This aspect of the technique can lead to the fabrication of improved nanocomposites, if explored.

2.4.2.3 Powder Precursor Casting

To improve the wettability of CNTs with the molten matrix, CNTs are coated with various types of coatings e.g. Al[5], Ni[136], Cu[137], and SiC[138]. The coated CNTs are then used as precursor for the incorporation in molten aluminum. In a typical work, Sehyun et al[139] first produced the powder precursor by mechanical milling of Al powder and CNTs and then they coated nickel on the milled powder to increase the wetting of the precursor in molten aluminum. They have investigated 10 and 20 wt. % of MWCNTs incorporation in Al. The nanotubes and aluminum powder were mixed in acetone and sonicated to avoid clustering; subsequently acetone was evaporated at 50 °C and partial pressure. Milling was performed (~24 hours) in argon filled container to reduce oxidation of the powder. The milled powder was then electro-less coated with nickel. The resultant cast Al-CNT nanocomposite exhibited good wetting of CNTs with matrix, although some segregation was also observed.

2.4.2.4 Stir Casting:

The technique emerged from the simplest idea of CNTs dispersion in molten metal, where a mechanical stirrer was used[140–142]. Recently, Rashad et al[143] used a novel approach, in which they first ball-milled aluminum powder and CNTs and prepared green billets. Then they incorporated these green billets in molten aluminum during stirring by mechanical means. A good dispersion and interfacial bonding was achieved which resulted in increased mechanical strength (~35%).

2.4.2.5 Compo-casting:

It is a modified form of stir casting, where CNTs are injected in the slurry through a coated tube. In Figure-2.11 the experimental setup is shown where a ceramic crucible is placed in a furnace with assemblies of stirring and powder injection mechanisms. A bottom pouring mechanism facilitates the subsequent pouring of treated melt. Argon gas was used to inject the powder.

Abbasipour et al[142] fabricated Al-CNT nanocomposite using A356 cast aluminum alloy. They reduced the segregation of CNTs by first coating CNTs by electro-less nickel plating and then injected the coated CNTs by the injector. Subsequently, the

slurry was cast in fully and semi-liquidus forms. They reported increased hardness along with good nanotubes' dispersion in the matrix.

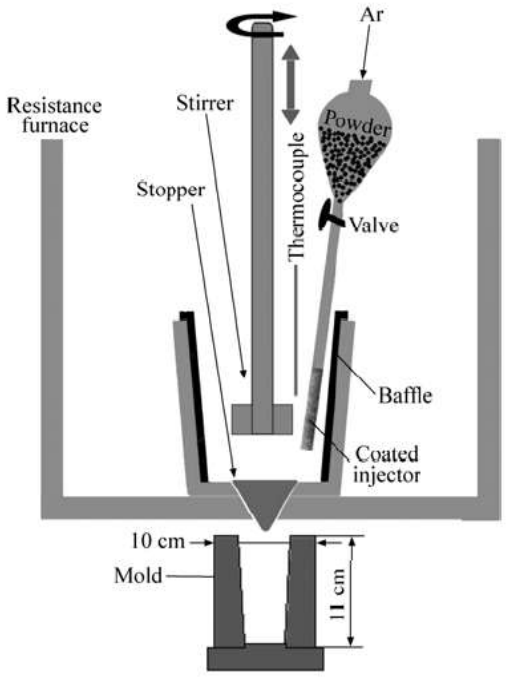

Figure-2.11 Schematic of the compo-casting setup[142].

2.4.2.6 Ultrasonic Assisted Casting:

Inducing ultrasonic waves into a molten metal causes cavitation, which may produce short duration (few nano-seconds) ultra-hot spots (up to 5000 °C) and extremely high pressure (up to 1000 atmospheres). Such high localized impacts of temperature and pressure can break the clusters of CNTs and increase their dispersion[144].

In 2009, the fact was first used by Donthamsetty et al[145] preparing Al-CNTs composite. They used CNTs, silicon and boron carbides in various percentages and dispersed them in aluminum melt using ultrasonic cavitation, which resulted in noticeable dispersion of the reinforcing agents. However, clustering and segregation was observed at isolated regions of the castings. Improvements in mechanical properties i.e. hardness and tensile strength were reported.

2.4.2.7 Squeeze Casting:

Two separate material processing techniques are combined in squeeze casting. Molten metal is poured into a mold (i.e. gravity casting) and pressure is inserted by the other half of the mold (i.e. closed die forging), Figure-2.12. Rapid heat transfer from the poured metal is effectuated by the physical contact and elimination/closure of casting defects (i.e. cavities) by applied pressure, consequently a defect-free casting is achieved which is comparable to wrought products. The process is featured with minimum porosity, splendid surface finish, low metal losses and economy of the process[146].

AbouBakr et al[147] reported on the fabrication of Al-CNTs nanocomposite by a combination of rheocasting and squeeze casting. They used hypoeutectic aluminum-silicon alloy as matrix material. Their method caused de-bundling and segregation of CNTs, additionally they observed refinement of grain size as well. Mechanical properties also increased significantly.

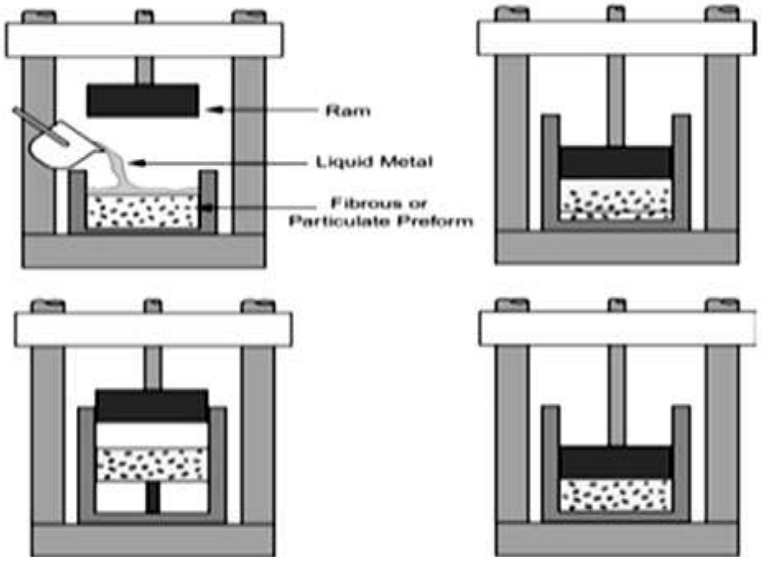

Figure-2.12 Process of Squeeze casting[146].

2.4.3 The Potentials

Powder metallurgy technique is more popular than melt processing for the fabrication of MM-CNTs nanocomposites due to a major challenge of CNTs dispersion in the molten metal. The root cause of the challenge is the feeble wetting of CNTs with most of the melts of structural metals and alloys. Therefore, rapid heating and solidification could be the solution by not permitting much time to the nanotubes for segregation. But dispersion of CNTs remained an issue to be addressed by continuous stirring and/or surface coating to increase wettability.

Chapter No: 3

Research Motivation and Approach

Emergence of aeronautical and aerospace industry, besides automotive industry, the urge for light weight and high strength structural materials has been increased considerably. Generally speaking, required mass for a load bearing application reduces due to increased pay load, fuel economy and environmental regulations. Both the monolithic metals and alloys cannot provide the specific combination of high strength and low mass, which instigated the development of MMCs. Using light weight metals and/or alloys as matrix material provides low mass and ductility, while reinforcing the matrix with strengthening materials (e.g. CNTs) may result in higher strength and stiffness. Specifically, aluminum matrix reinforced with CNTs has potentials to attain higher strength to mass ratio, which is the alluring aspect to instigate present research in the field of Al-CNTs based MMCs.

3.1 Motivation

In the preceding discussion of literature review, it has been established that Al-CNT nanocomposite is a potential candidate material for engineering applications due to its expected mechanical and physical properties. However, the expected properties in a composite having the CNTs as strengthening material could only be achieved if following two issues could be address prudently:

- Dispersion of the nanotubes in the matrix material
- Wetting of the nanotubes with the matrix material

CNTs being excellent reinforcement material, due to their extra ordinary set of mechanical and physical properties, might only render their strengthening effects, from nano to micro and then macro scales, if and only if they are well dispersed within the matrix and substantially wet or bonded with the matrix.

The above mentioned hypothesis was the motivation of the present research, where it was planned to achieve both the required aspects (i.e. dispersion and wetting) for amelioration in mechanical properties of Al-CNTs nanocomposite.

Additionally, it was also planned to find such a route for the fabrication of the composite, which may render scale-up capabilities along with justified processing cost. As discussed in literature review, many research groups had quoted appreciable improvement in mechanical properties of Al-CNT nanocomposite but their methodologies were complex with certain limitations of process control and yield. Moreover, their routes were expensive not only in terms of capital investment but also for process cost. Therefore, the motivation of the present research also includes a feasible processing.

3.2 Approach

To achieve the objective of increased mechanical properties in Al-CNTs composite through dispersion and wetting of the nanotube in matrix, the research plan was divided into following stages:

I. Synthesis of MWCNTs; production of characteristic MWCNTs, which can support their easy dispersion in subsequent processes of the composite fabrication.
II. Dispersion of CNTs in aluminum; using innate stirring action of induction melting to disperse the nanotubes in molten aluminum.
III. Coating of CNTs with aluminum; to develop a process that could facilitate wetting/coating of aluminum on the nanotubes.
IV. Fabrication of Al-CNT nanocomposite; combining the results of stages 1, 2 and 3 such that appreciable dispersion and wetting of the nanotubes could occur, hence improving the mechanical properties of the composite.

3.2.1 Synthesis of MWCNTs

3.2.1.1 Background

Among the various means for CNTs synthesis, CVD shows the most promising industrial scale deposition in terms of its economics. There are additional advantages associated to the CVD synthesis of CNTs: unlike the other methods, CVD is capable of growing nanotubes directly on a desired substrate, whereas other processes demand an additional step for collection of CNTs; the growth sites are controllable by careful deposition of the catalyst; moreover, CVD also supports to grow vertically aligned carbon nanotubes (VACNTs) using various carbon precursors with the liberty of supported or floating catalysts. One of the popular methods to synthesize VACNTs is co-evaporation technique, where catalyst and carbon precursor are mixed. The mixture is then evaporated and passed through the CVD reactor having inert atmosphere, where synthesis and deposition of CNTs occurs. Main advantage of the process is "long active growth period" for the synthesis of CNTs due to continuous supply of catalyst along with carbon precursor. Resultant CNT products are usually a thick mat of vertically aligned CNTs[148–151].

Maruyama et al[82] are the pioneer researchers who reported synthesis of SWCNT using ethanol. They prepared dual metallic catalyst supported on zeolite by sonication-assisted mixing of iron acetate and cobalt acetate in ethanol with Y-type zeolite powder. In a CVD reactor the catalyst mixture was placed and ethanol vapors were passed from an ethanol reservoir (at room temperature) using a vacuum pump. The SWCNTs were synthesized at 700-800 °C.

Extending the Maruyama's work, Kouravelou et al[152] exhibited their work on dynamic study of CNT growth using ethanol. They used iron oxide particles supported on alumina and studied the effect of catalytic particle loadings on the carbon yield. A mixture of ethanol, methanol, hydrogen and helium was used for CNT synthesis. The CNTs produced were of multi-walled type.

Mendoza et al[85] introduced a variation in Maruyama's approach by passing hydrogen gas through an ethanol bubbler and synthesizing MWCNTs at 700 and 900 °C on

quartz supported catalyst (iron nitrate). They increased the length of MWCNTs using a process temperature of 700 °C, by inhibiting generation of amorphous carbon caused by -OH radicals.

In 2009, Maruyama and his team again reported their work with an approach to reactivate the catalyst by introducing acetylene in ethanol assisted CNT growth. This time they used Co-Mo mixture as catalyst at a process temperature of 800 °C and ethanol-acetylene as precursor. They observed a 10-fold increase in the growth of SWCNTs by catalytic reactivation[153].

Another research group, Ren et al[154] demonstrated synthesis of free standing SWCNTs film using ferrocene and ethanol. They employed two furnaces for this purpose; one for the evaporation of ferrocene-ethanol mixture at 100 °C and the other for pyrolysis of ethanol and synthesis of the CNTs. By varying the flow rate of ethanol they observed variations in the CNTs diameter, however, they did not show explicit data about the ethanol flow rates.

Recently, Jaime et al[155] has mentioned the effect of ethanol precursor on the synthesis of MWCNTs using perovskite-type oxide $LaNiO_3$ as catalyst. They found that the catalyst is quite efficient for ethanol decomposition producing higher CNTs yield at 700 °C and 50ml·min^{-1} of ethanol in He (50 % - v/v).

As mentioned above, the previous researchers[82,85,152–156] had shown their work on alcohol assisted SWCNT growth by CVD but the effect of ethanol flow rate for the synthesis of MWCNTs associating catalytic activity of nickel particles during CVD was ignored.

3.2.1.2 Hypothesis and Approach

In the present work, it was planned to grow MWCNTs on quartz substrates in a CVD reactor where ethanol would be used as a precursor with nitrogen and hydrogen as inert carrier and reducing medium, respectively. The flow rate of nitrogen gas would be used to introduce various concentrations of ethanol during the synthesis of MWCNTs and subsequently, the ethanol flow rates would be optimized to synthesize mono strands of characteristic CNTs having uniform diameter offering easy dispersion in molten aluminum. The optimization of the process would be associated with the catalytic activity of the catalyst used for the synthesis.

3.2.2 Dispersion of CNTs in aluminum

3.2.2.1 Background

To improve the dispersion and wettability of the nanotubes in molten aluminum, several researchers had used various types of coatings e.g. Ni[136], Cu[137] and SiC[138]. The coated CNTs were then used as precursor for incorporation in molten aluminum. In a typical work, Sehyun et al[139] initially produced the powder precursor by mechanical milling of Al powder and CNTs. Subsequently, they coated nickel on the milled powder to increase the wetting of the precursor in molten aluminum. They investigated 10 and 20 wt. % of multi wall carbon nanotubes (MWCNTs). The resultant cast Al-CNTs nanocomposite exhibited good wetting of CNTs with matrix, although some segregation was also observed.

A further improvement in the dispersion of CNTs in the molten matrix occurred by the emergence of the melt stirring by mechanical means[140–142]. Recently, Rashad et al[143] used a novel approach, in which they first ball-milled aluminum powder and CNTs. Then green billets of the milled powder were prepared and incorporated in molten aluminum during stirring by mechanical means. A good dispersion and interfacial bonding was achieved which resulted in increased mechanical strength (~35%).

Abbasipour et al[142] fabricated Al-CNTs nanocomposite of A356 cast aluminum alloy using compocasting technique, which was basically a stir casting method but it allowed casting the composite in semi-molten state. They first coated CNTs by electro-less nickel plating and then injected them into the melt using an injector. Subsequently, the composite was cast in semi-liquid form. They reported increased hardness along with good dispersion of the nanotubes in the matrix.

Similarly, Hamed et al[147] reported on the fabrication of Al-CNTs nanocomposite by a combination of rheocasting and squeeze casting. They used hypoeutectic aluminum-silicon alloy as matrix material. Their method caused de-bundling and dispersion of CNTs; additionally they observed refinement of grain size and increased mechanical properties.

3.2.2.2 Hypothesis and Approach

It is mentioned in preceding discussion that many researchers had tried various melt-cast routes to fabricate Al-CNT nanocomposite, however their efforts were mainly limited to mechanical stirring. The present work was based on hypothesis of using induction melting due to the following reasons:

- The innate electromagnetic stirring action of the process will facilitate dispersion of the nanotubes in molten aluminum.
- The rapid heating rate of induction melting will assist to reduce degradation of the nanotubes, which in-turn increases the contribution of the nanotubes towards strengthening of the composite.
- Scale up capabilities of the process, so that larger quantities of the composite could be processed.
- The processing route is more economical.

A major hindrance in using induction melting for aluminum was its reduced thermal efficiency due to high electrical and thermal conductivity of aluminum. In usual practice, graphite susceptors are used to increase thermal efficiency of the process, however, it limits the stirring action of the induction melting. Therefore, a specific induction coil would be designed, which would render substantial thermal efficiency along with stirring to melt aluminum and disperse CNTs.

For this purpose, a coil was designed on the basis of geometrical, thermal and electromagnetic analyses[157,158]. The results of the analyses are given in Table-3.1. Using these design parameters, the heating efficiency of the coil and stirring force in the melt were calculated according to the simulation work of Julio et al [159] using finite element method magnetic software (FEMM 4.2). The coil design considerations, relevant simulation and efficiency factors have been discussed elsewhere[160] and in Annexure-1. Figure-3.1 represents distribution of magnetic fields in two types of induction melting approaches. In Figure-3.1a, magnetic field lines were plotted with no susceptor material while in Figure-3.1b a graphite susceptor was placed between the coil and the crucible. It was observed that presence of susceptor had limited the magnetic field lines. The calculations indicated that a heating efficiency greater than

60% and stirring force ~3 mN was achievable at the operating parameters of the induction generator (i.e. frequency of 10 kHz and current of 100 A). The designed coil was employed for the subsequent experimental work.

Table-3.1 Results of the coil design analyses

Geometrical analysis	
Height of molten metal	5.5 cm
Diameter of molten metal	3.0 cm
Volume of the molten melt	38.9 cm^3
Internal diameter of the induction coil	45.0 cm
Height of the inductor coil	6.0 cm
Thermal analysis	
Energy to melt aluminum	69850 J
Energy to superheat molten aluminum	32042 J
Energy to melt slag	144 J
Total heat energy required	102036 J
Electromagnetic analysis	
Maximum magnetic flux density	0.00409 T
Current density through the coil	5.67 $A.mm^{-2}$
Number of turns of the coil	4.47 turns

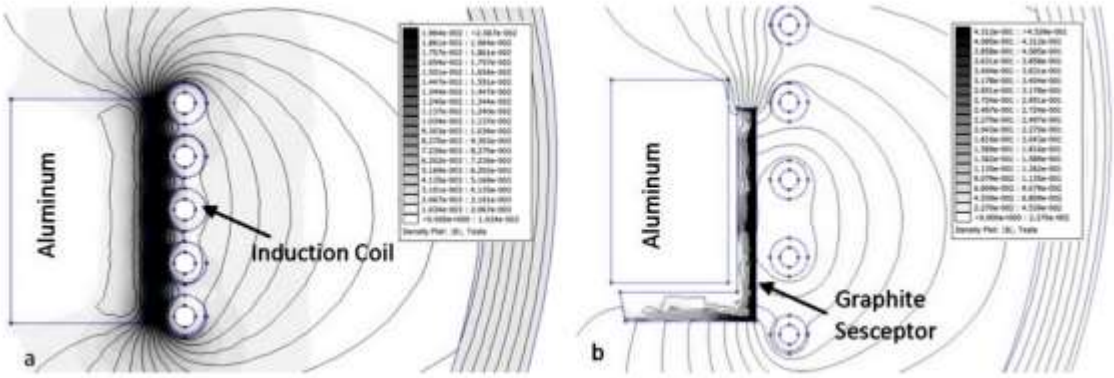

Figure-3.1 FEMM simulated magnetic flux lines for induction melting a) without susceptor and b) with graphite susceptor. It is evident that susceptor has limited the magnetic flux lines to enter in aluminum.

3.2.3 Coating of CNTs with aluminum

3.2.3.1 Background

Aluminum based carbon nanotubes (Al-CNTs) composite, is a promising materials for many conventional and contemporary applications. However besides dispersion, wetting of carbon nanotubes (CNTs) in molten aluminum (Al) is quite difficult owing to their large differences of surface tension forces i.e. 45 mN/m and 860 mN/m, respectively[125]. Many researchers addressed the issue by coating copper oxide[161], nickel[162], titanium[163]or tin oxide[164] on CNTs, which reduced the surface tension between the nanotubes and molten aluminum improving the wetting and dispersion.

In recent years, Arai et al reported their sequential work for the coating of nickel on CNTs and their subsequent use in Al-CNTs composite fabrication[165–167]. They coated MWCNTs with pure nickel using electro-less deposition technique. For a typical work they used hydrazine and gluconic acid as reducing and complexing agents, respectively. After annealing treatment they observed the treated nanotubes in electron microscope and found a complete but rough coating of nickel on the CNTs. The roughness of the coating smoothened after another heat treatment at relatively higher temperature.

Similarly, Maqbool et al[168] has reported on the copper electro-less coating of the nanotubes. After the coating, the nanotubes were dispersed in aluminum using molecular level mixing. The process was assisted by sonication and ball milling. The compacted specimens were pressure-less sintered in vacuum. Subsequently, the sintered composites were rolled to attain uniformity in the structure. They compared the composites having uncoated and coated CNTs and found that the composite prepared with coated CNTs have yield and tensile strengths almost twice to that of the composites prepared by uncoated CNTs. They believed that there was enhancement of interfacial bonding between CNTs and aluminum matrix due to copper coating.

Limited work is available on the coating of Al on CNTs. So et al[5] coated Al on substrate supported vertically grown CNTs using electrolysis of aluminum chloride. It was a two-step coating process: in first step, aluminum was coated on the CNTs by electroless deposition; spreading excess aluminum powder on the coated CNTs and

annealing at high temperature. In this way they formed aluminum carbide on the surface of the CNTs, which subsequently provided wetting for aluminum to coat.

3.2.3.2 Hypothesis and Approach

It is established so far that aluminum has partial or negligible wetting with CNTs, which is the primary factor of limited augmentation in the mechanical properties of Al-CNTs composite.

As described in foregoing discussion that limited work has been reported on the wetting of aluminum with CNTs, however, Baumli et al demonstrated improved wetting of aluminum with graphite[169,170] and carbon fibers[171] using multifunctional flux. They used a mixture of chloride flux and potassium hexafluorotitanate ($MCl+K_2TiF_6$) during melting of aluminum having graphite powder or carbon fiber at 750 °C. The multifunctional flux effectuated dissolution of the oxide layer present on aluminum and formation of titanium carbide by an exchange reaction between titanium present in molten aluminum and carbon.

The current study was inspired from Baumli's work which led to the developed of a hypothesis that by using potassium hexafluorotitanate during fabrication of Al-CNT composite might increase the wettability of aluminum with CNTs due to the following assumptions:

- CNTs are basically rolled sheets of graphite. Therefore, the surface crystalline structure or precisely speaking the unit mesh on the surface of both the materials is comparable.
- Outer surface of the CNTs is always accompanied by certain amount of amorphous carbon, which may promote direct formation of titanium carbides prior to the exchange reaction. Hence it could be expected that titanium carbides may form at even lower temperatures than reported by Baumli (i.e. <750 °C).
- Additionally, surface imperfections (discontinuities, voids, contours, bends, etc.) of the nanotubes may provide easy nucleation/formation sites for titanium carbides.

To validate the above hypothesis, a separate experimental regime was planned, where substantial quantities of CNTs and potassium hexafluorotitanate were used along with aluminum.

3.2.4 Fabrication of Al-CNT nanocomposite

3.2.4.1 Background

Aluminum based carbon nanotubes (Al-CNTs) composite is a promising materials for many conventional and contemporary applications. However, wetting and dispersion of carbon nanotubes (CNTs) in molten aluminum (Al) is quite difficult owing to their large differences of surface tensions i.e. 45 mN/m and 860 mN/m, respectively[5]. Many researchers addressed the issue by coating nickel on CNTs[172,173], which reduced the surface tension and improved the wetting and dispersion. However, their work mainly encompassed electro-less plating approach, which in turn was a lengthy process beside risk of contamination. Limited evidence is available on the coating of Al on CNTs. So et al[5] coated Al on substrate supported vertically grown CNTs using electrolysis of aluminum chloride.

3.2.4.2 Hypothesis and Approach

The hypothesis of the present work is based upon the experimental findings "Synthesis of MWCNTs", "Dispersion of CNTs in aluminum" and "Coating of CNTs with aluminum".

- In step-1, synthesis of characteristic MWCNTs will be demonstrated using ethanol assisted CVD process. Uniform, mono-strands and less tangled nanotubes will be produced by optimization of the ethanol flow rate with respect to the catalytic activity of the nickel catalyst. It is logical that if the CNTs to be used are mono-strands and not tangled ones their dispersion would be easier. Therefore, characteristic nanotubes will be synthesized in excess quantity, and would be used in subsequent fabrication of Al-CNT composites.
- It will be experimentally shown in step-2, that substantial amount of dispersion of the nanotubes could be achievable using induction melting along with appropriate flux, which might be reflected by the increase in

mechanical properties of the Al-CNTs composite Therefore, the idea could be extended for the present work.

- In step-3, it will be established that the flux (potassium hexafluorotitanate) effectuated a facile coating of aluminum on the nanotubes. This finding will lead to the fact that presence of potassium hexafluorotitanate in molten aluminum may facilitate wetting of the nanotubes with molten aluminum. It is believed that the mechanism of wetting is based upon an in-situ reaction forming titanium carbide on the surface of the nanotubes, hence providing wetting sites for aluminum on the walls of the nanotubes. Therefore, the finding will be utilized for the wetting of the nanotubes during Al-CNTs composite fabrication.

The prime function of the flux is to induce wetting between aluminum and the nanotubes. Therefore, a specific amount of the flux will be needed for the purpose. Baumli et al[174] demonstrated experimentally that the addition of 4 wt. % of titanium in K_2TiF_6, along with other fluxes, reduced the contact angle form 130° to almost zero degree between molten aluminum and carbon. However, 4 wt. % of K_2TiF_6, without using additional fluxes has been proposed in the current research.

For a melt of 20 grams of aluminum, 800 mg of K_2TiF_6 will be used in two steps. In first step, a mixture of the nanotubes and 400 mg of the flux will be added in the crucible along with 20 gram of aluminum and heated. In second step, when aluminum will become molten another 400 mg of the flux will be added and held for a specific time at 760 °C.

The two-step addition of the flux in the melt will be adapted due to following reasons:

- In first step, presence of the flux along with the nanotubes in molten aluminum will effectuate removal of surface oxides from aluminum and achieves efficient melting.
- Meanwhile, the titanium reduced by the aluminum from the flux will form titanium carbide on the surface of the nanotubes by a set of exchange reactions:

$$3K_2TiF_6 + 13Al \rightarrow K_3AlF_6 + 3KAlF_4 + 3Al_3Ti \quad (3.1)$$

$$Al_3Ti + C \rightarrow 3Al + TiC \quad (3.2)$$

Accomplishment of reaction-3.2 could only be favorable if the temperature of the melt will be more than 750 °C and titanium contents will be more than 0.4 wt. % [169]. To replenish the amount of titanium in the melt, more flux (i.e. 400 mg) will be added into the melt in second step.

Although, additional flux will be added to execute reaction-3.2 but it will also serve for effective separation between molten aluminum and flux because the densities of aluminum and the flux are 2.32 Kg/m^3 and 2.10 Kg/m^3 at 1100 K, respectively[175], [176]. The difference in the molten densities will cause the formation of crust of the molten flux on the surface of molten aluminum, which would be impermeable to oxygen hence, restrict further oxidation of the nanotubes and aluminum during the process.

Chapter No: 4

Experimental

4.1 Introduction

The approach to fabricate Al-CNTs composite with appreciable dispersion and wetting of CNTs with aluminum matrix was elaborated in Chapter No: 3, where a specific sequence was followed. During experimental work same sequence was pursued such that the results of the previous section(s) could be profited to ameliorate experimental work of succeeding section(s). Therefore the first stage of experimental was the synthesis of MWCNTs. Bulk nanotubes were synthesized after the optimization of synthesis process for characteristic MWCNTs, which were to be used for subsequent stages of composite fabrication. In second stage, dispersion of the CNTs in molten aluminum was carried out using induction melting. In third stage, a separate experimental was carried out to find the wetting/coating of CNTs with aluminum, assisted by potassium hexafluorotitanate. Finally, using all the previous experimental results (stage-1 to stage-3), Al-CNTs composite was prepared having dispersion (assisted by induction melting) and wetting (assisted by potassium hexafluorotitanate).

4.2 Synthesis of MWCNTs

The experimental work comprises of selection of materials to be used, equipment, process description, and synthesis sequence.

4.2.1 Materials

4.2.1.1 Carbonaceous material

Anhydrous ethanol, having purity >99.5 %, was used as carbonaceous source for the synthesis, which was procured from Sigma-Aldrich, USA. The product number was 459836, and claimed trace residues were less than 0.005 % on evaporation.

4.2.1.2 Catalyst

Nickel nanoparticles were used as catalyst for the synthesis of the present work. The particles were produced using hydrated nickel nitrate [Ni $(NO_3)_2.6H_2O$)]. The salt was obtained from AlfaAesar under the trade name of "Puratronic" having purity more than 99.9985 %.

4.2.2 Equipment

Besides laboratory glass wares, following equipment were used during the experimental work:

- Three zones horizontal tube furnace: Carbolite-TZF: 12/75/700 having 750 mm tube length and 75 mm inside diameter.
- Oven: TAISITE-CE/GP, maximum temperature ~450 °C.
- Spin coater: Precision spin coater, Model KW-4A with dispenser supplied by SPI supplies, USA.

4.2.3 Synthesis of MWCNTs using supported catalyst CVD

4.2.3.1 Description of CVD Process

The horizontal tube furnace was used with nitrogen as a carrier gas and as dilution medium for the injection of ethanol whereas hydrogen was used as a reducer gas. A quartz substrate was coated with nickel nitrate solution as catalyst. A hydrogen

treatment was carried out for nickel nitrate reduction prior to the CNT synthesis. Subsequently, a controlled flow of ethanol, hydrogen and nitrogen was introduced at 750 °C for CNT growth. Ethanol bubbler was kept at 45 °C during bubbling process. Typically, a process of 20 minutes of CNT growth was used to deposit CNTs at a flow rate of 10 sccm of hydrogen and 10, 25, 40 and 55 sccm of ethanol vapors via nitrogen bubbler. A schematic view of the CVD reactor is shown in Figure-4.1. The CNTs batches synthesized at 10, 25, 40 and 55 sccm of ethanol vapors were named as A-CNTs, B-CNTs, C-CNTs and D-CNTs, respectively.

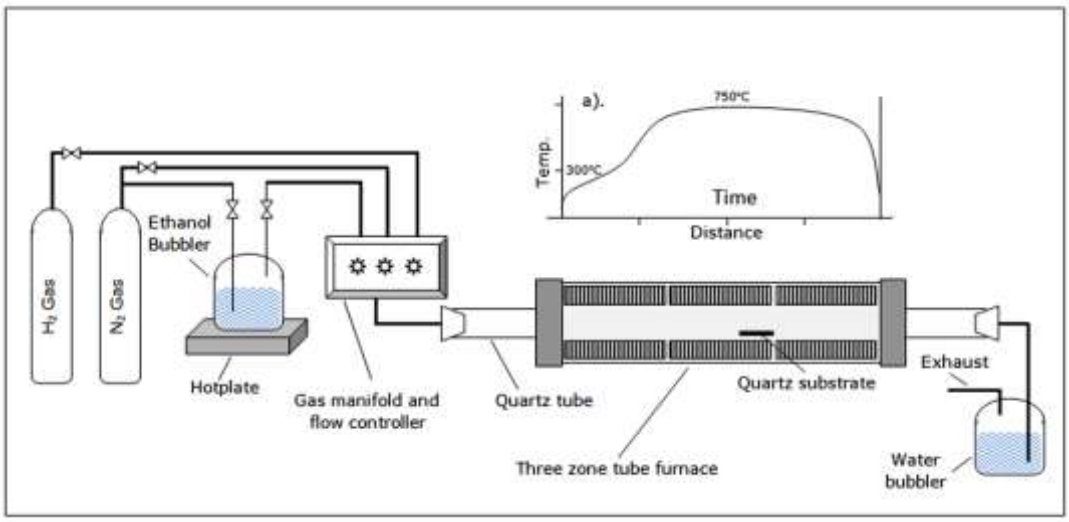

Figure-4.1 Schematic of the CVD apparatus; a) is the inset of the reactor's temperature profile during CNT synthesis.

4.2.3.2 Synthesis Sequence

The synthesis of CNTs was carried out in five stages:

I. Coating: A homogeneous thin film of nickel nitrate solution (50 mmol/l) was coated on the quartz substrates using a spin coater. Thickness of the deposited film was assured to be same in each case by using fixed coating parameters (i.e. solution concentration, feed quantity, feed rate and spinning speeds). Subsequently, the coated substrates were dried in an oven at 65 °C for 2 hours. After drying, the coated substrates were placed in the CVD reactor.

II. Decomposition: Nickel nitrate thermally decomposes at 350 °C to nickel mono-oxide according to the equation-4.1 [156]:

$$2Ni\,(NO_3)_2 \rightarrow 2NiO + 4NO_2 + O_2 \qquad (4.1)$$

Therefore, the coated substrates were heated to 350 °C at the rate of 5 °C/min. and held at this temperature for 30 minutes to attain a complete decomposition to nickel mono-oxide. The slower heating rate was desired to favor a gradual decomposition of the catalyst; or it might cause splashes resulting in heterogeneous distribution of the catalyst on the substrate.

III. Reduction: The reactor temperature was raised to 450 °C and hydrogen gas (10 sccm) along with nitrogen gas (25 sccm) were introduced in the reactor for 10 minutes to reduce the nickel oxide into nickel nano particles.

IV. Synthesis: Finally, the reactor temperature was raised to 750 °C at a heating rate of 25 °C/min. A relatively fast heating rate was helpful to avoid coarsening of nickel nano particles due to high temperature and longer time period. At reaction temperature, hydrogen gas was maintained at the same flow rate whereas nitrogen gas was bubbled through ethanol; various ethanol flow rates were used to synthesize CNTs. This process was continued for 20 minutes.

V. CNTs removal: The processed substrates were washed in 0.4 M HCl at 45 °C to remove the CNTs deposit. The removed deposits were washed and filtered with de-ionized water and heated in oven at 65 °C for 1 hour before desiccation. Various stages of the synthesis are graphically presented in Figure-4.2.

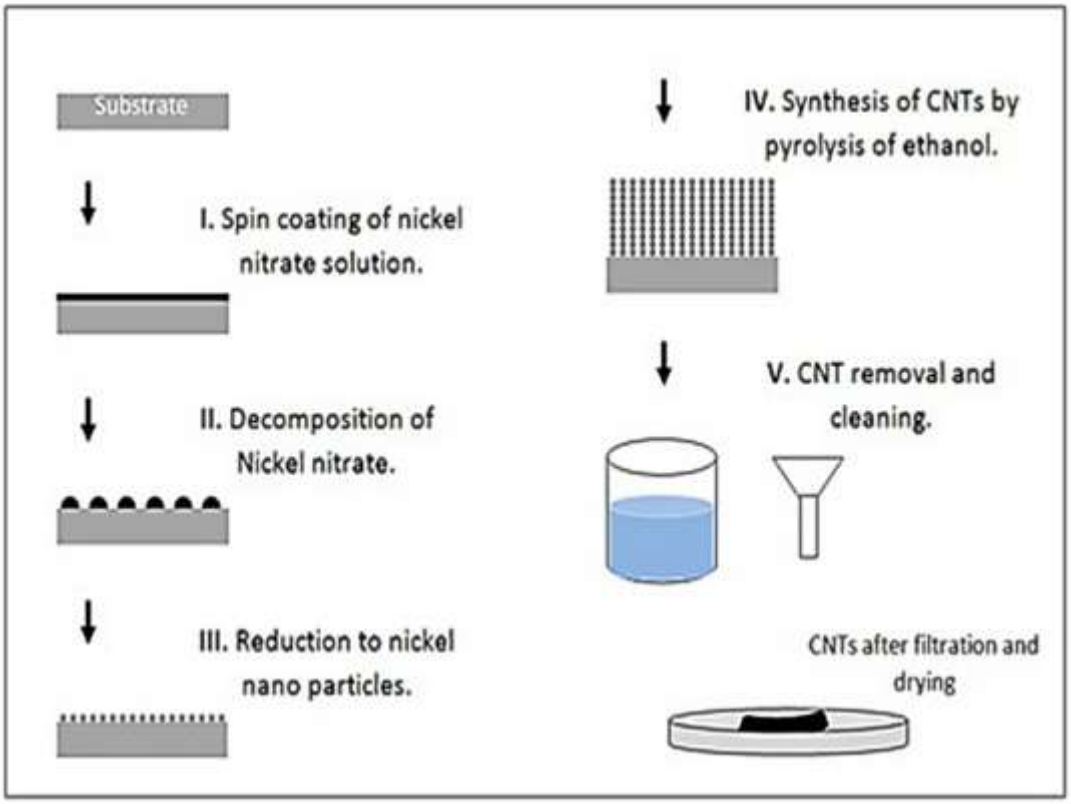

Figure-4.2 Various stages for the synthesis of CNTs.

4.3 Dispersion of CNTs in Aluminum

4.3.1 Materials

4.3.1.1 Matrix Material

High purity aluminum (AA1199) used for the matrix material was available in wire form (diameter: 4mm). The aluminum wire was cut into 1 inch staples and treated with 10 % solution of sodium hydroxide before a final wash with water, in order to degrease or remove any oxide layer on the surface. Subsequently, the washed aluminum was preheated for 30 minutes at 150 °C for complete drying.

4.3.1.2 Reinforcement Material

Multiwalled carbon nanotubes (MWCNTs) synthesized using CVD were used to strengthen the aluminum matrix in present work. Detailed synthesis technique for MWCNTs is discussed elsewhere[177], and in "synthesis of MWCNTs" (Section No. 5.2) of the present thesis. The MWCNTs had average diameter 10 nm and length 1.5µm.

4.3.1.3 Melting Fluxes

The flux used for the melting purpose was a mixture of "recycling and remelting flux" and "cleaning flux" supplied by FOSECO under the trade names of COVERAL-912 and ALUFLUX-3, respectively. The purpose of using multi-flux was to reduce the melting temperature of aluminum and to remove impurities from the melt. A mixture of the flux and pre-weighed MWCNTs was manually prepared using mortar and pestle. Each batch of 20 g of aluminum used 2 g of flux [50 wt. % COVERAL + 50 wt. % ALUFLUX], however, CNTs were used in varying concentrations [0, 0.1 and 0.2 vol. %]. Fabrication of the composite was carried out in air induction furnace using the previously described coil's design.

The excess amount of flux was purposely used for the fabrication of the composite as the melting was to be carried out in an air induction furnace and CNTs had tendency to oxidize before the melting temperature of aluminum[177,178]. Excess amount of the flux would provide a cover of low density molten salts at top of the melt, preventing oxidation of the nanotubes and aluminum besides other benefits like early melting, removal of dross and impurities sink. However, high flux contents might cause retention of elements (like potassium, sodium, calcium etc.) in the melt. To avoid the

retention of the impurities in the melt, a “cleaning flux” (ALUFLUX-3) was added into the “recycling and remelting flux” (COVERAL-912). The cleaning flux has a strong tendency to remove oxides, dross and inclusions [179]. Moreover, the operating temperature was kept below 790 °C, since exceeding this temperature the tendency of molten aluminum to pick up hydrogen from the atmosphere and retain impurities from flux could increase remarkably[180,181].

4.3.2 Melting Furnace

Fabrication of the composite was carried out using an air induction furnace. The heating coil of the induction furnace was specifically designed for the application to ensure maximum magnetic flux density, consequently maximum stirring, within the melt. The coil design considerations, relevant simulation and efficiency factors are discussed in detail elsewhere[160] and in Annexure-1.

4.3.3 Method

The procedure used in the present work to fabricate Al-CNT composite is as follows: an alumina crucible (diameter: 30mm) was placed in the induction coil and aluminum staples were positioned vertically in it (step-I). The mixture of the flux and the nanotubes was poured in the crucible when aluminum became semi-molten at around 660 °C (step-II). Addition of the flux caused removal of the surface oxide and rapid melting of aluminum. Meanwhile, the flux became molten and covered the top surface of the melt preventing it from oxidation. In step-III, the nanotube present in the flux moved towards the interface of molten flux and aluminum, under gravity. At this stage, the temperature of the melt was 760 °C. Generic stirring action of induction heating picked the nanotubes from the interface of flux-aluminum and dispersed them into the melt. Low density of the molten fluxes prevented their sinking/dispersion in molten aluminum. Step- IV was basically dispersion stage, where the melt was held for 10 minutes while keeping the temperature around 760 °C. No manual or mechanical stirring was carried out. Various steps involved in the fabrication of the composite are schematically shown in Figure-4.3. After the hold

time the molten flux was skimmed using a stainless steel spatula and the melt was poured into a rectangular copper mold (65 mm x 20 mm x 10 mm) preheated to 150

°C. The solidified ingots were homogenized at 540 °C for one hour in argon atmosphere; subsequently the ingots were cold rolled to attain a final thickness of 0.5 mm using two-high roll mills. It is worth mentioning that all the castings (pure aluminum, Al-0.1% MWCNT and Al-0.2% MWCNT) were carried out under the same processing conditions to establish the effect of CNTs addition.

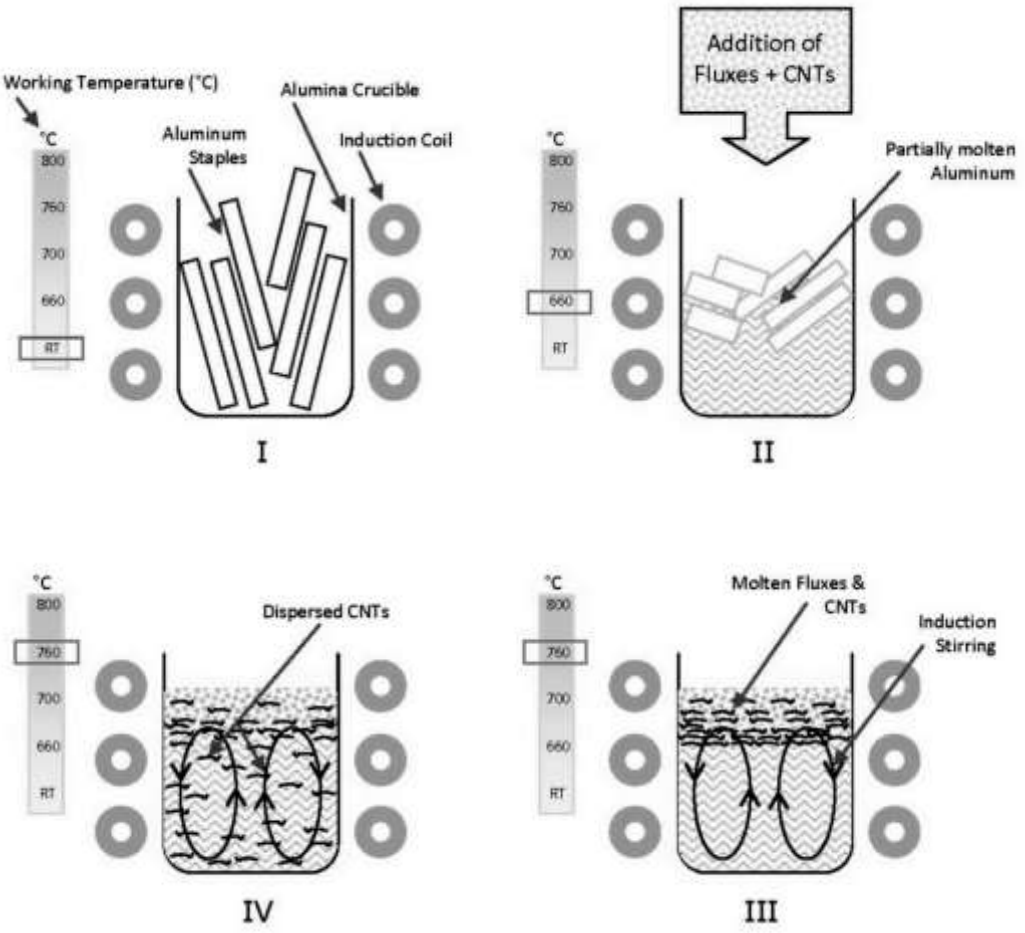

Figure-4.3 Schematic of the various stages during fabrication of Al-CNT nanocomposite using air induction furnace

4.4 Coating of CNTs with Aluminum

4.4.1 Materials

The nanotubes used for the present work were multi wall carbon nanotubes (MWCNTs), synthesized by chemical vapor deposition. The average diameter and length of the nanotubes was 10 nm and 7.5 µm, respectively.

The flux used was potassium hexafluorotitanate (K_2TiF_6), having purity more than 98%, supplied by Sigma-Aldrich. The Al powder, having 125 µm particle size and more than 99.5% purity, was purchased from GoodFellow-UK.

4.4.2 Method

1.3 g of MWCNTs and flux mixture, having titanium to carbon ratio of 5 and 1.25 g of aluminum powder was placed in an alumina crucible and heated to 790 °C in an argon atmosphere furnace. A heating rate of 10 °C/min was used to achieve the temperature and the mixture was heated for 60 minutes. Subsequently, the furnace was cooled to room temperature and the crucible was removed.

4.5 Fabrication of Al-CNT Nanocomposite

4.5.1 Materials

4.5.1.1 Matrix Material

AA 1199 grade aluminum was used as matrix material. For details refer to section 4.3.1.1.

4.5.1.2 Reinforcement Material

The reinforcement material is same as described in section 4.3.1.2. For various melting batches, 0.1, 0.2, 0.4, 0.8, and 1.6 vol. % of the nanotubes were added in molten aluminum.

4.5.2 Melting Flux

The flux used was potassium hexafluorotitanate (K_2TiF_6), having purity more than 98%, supplied by Sigma-Aldrich. The flux was heated in an air oven at 120 °C for two hours and ground to fine powder using a ball mill. The powder was sized to ~220 µm by its retention at mesh No: 70 using a sieve shaker with a set of two mesh sizes i.e. mesh No: -60 and +70.

4.5.3 Melting Furnace

Fabrication of the composite was carried out according to the parameters described in Annexure-1, using an air induction furnace.

4.5.4 Method

The procedure used in the present work for fabricating of Al-CNT composite is similar to the procedure described in section 4.3.3 with some additional steps of flux incorporation into the melt. The process is schematically shown in Figure-4.4. In step-I, a 30 mm diameter alumina crucible was charged with the materials (i.e. aluminum staples, MWCNTs and flux) and heated in the induction furnace.

When the charge became molten, second addition of the flux was made (step-II). The temperature of the melt was ~700 °C at this stage. Addition of the flux caused formation of a surface crust on the melt, which prevented further oxidation of the melt and the nanotubes. Moreover, the nanotube present in the melt dispersed under the innate stirring action of induction heating, which continued in next step as well.

Step- III was a holding stage, where the melt was kept at 760 °C for 10 minutes to accomplish following occurrences:

- Formation of Al_3Ti after the reaction between aluminum and K_2TiF_6.
- Formation of TiC on the surface of the nanotubes after the reaction between Al_3Ti and carbon. TiC provided the wetting of the nanotubes with molten aluminum.
- Removal of the by-products (fluorides of aluminum and potassium) from the molten aluminum to the surface molten flux. These by-products shifted to the surface due to their lower densities and stirring action of the induction furnace.

Once the hold time lapsed, the crust of the molten flux was broken and skimmed off using a stainless steel spatula. The melt was then poured into a rectangular copper mold (65 mm x 20 mm x 10 mm) preheated to 150 °C. The solidified castings were homogenized at 540 °C for one hour in argon atmosphere; subsequently the ingots were cold-rolled to attain a final thickness of 0.5 mm using two-high roll mills. All the castings (pure aluminum, Al-0.1 % MWCNT, Al-0.2% MWCNT, Al-0.4 % MWCNT, Al-0.8% MWCNT and Al-1.6 % MWCNT) were carried out under the same processing conditions to establish the effect of the nanotubes addition.

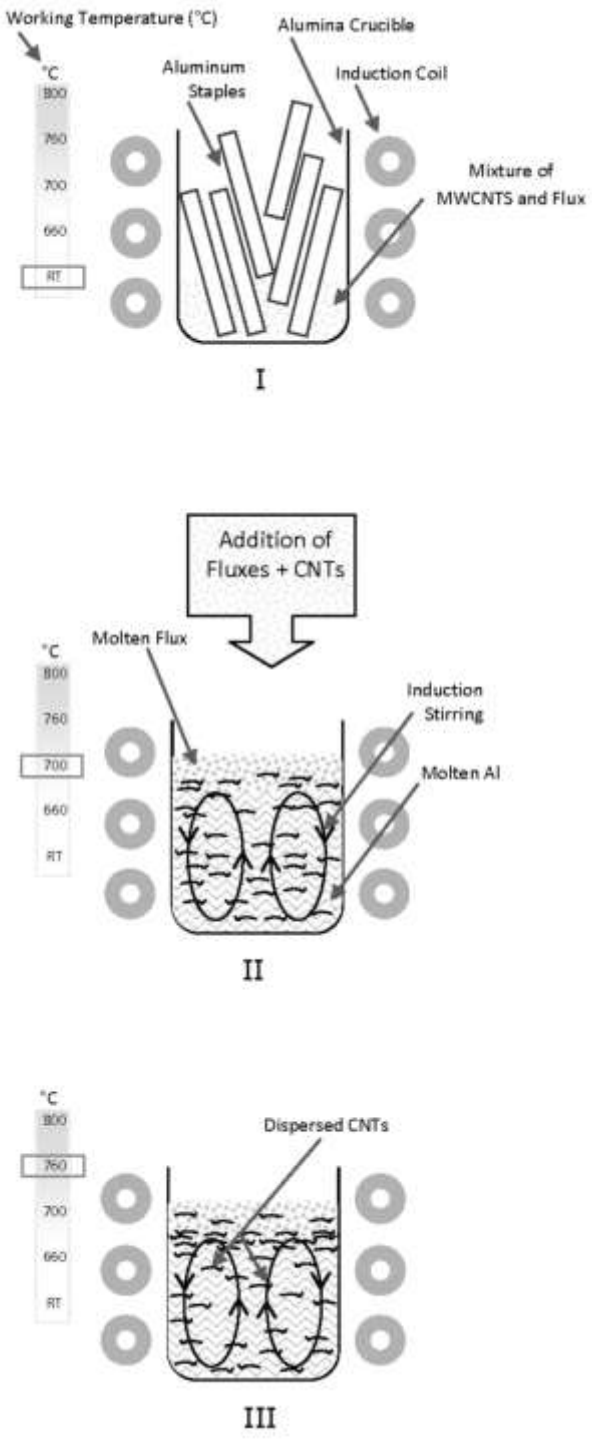

Figure-4.4 Schematic of the various stages during fabrication of Al-CNT nanocomposite using air induction furnace

4.5.5 Nomenclature

Various materials were melted and solidified using air induction furnace under same processing conditions for evaluation and comparison purpose. Following is the nomenclature of the specimens used in present experimental regime:

Table-4.1 Nomenclature and description of fabrication conditions for various specimens using multifunctional flux.

Specimen ID	Description
T0	Pure aluminum melted under KCl-NaCl flux.
TM	Aluminum + K_2TiF_6 (0.4 wt. % Ti contents)
T1	Aluminum + K_2TiF_6 (0.4 wt. % Ti contents) + 0.1 vol. % of MWCNTs
T2	Aluminum + K_2TiF_6 (0.4 wt. % Ti contents) + 0.2 vol. % of MWCNTs
T3	Aluminum + K_2TiF_6 (0.4 wt. % Ti contents) + 0.4 vol. % of MWCNTs
T4	Aluminum + K_2TiF_6 (0.4 wt. % Ti contents) + 0.8 vol. % of MWCNTs
T5	Aluminum + K_2TiF_6 (0.4 wt. % Ti contents) + 1.6 vol. % of MWCNTs

4.6 Characterization

4.6.1 Etching

To reveal the grain boundaries “Hume-Rothay’s etchant” was used. All the specimens studied in the present work were etched using the etchant. The etching regents and method are as follows:

- A 15 wt. % aqueous solution of copper chloride was used to etch the structure of the materials by swabbing. To reveal embedded nanotubes in aluminum matrix excessive etching was carried out to remove maximum matrix material. For such excessive etching, swabbing continued for 30 to 45 seconds.
- After etching, the etched specimens were placed vertically in 5vol. % solution of hydrochloric acid using a beaker, which was then sonicated for 10 to 20 seconds. The treatment removed the etching deposits from the surface of the specimen. Later on, the specimens were washed in cold water and dried in pressurized air.

The etched specimens were preserved in a dried silica gel desiccator in order to avoid any surface contamination/degradation.

4.6.2 Optical Microscopy

A stereo optical microscope (OLYMPUS SZX9) was used to study the etched specimens of various materials (i.e. pure aluminum and Al-CNT composites with different fractions of the nanotubes) in as cast condition. An OLYMPUS BZ51 optical microscope was used to study the microstructure of various specimens.

4.6.3 Scanning Electron Microscopy

A scanning electron microscope JEOL JSM 5910LV was used for SEM studies.

4.6.3.1 Carbon Nanotubes

Loose powder of the CNTs was directly sprinkled on the adhesive carbon tape supported by an aluminum stub. Further the sprinkled CNTs were gently pressed with

a glass slide to ensure the CNTs were properly fixed on the carbon tape. All the observations were carried out in secondary electron imaging mode at 20KV.

4.6.3.2 Pure Aluminum and the Composites

The structure of as cast and rolled specimens of the nanocomposites was studied using scanning electron microscope (SEM) in secondary electron mode with working distance of 10 mm at 20 KV. Deep etching of the composite specimens was performed. SEM and energy dispersion spectroscopy (EDS) were used to conduct fractography and area analyses of the fracture surfaces of the broken tensile specimens, respectively.

4.6.3.3 Aluminum Coated CNTs

The treated mass (agglomerated powder) was subjected to scanning electron microscopic (SEM) using secondary electron imaging mode at 20 kV accelerating potential. The powder was slightly ground in mortar and pestle then it was sprinkled on a steel stub.

4.6.4 Transmission Electron Microcopy

A transmission electron microscope JEOL JEM 2000FX was used to study the dispersions of CNTs and thin foils of various composite specimens.

4.6.4.1 Carbon Nanotubes

The nanotubes were first sonicated in ethanol to form dispersion and then dropped on a carbon coated grid. The grid was dried in a vacuum desiccator prior to its use. All the observations were carried out in bright field mode at a potential difference of 120 KV.

4.6.4.2 Pure Aluminum and the Composites

For TEM studies of the composite, 3 mm discs were punched from the rolled strips and thinned to <0.3 mm. The discs were perforated using twin-jet method with 10% perchloric acid solution. TEM studies were carried out in bright field illumination mode at 120KV working potential difference.

4.6.5 X-ray Diffraction

A Siemens D-500 X-ray diffractometer with cobalt radiation source was used to study various specimens in the present study.

4.6.5.1 Carbon Nanotubes

Powder samples of various CNT batches were subjected to XRD analysis using a Cu Kα radiation source and a scan rate of 0.05° s^{-1} from 18°-75° (2θ). During scanning the tube potential and current was maintained at 40 KV and 30 mA, respectively.

4.6.5.2 Pure Aluminum and the Composites

To find the crystallite size and lattice strain, various rolled samples were studied using Siemens D-500 X-ray diffractometer (XRD). A cobalt X-ray source with CoK_{α} radiation having wavelength of 1.78897 Å was used. The diffractometer was operated at 40 kV and 40 mA tube potential and current, respectively, with a scan rate of 0.1° per minute and a step size of 0.02° 2θ. To calculate crystallite size and lattice strain, one needs to eliminate instrumental broadening from the full width half maximum (FWHM) of the specimens under investigation. Therefore, a full annealed aluminum specimen was used to find instrumental broadening. In present study, first three peaks of the aluminum spectrum (i.e. 111, 200 and 220) were used for profile analyses, while higher order peaks were not used due to the appearance of alpha 1 and 2 doublets. These alpha doublet peaks cause confusions in finding respective FWHM values.

The crystallite size and lattice strain were calculated using slope-intercept method, considering the combined effect of peak broadening by small crystallites and lattice strain[182]. According to this method the broadening of diffraction peaks (B_r) is sum of individual broadening due to small crystallite size (B_c) and lattice strain (B_s):

$$Br = Bc + Bs \tag{4.2}$$

where;

$$Br^2 = Bo^2 - Bi^2 \tag{4.3}$$

and

$$Bc = k\lambda/L\cos\theta \tag{4.4}$$

$$Bs = \eta tan\theta \tag{4.5}$$

where B_o is FWHM value of the peak under investigation, B_i is FWHM value of instrumental broadening, k is a constant, λ is wavelength of the radiation used, θ is diffraction angle, L is crystallite size and η is lattice strain. Substituting Eqs. (4.4 and 4.5) into Eq. (4.2), we have

$$Br\cos\theta = k\lambda/L + \eta\sin\theta \quad (4.6)$$

In Eq-4.6, kλ/L and η represent intercept and slope of the straight line, which were used to calculate crystallite size and lattice strain, respectively.

4.6.5.2 Aluminum Coated Carbon Nanotubes

To find the phases present in the mixtures treated at various temperatures a Siemens D-500 X-ray diffractometer (XRD) was used. A copper X-ray source with CuK_α radiation having wavelength of 1.54173 Å was used. The diffractometer was operated at 40 kV and 30 mA tube potential and current, respectively, with a scan rate of 0.1° per minute and a step size of 0.02° 2θ.

4.6.6 Thermal Analysis

4.6.6.1 Carbon Nanotubes

For thermogravimetric analyses (TGA), 10 mg of the CNTs from each formulation were heated to 900 °C in air using a Netzsch STA 409C system. A heating rate of 10 °C/min and a constant flow of air were maintained throughout the heating cycle.

4.6.6.2 Aluminum Coated Carbon Nanotubes

To evaluate various reactions in the mixture at different temperatures differential scanning calorimetric (DSC) studies were carried out. For the purpose, 10mg of the mixture, having same composition, was heated to 850°C in argon using a Netzsch STA 409C system. A heating rate of 10°C/min and a constant flow of argon were maintained throughout the heating cycle.

DSC scan exhibited four distinguishable peaks at various temperatures, therefore the mixture was heat to those temperatures separately and treated masses were subjected to XRD for phase analyses.

4.6.7 Raman spectroscopy of the Nanotubes

Raman analysis was carried out using a Raman Renishaw (inVia) spectrometer operating with a wavelength of 785 nm. The specimens were manually compressed between two glass slides in order to improve density to get measurable spectrum. Each specimen was scanned in the Raman shift range of 100-3000 cm^{-1}.

4.6.8 Mechanical Testing

Hardness testing was carried out on cold rolled strip specimens using a Vickers hardness testing machine (LECO V100) according to ASTM E384 standard. Tensile specimens were prepared by wire-cut electric discharge machine in accordance with ASTM standard E8/E8M-11. An INSTRON-1195 universal testing machine with 0.02 s^{-1} strain rate and 25 mm gauge length was used to determine the tensile properties.

To find the stress relaxation behavior, specimens were tested in accordance with ASTM E328-02 at a strain rate of $1x10^{-4}$ $s^{-1}$for annealed specimens. Stress relaxation data was acquired using a digital interface operating at 500 Hz. At a certain stress level ($\sigma_{\circ}$), cross-head movement of the machine was arrested for a relaxation time of 300 seconds, in each case. All the tests were carried out at room temperature.

Chapter No: 5

Results and Discussion

5.1 Introduction

In this chapter, the results obtained during various experimental and characterization carried out (as mentioned in Chapter No: 4) will be presented and discussed sequentially. Though, the results will be presented and discussed separately for each experimental stage, these will also be correlated with previous findings where needed.

5.2 Synthesis of MWCNTs

5.2.1 X-ray Diffraction

The XRD scans of the various batches of the synthesized nanotube are given in Figure-5.1. The scans are superimposed on each other with a vertical off-set of 1000 CPS.

Three peaks of different intensities observed in each scan i.e. 26.5°, 45° and 52° are shown in the figure. The major peak which can be attributed to hexagonal graphite (JCPDS card No. 41-1487) occurred around 26.5° and it represents (002) planes of CNTs[164,183]. Other two minor peaks represent the nickel catalytic particles [PDF card No: 040850]. The intensity of the 26.5° peak reflects the quantity and the crystallinity of carbon phase in the form of CNTs[184]. The scans indicated that at flow rate of 10 standard cubic centimeters per minute (sccm) i.e. for A-CNTs, amount of amorphous carbon was relatively high; the amorphousness, however, decreased with a rise in the flow rate to 25 sccm (B-CNTs). However, it again increased with further high flow rates 40 and 55 sccm as represented by C- and D- CNTs scans, respectively. The other two peaks at 45° and 52° represent variation in the amounts of nickel particles as shown by their intensities; the peak broadenings depict their nanocrystalline size.

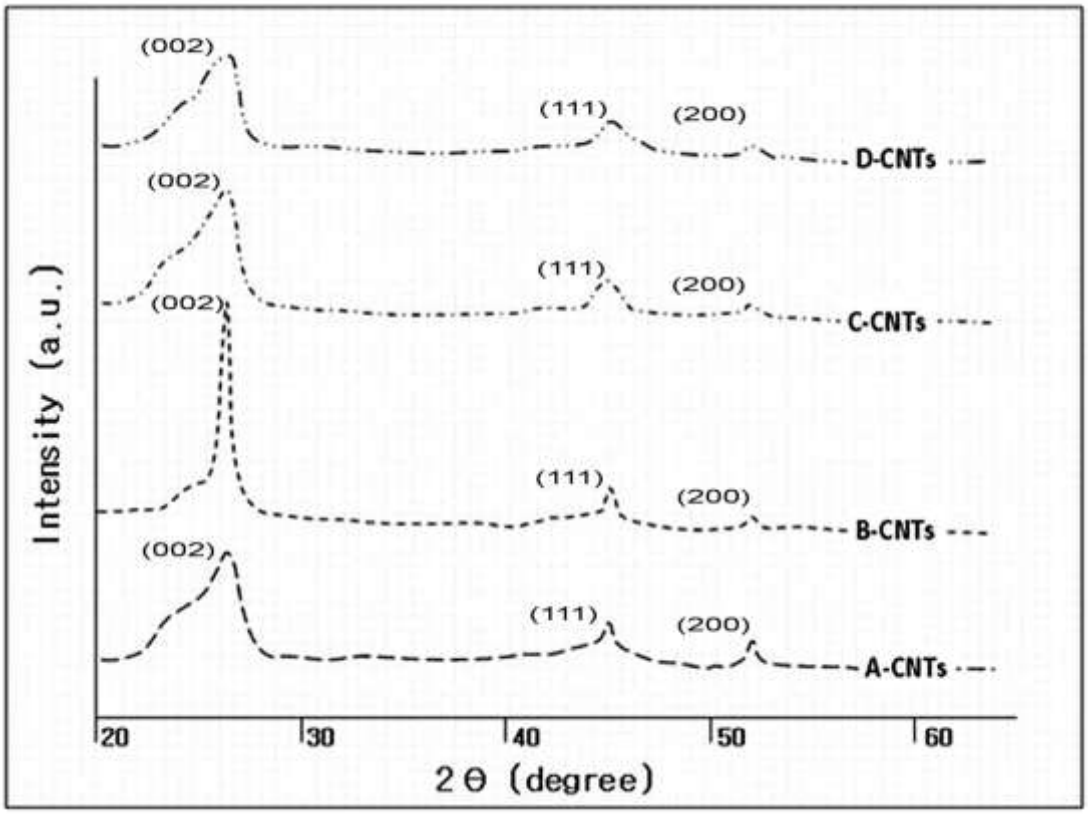

Figure-5.1 Superimposed XRD scans of various CNT batches: peaks at 26.5° represent graphite, while peaks at 45° and 52° represent nickel catalytic particles entrapped in the CNTs.

5.2.2 Scanning Electron Microscopy

Scanning electron micrographs of Al-CNTs specimens exposed to secondary electron imaging mode at 20KV are shown in Figures-5.2 to 5.5. In A-CNT specimen the CNTs were irregular in shape, structurally inconsistent and heterogeneous (Figure-5.2). Fine CNTs appeared to be stemming out of the coarse CNTs. Trapped catalyst nickel particles were also found to be present at the ends and body of the CNTs; presumably the fine CNTs were nucleated from the trapped nickel particles causing more heterogeneous growth pattern during synthesis.

In B-CNT specimen, regular and uniform strands of CNTs were observed (Figure-5.3). Amorphous carbon was seen in isolated regions in minute quantity. In C-CNT

and D-CNT specimens, an increasing trend of structural heterogeneity, randomness and amorphous carbon were observed. The maximum heterogeneity was observed in case of D-CNT specimen (Figure-5.4 & 5.5).

The behavior of CNTs' synthesis during the process could be attributed to the variation of ethanol flow rates as well as to the catalytic activity. Since the other process parameters were kept constant in all formulations, equal amount of catalyst (ca.) were available for reaction in various ethanol concentrations, which helped in cracking and subsequent growth of carbon molecules in to CNTs. Increasing flow rate of ethanol from 10 sccm to 25 sccm resulted in better structural control and uniformity in growth of the CNTs. The CNTs were more regular in shape, uniform in structure and less contaminated by amorphous carbon. A further increase in ethanol flow rate caused structural damage to the synthesized CNTs; this could be attributed to sluggish activity of the catalyst particles, which was unable to decompose significant carbon contents into MWCNTs. This hypothesis was further supported by TGA results.

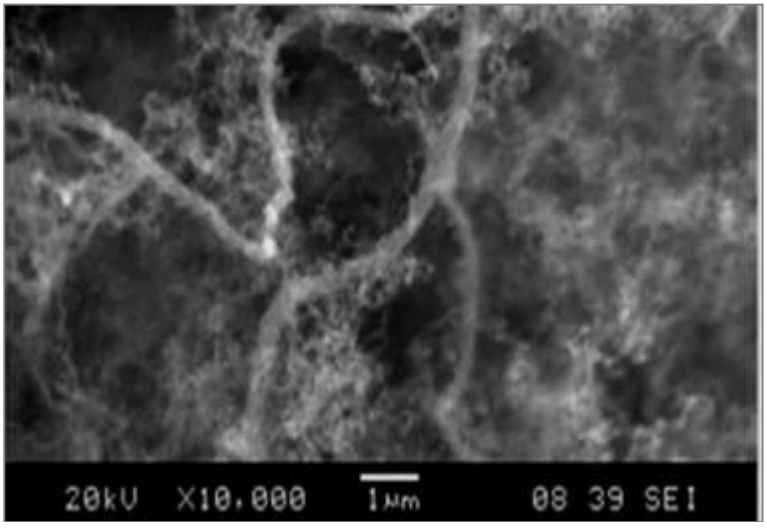

Figure-5.2 SEM micrograph of A-CNTs

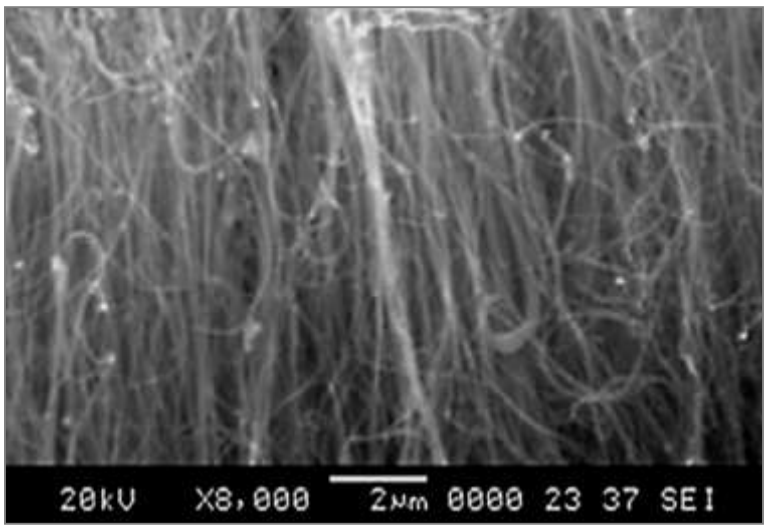

Figure-5.3 SEM micrograph of B-CNTs

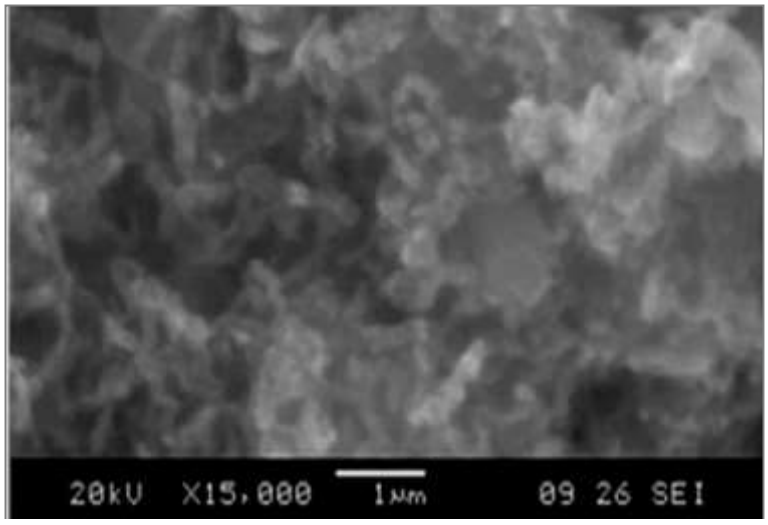

Figure-5.4 SEM micrograph of C-CNTs

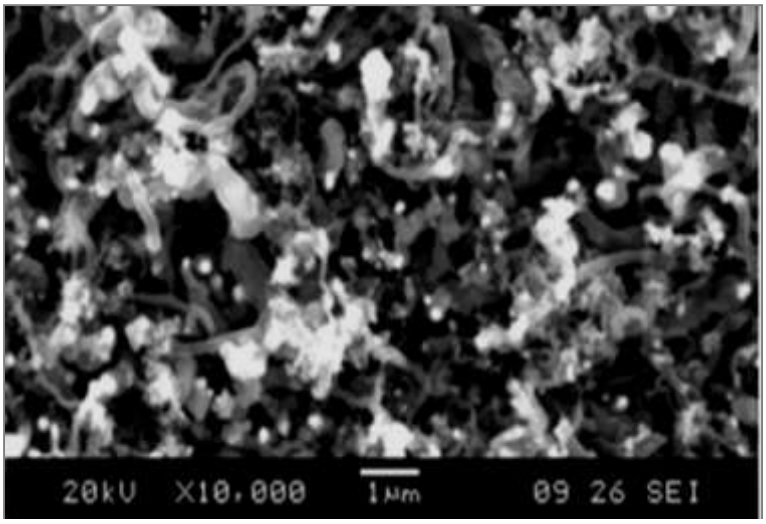

Figure-5.5 SEM micrograph of D-CNTs

5.2.3 Transmission Electron Microscopy

During TEM studies, it was observed that the nanotubes were distributed uniformly exhibiting uniform diameter and extended length (Figure-5.6). At higher magnifications, diameter distribution appeared to be more uniform along with amorphous carbon on the outer walls of the nanotubes (Figure-5.7 and 5.8). Figure-5.9 exhibits diffraction pattern of the nanotubes showing their multi-walled nature with (002) and (004) reflections, indicating their reasonable crystallinity[185]. The diameters of the nanotubes were measured and a histogram (Figure-5.10) was plotted against frequency function (260 measurements) to find the spread of the nanotubes' diameter; calculated to be 10.3±1.8 nm.

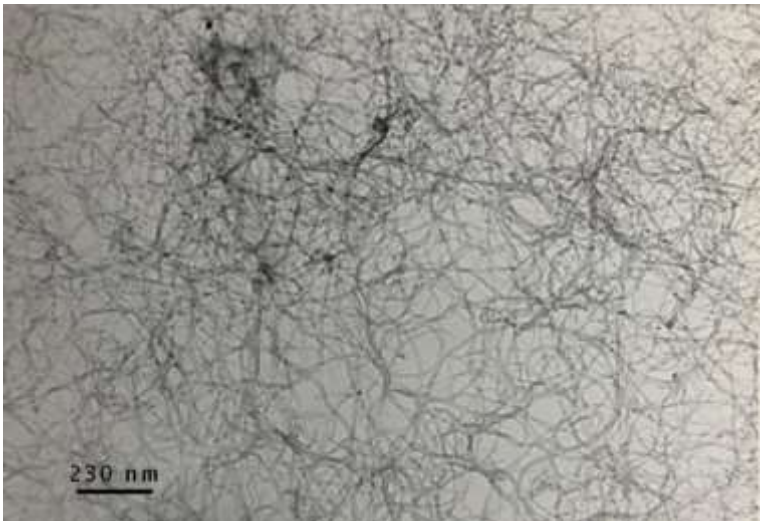

Figure-5.6 TEM micrograph of B-CNTs, showing spread and length of the nanotubes

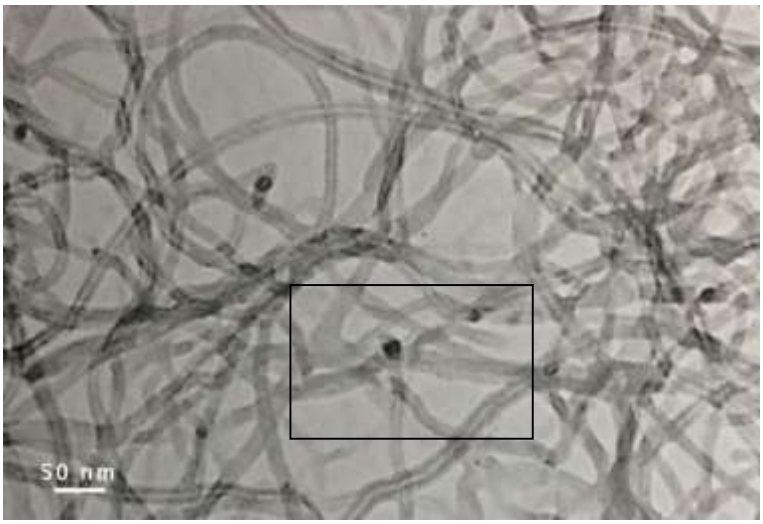

Figure-5.7 Same as Figure-5.6 but at higher magnification

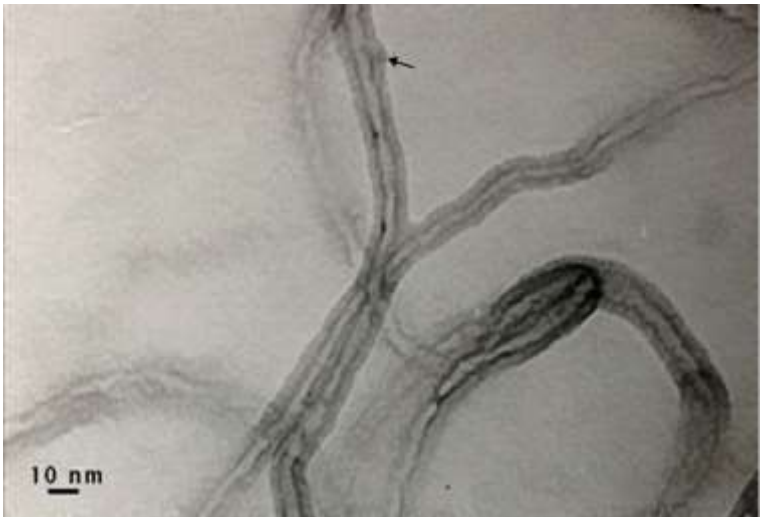

Figure-5.8 Higher magnification of the marked region in Figure-5.7, showing amorphous carbon on the walls of nanotubes

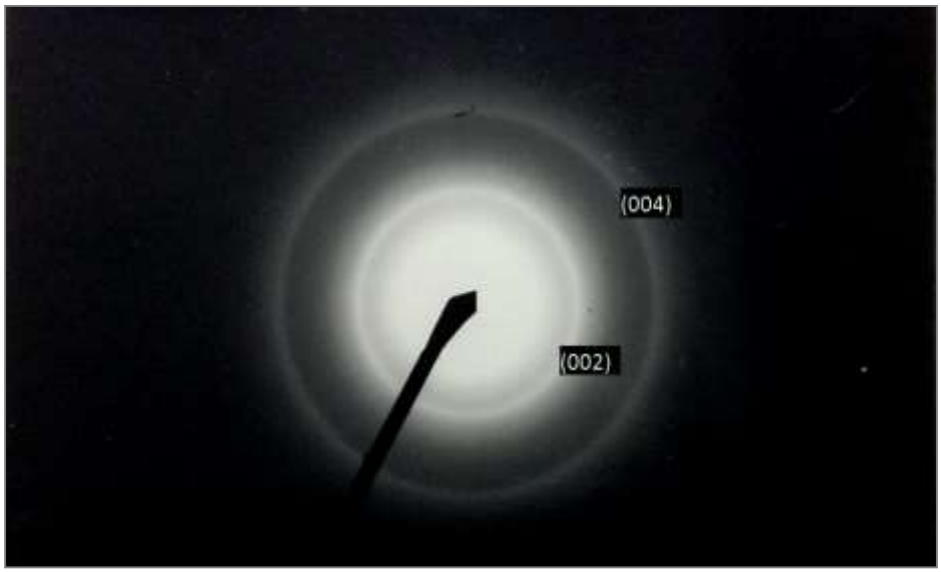

Figure-5.9 Diffraction pattern of CNTs

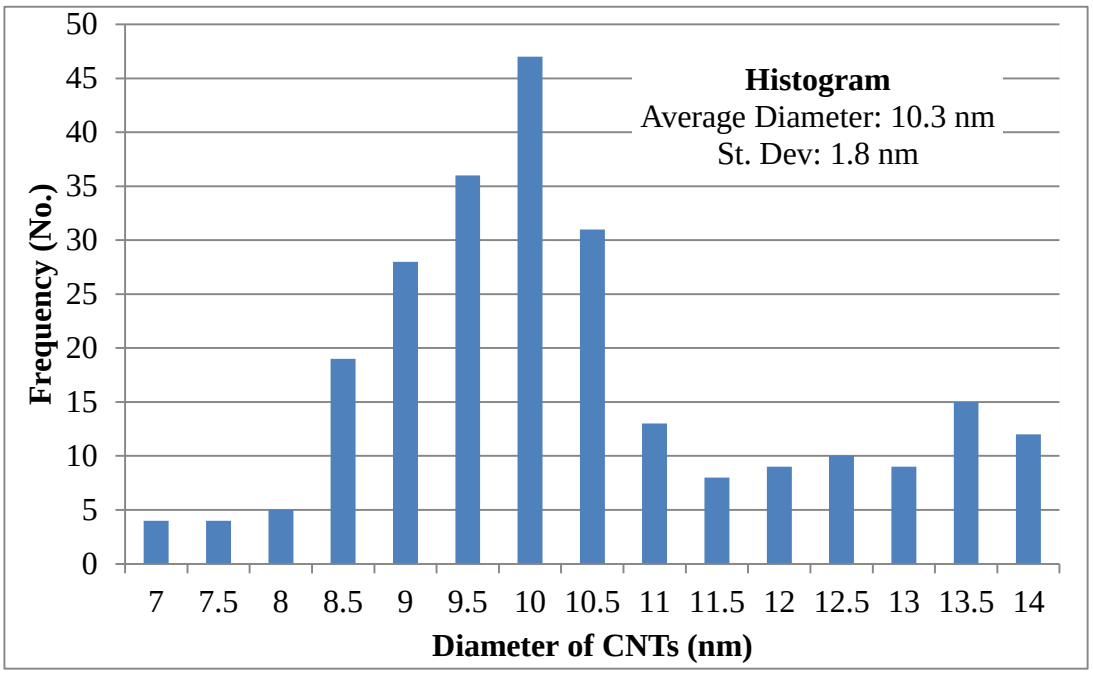

Figure-5.10 Spread of CNTs diameter as a function of frequency in B-CNTs specimen, derived from TEM observations

5.2.4 Thermogravimetric Analyses

The TGA plots along with the analyses of the various CNTs specimens are shown in Figures-5.11 to 5.16, which indicate fractional thermal stability of CNTs in terms of variation in mass during heating in air. Each plot consists of three curves, TGA, DTGA and Lorentzian fitting of DTGA, represented by solid line, dash-dot line and dash line, respectively.

5.2.4.1 Phase Analyses

The TG curves demonstrated oxidation start temperatures of various specimens at temperatures in the range of 310-360 °C representing the oxidation temperature of amorphous carbon present; the variation in the oxidation start temperatures suggests various levels of defects in the specimens[186]. Similar results have also been reported by other researchers[187,188]. After initial drop in mass, the curves overlapped during the later stages and were difficult to interpret directly. Therefore, their differential curves (DTGA) were plotted to elucidate the change in mass with increasing temperatures.

The DTGA curves showed mass changes at documented temperature ranges for different phases present in the samples: 315-355°C for amorphous carbon, 429-486°C for SWCNTs, 582-602°C for MWCNTs and 670 °C for carbon nano-particles (CNPs)[189].

The quantitative analysis of each phase corresponds to its area under the peak, and was executed by means of Lorentzian fitting of the DTGA curves. Lorentzian curve fitting resulted in up to four fractional steps marked as step-I, step-II, step-III and step-IV, representing amorphous carbon, SWCNTs, MWCNTs and CNP, respectively[189,190].

In A-CNTs (Figure-5.11), a heterogeneous multiphase deposit was observed since maximum fraction was represented by amorphous carbon and SWCNTs. However, small quantities of MWCNTs and CNPs were also present in the specimen. In B-CNTs (Figure-5.12), more than 80% of the specimen fraction was occupied by MWCNTs besides diminishing fractions of amorphous carbon and SWCNTs. In C-CNTs and D-CNTs specimens (Figure-5.13 and 5.14), increasing tendencies of amorphous carbon along with decreasing fractions of MWCNTs were observed.

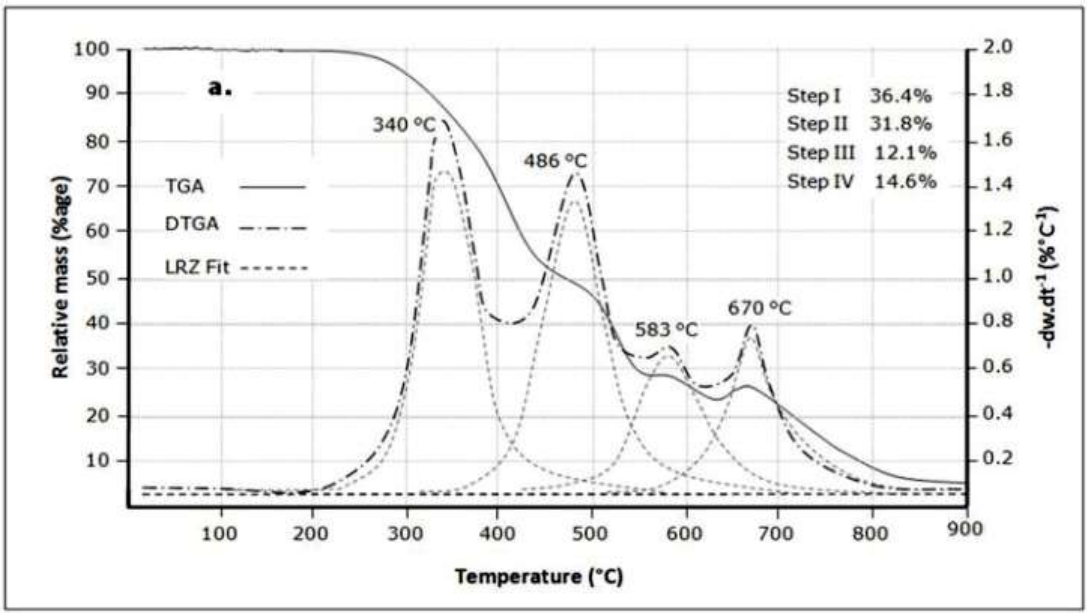

Figure-5.11 TGA curves of various A-CNTs specimens showing worked graphs of DTGA and Lorentzian fitting along with quantitative analysis results of various phases present in the specimens.

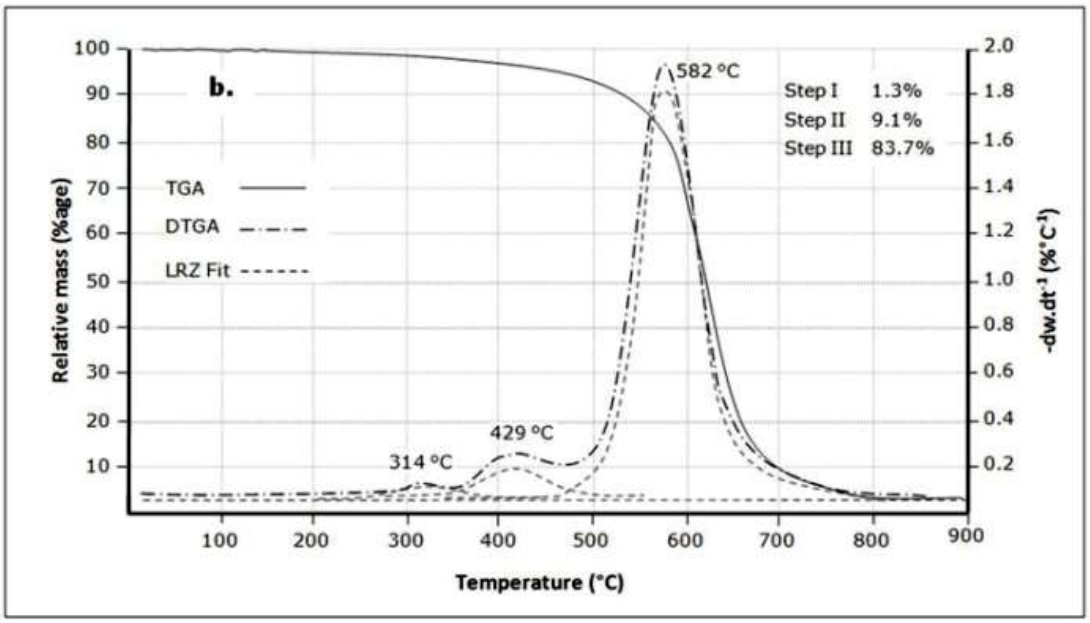

Figure-5.12 TGA curves of various B-CNTs specimens showing worked graphs of DTGA and Lorentzian fitting along with quantitative analysis results of various phases present in the specimen.

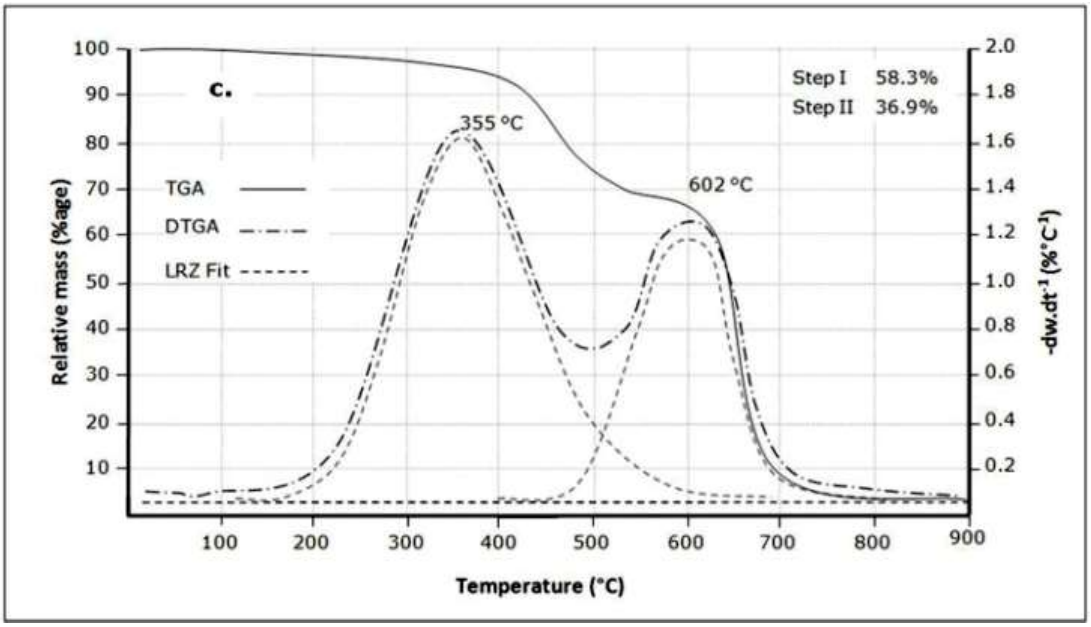

Figure-5.13 TGA curves of various C-CNTs specimens showing worked graphs of DTGA and Lorentzian fitting along with quantitative analysis results of various phases present in the specimen.

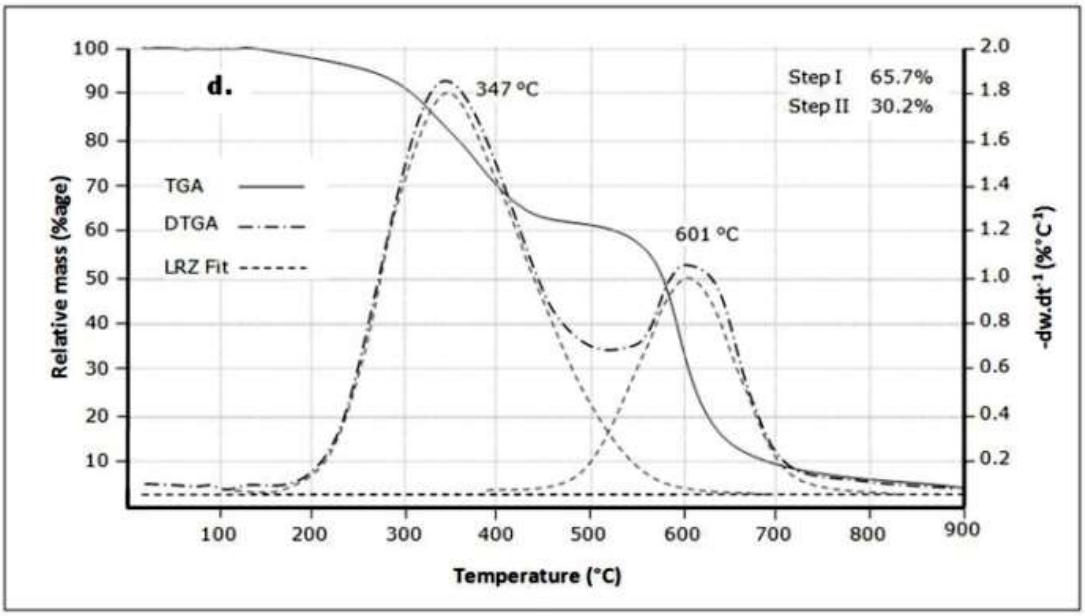

Figure-5.14 TGA curves of various D-CNTs specimens showing worked graphs of DTGA and Lorentzian fitting along with quantitative analysis results of various phases present in the specimen.

5.2.4.2 Catalytic Activity

To find activity of the catalyst, a modified approach was adopted, where the amount of MWCNTs synthesized was assumed to be directly related with activity of catalytic particles (i.e. nickel). The catalytic activity (H_{ct}) was calculated using following formula[191]:

$$Hct(\%) = 100(Mp - Mr)/Mr \qquad (5.1)$$

where:

M_r = the weight of the catalyst retained during TGA, which was actually consumed to decompose ethanol.

$M_{p=}$ the weight of the resulted CVD product (here the product is specifically MWCNTs).

To control the skewness of the calculated H_{ct} values, the catalytic activity was converted into log values. The results obtained after TGA analyses are shown in Table-5.1 and graphically represented in Figure-5.15.

Table-5.1 The results obtained by TGA analyses of various synthesized CNTs specimens.

Sample	A-CNTs	B-CNTs	C-CNTs	D-CNTs
Ethanol Flow Rate (sccm)	10	25	40	55
Amorphous Carbon (%age)	36.4	1.3	58.3	65.7
SWCNTs (%age)	31.8	9.1	-	-
MWCNTs (%age)	12.1	83.7	36.9	30.2
Carbon Nano Particles (%age)	14.6	-	-	-
Retained Catalyst (%age)	5.1	5.9	4.8	4.1
Catalyst Activity (log scale values)	2.1	3.1	2.9	2.8

Table-5.1 indicates that maximum purity of synthesized MWCNTs was achieved with an ethanol flow rate of 25-30 sccm, whereas minimum littering by other phases was also occurred. Any further increase in the flow rate resulted in increased levels of other phases. Moreover, a varying quantity of retained catalytic particles were also observed with ethanol flow rates, which suggests that with increasing flow rate a saturation in the activity of nickel particles occurs, as indicated in Table-5.1. The low activity of the nickel particles resulted in copious generation of unwanted phases especially amorphous carbon.

In Figure-5.15, calculated catalytic activity of nickel particles at different ethanol flow rates is plotted. It was observed that catalytic activity of Nickel particles increased rapidly by increasing ethanol flow rate and attained its optimum values at 25-30 sccm, afterwards it decreased rapidly and became steady around 50-55 sccm of ethanol flow rate.

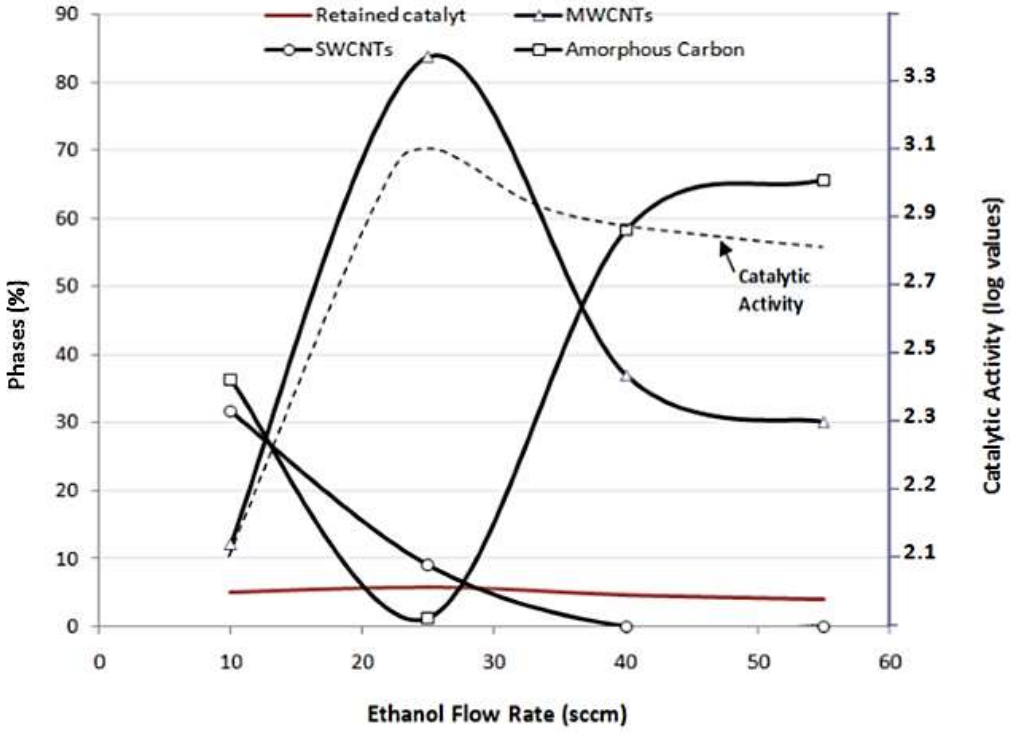

Figure-5.15 Graphs of the variation in different phases along with ethanol flow rates (solid lines), changes in catalytic activity with ethanol flow rates (dashed line).

5.2.5 Raman Spectroscopy

A superimposed montage of the curves is shown in Figure-5.16, where three critical Raman shift ranges for D, G and G' bands have been collected. The D-band represents defects in MWCNTs including sp^3 bonded carbonaceous impurities and broken sp^2 bonds. G-band emerges owing to graphitic nature of the specimen exhibiting crystallinity and the atomic structure. Whereas G'-band appears due to the long-range ordering of the structure and is developed from two-phonon second order scattering process resulting in generation of an inelastic phonon[192].

Instead of using intensity ratios of D- and G- bands to qualitatively assess purity levels of MWCNTs specimens[187], the mathematical formulae proposed by DiLeo et al[193] were used. They used a set of reference samples with known percentage of MWCNTs and selective synthesized by-products. Changes in the characteristic Raman peak ratios were measured as a function of MWCNTs contents. They also proposed following three equations to calculate ratios of D-, G-, and G'- bands in order to evaluate purity of the respective MWCNTs specimens:

$$\frac{D}{G} = 0.96 - 0.006X \quad (5.2)$$

$$\frac{G'}{G} = 0.33 + 0.0045X \quad (5.3)$$

$$\frac{G'}{D} = 0.31\exp(0.21X) \quad (5.4)$$

where:

'X' is the percentage of MWCNTs.

By taking the intensities of the characteristic peaks from individual Raman spectrum, the amount of MWCNTs present in each specimen was calculated using above mentioned equations. The results are shown in Table-5.2. It could be seen that the results obtained by Raman spectrometry are quite comparable with TGA with only exception of A-CNT specimen, which probably arises due to the presence of SWCNTs and CNPs as the above mentioned equations were derived for the specimens containing MWCNTs and synthesis products other than SWCNTs.

Table-5.2 Measured intensities of various Raman spectrums along with calculated purity (in terms of MWCNTs) by the curve fitting formulae.

Specimen ID	**D-band**	**G-band**	**G'-band**	**MWCNT present in various specimens (%age)**			
				D/G Curve fit	***G′/G curve fit***	***G′/D curve fit***	***Average Purity***
A-CNTs	42	58	30	35.7	41.6	39.7	39.0
B-CNTs	35	89	62	85.8	81.5	83.0	83.4
C-CNTs	41	56	27	34.5	33.8	35.9	34.7
D-CNTs	42	55	24	29.7	27.7	29.1	28.8

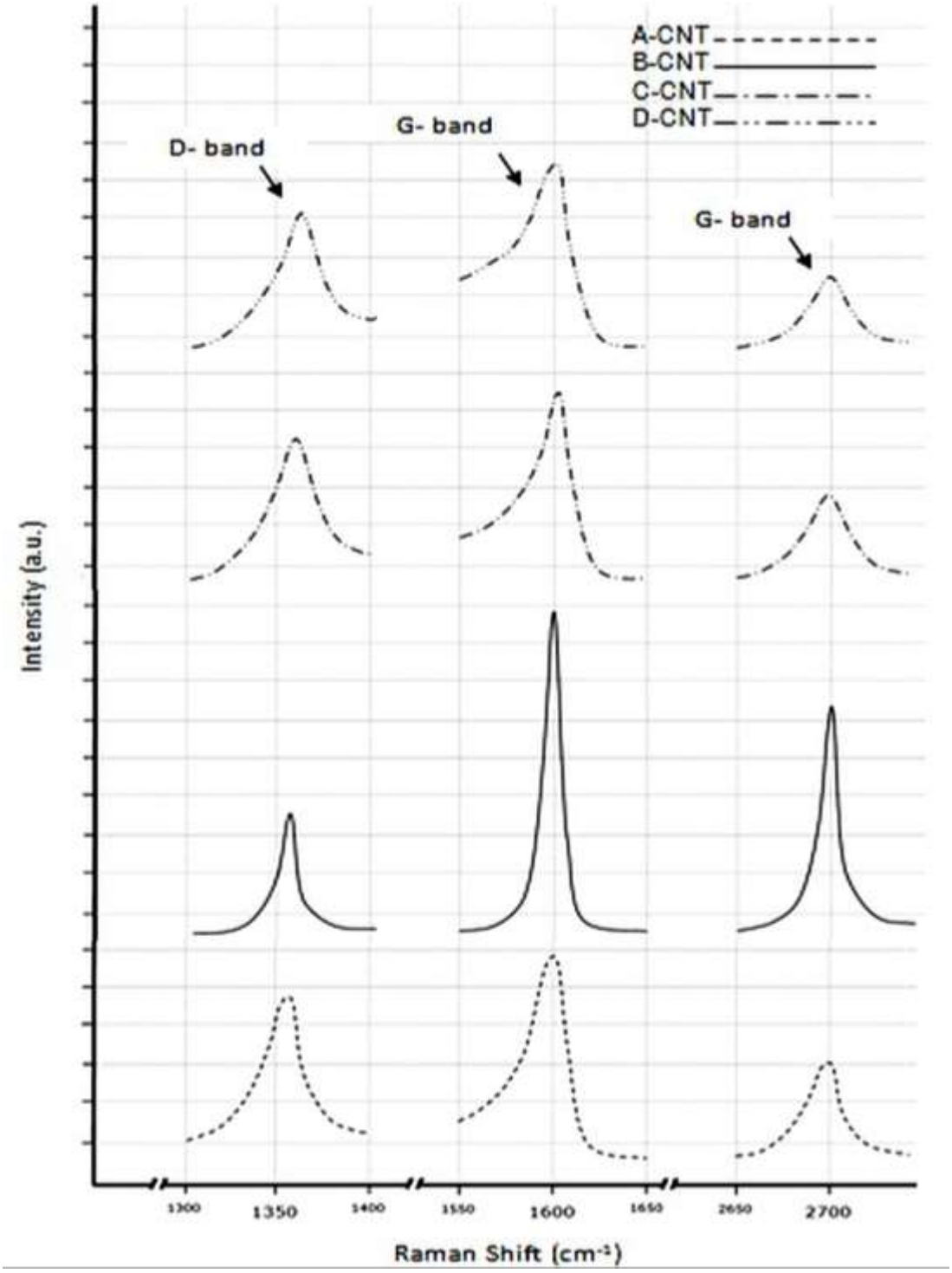

Figure-5.16 A superimposed montage of the Raman curves of the specimens encompassing selection of the critical Raman shift ranges for MWCNTs.

5.3 Dispersion of CNTs in Aluminum

5.3.1 TEM

As mentioned earlier, specimens for TEM studies were prepared from rolled strips of the pure aluminum and the composite, highly stressed microstructures were observed during TEM studies. In Fig. 5.17a, microstructure of pure aluminum is shown, which revealed abundant dislocation bands. It was also observed that a uniform thinning of the foil specimen occurred, which produced larger area of the specimen for electron transmission. In case of the composite, heterogeneous thinning occurred and fewer areas of the specimens were available for microscopic observation. The nanotubes were seen embedded in the matrix; however, no evidence of the nanotubes' clustering was noticed, (Figures-5.17b and 5.17c). Fine grains were also seen in the composite specimens. The size of the grains varied from 180 to 430 nm (Figure-5.17d).

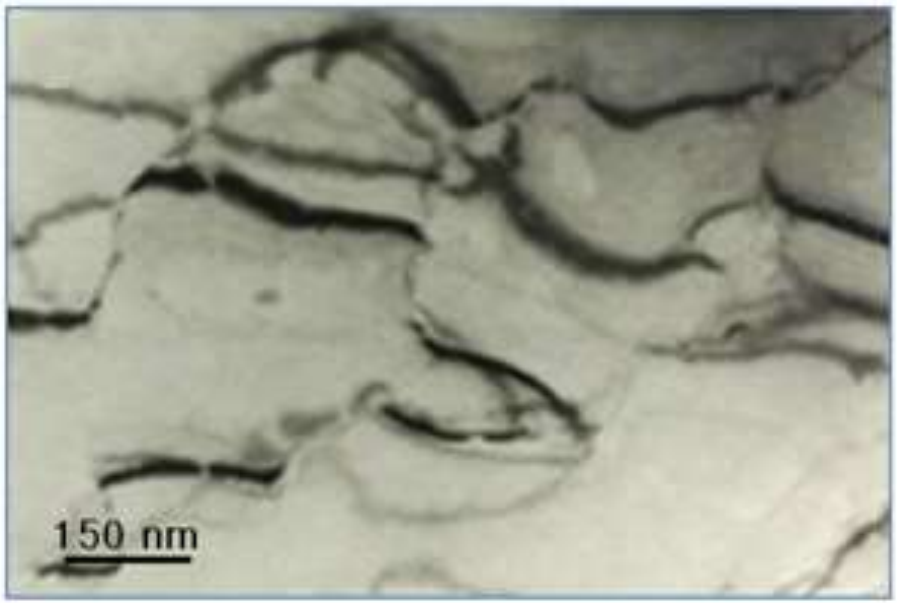

Figure-5.17a) TEM of micrograph of pure aluminum.

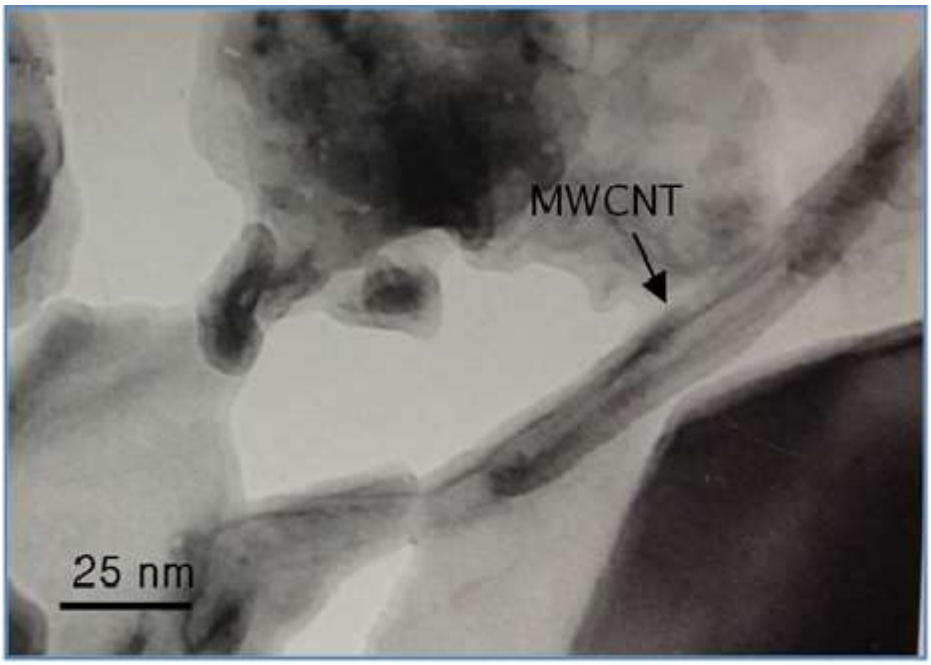

Figure-5.17 b) TEM micrograph of 0.1 vol.% MWCNTs-Al composite.

Figure-5.17 c) TEM micrograph of 0.2 vol.% MWCNTs-Al composite.

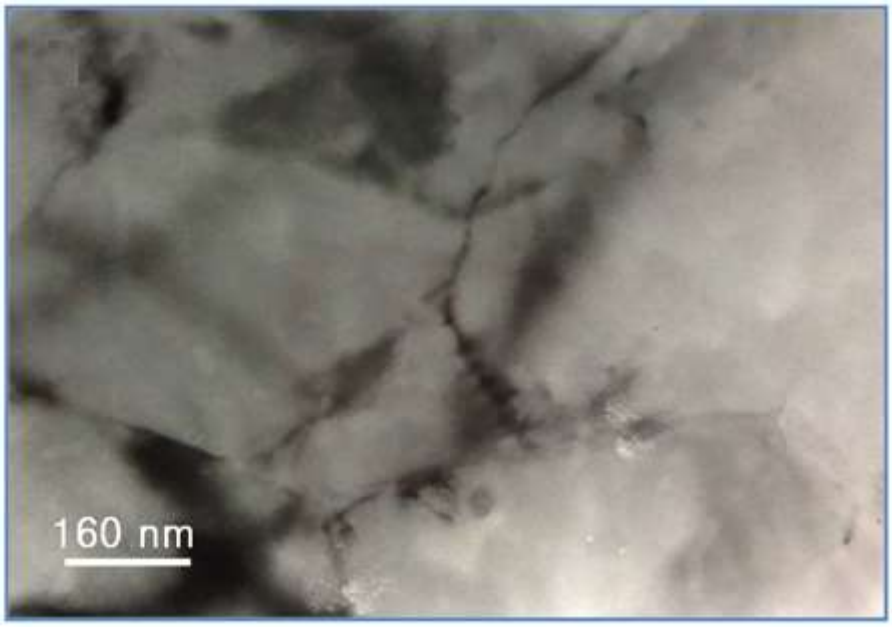

Figure-5.17 d) The micrograph of 0.2 vol. % MWCNTs-Al composite showing grain size of the composite.

5.3.2 SEM

5.3.2.1 Cast Specimens

During SEM studies, polished specimens of pure aluminum revealed fine particles of retained flux in isolated regions, comprising K, Ca, F and Cl. These particles were fewer in number and small in size (< 2 μm). The SEM micrographs of the composite specimens are shown in Figure-5.18 (a and b). The cast structure was accompanied by porosity (Figure-5.18a). However, at higher magnification, the porosity appeared to be the removal of some phase, most likely MWCNTs, due to aggressive etching (Figure-5.18b).

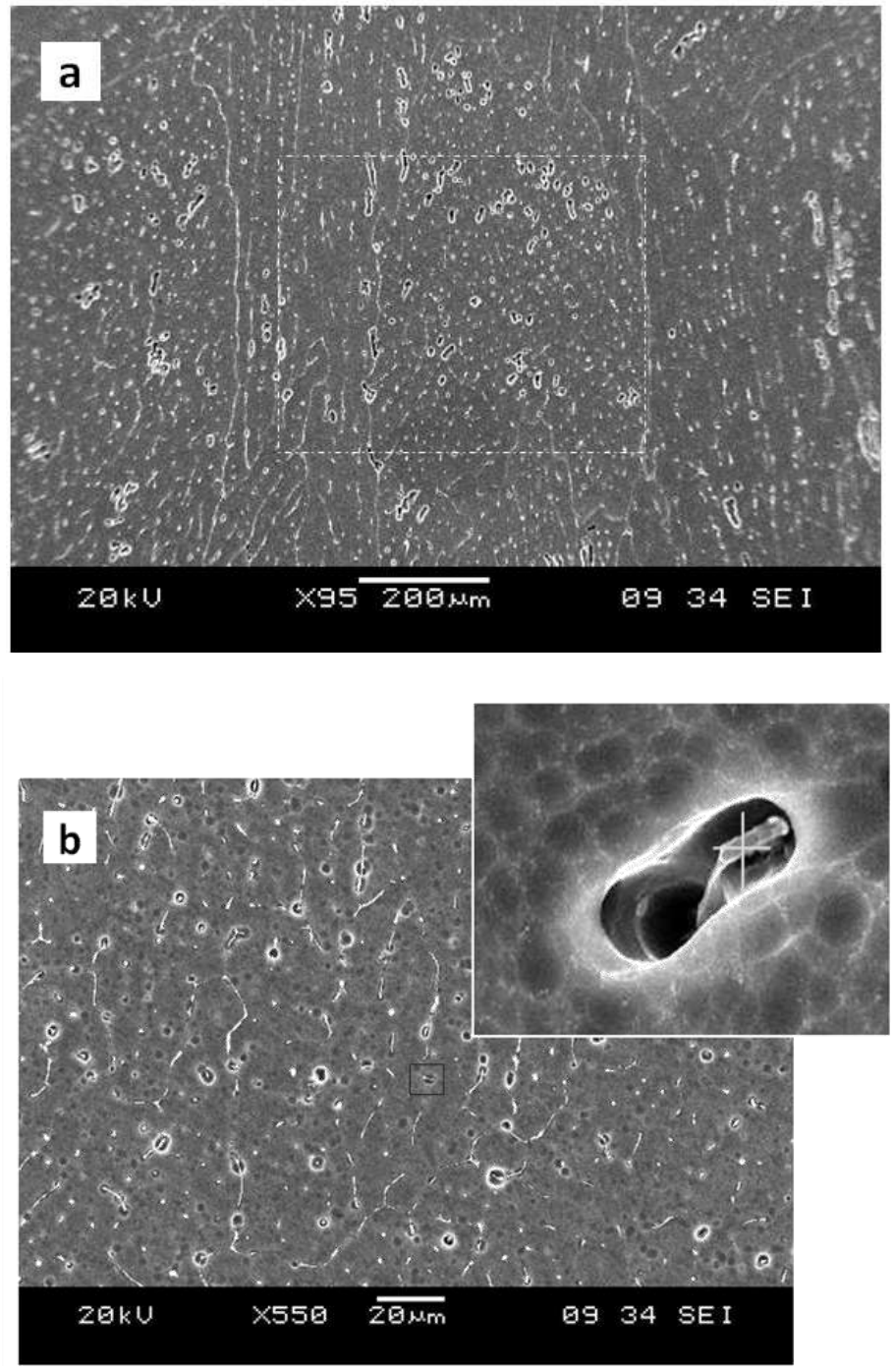

Figure-5.18 a) SEM micrographs of the cast 0.2 vol. % MWCNTs nanocomposite in etched condition and b) SEM micrograph showing the distribution of the nanotubes in aluminum matrix. Inset is at higher magnification (15 kX)

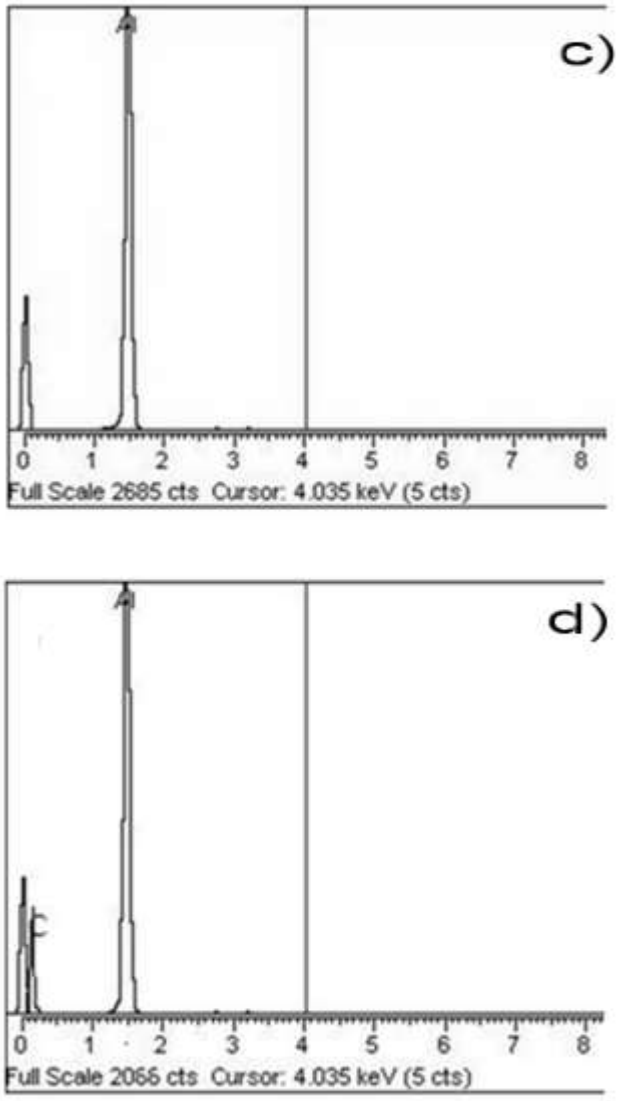

Figure-5.18 c) and d) are EDS spectrums of the marked regions in 6a) and inset of 6b), respectively.

Aluminum is a passive metal in water, forming a protective hydroxide layer on its surface; however presence of sodium hydroxide forms dissolvable aluminates of aluminum[194], according to the reaction 5.5 and 5.6:

$$2Al + 6H_2O \rightarrow 2Al(OH)_3 + 3H_2 \quad (5.5)$$

$$Al(OH)_3 + NaOH \rightarrow Na^+ + [Al(OH)_4]^- \quad (5.6)$$

Deep etching was required to reveal the dispersion of the nanotubes in the matrix; therefore strong etchant was used, which preferentially attacked the interface between aluminum and the nanotubes (inset of Figure-5.18b). It was also observed that the MWCNTs were dispersed in the matrix along the grain boundaries. No clustering or segregation of the nanotubes was observed. Figures-5.18c and 5.18d are the EDS spectra of the marked regions of Figures-5.18a and 5.18b, respectively. Area analysis at low magnification did not show presence of the nanotubes due to their low concentration, however, carbon peak appeared during point analysis at higher magnification, confirming the presence of the nanotubes along the grain boundaries.

5.3.2.2 Rolled Specimens

Etched cross sections of rolled pure aluminum and composite are shown in Figure-5.19. In pure aluminum specimen, elongated grains with large aspect ratio were seen. The general grain structure was etched in a certain crystallographic orientation, while grain boundaries were easily distinguishable due to the mismatch of the crystalline planes of adjacent grains (Figure-5.19a). At higher magnification the structure appeared to be pitting or etching of numerous crystallites within a grain (Figure-5.19b).

In composite specimens (Al-0.2 vol. % MWCNTs), no grain boundaries could be seen. However, at higher magnification isolated CNTs were seen in and around the etched pits (Figure-5.19c). Presence of CNTs in those regions was confirmed by EDS analyses (Figure-5.19e). These nanotubes were singly dispersed and aligned in the direction of rolling (Figure-5.19d). No evidence of clustering or aggregation of the nanotubes was found.

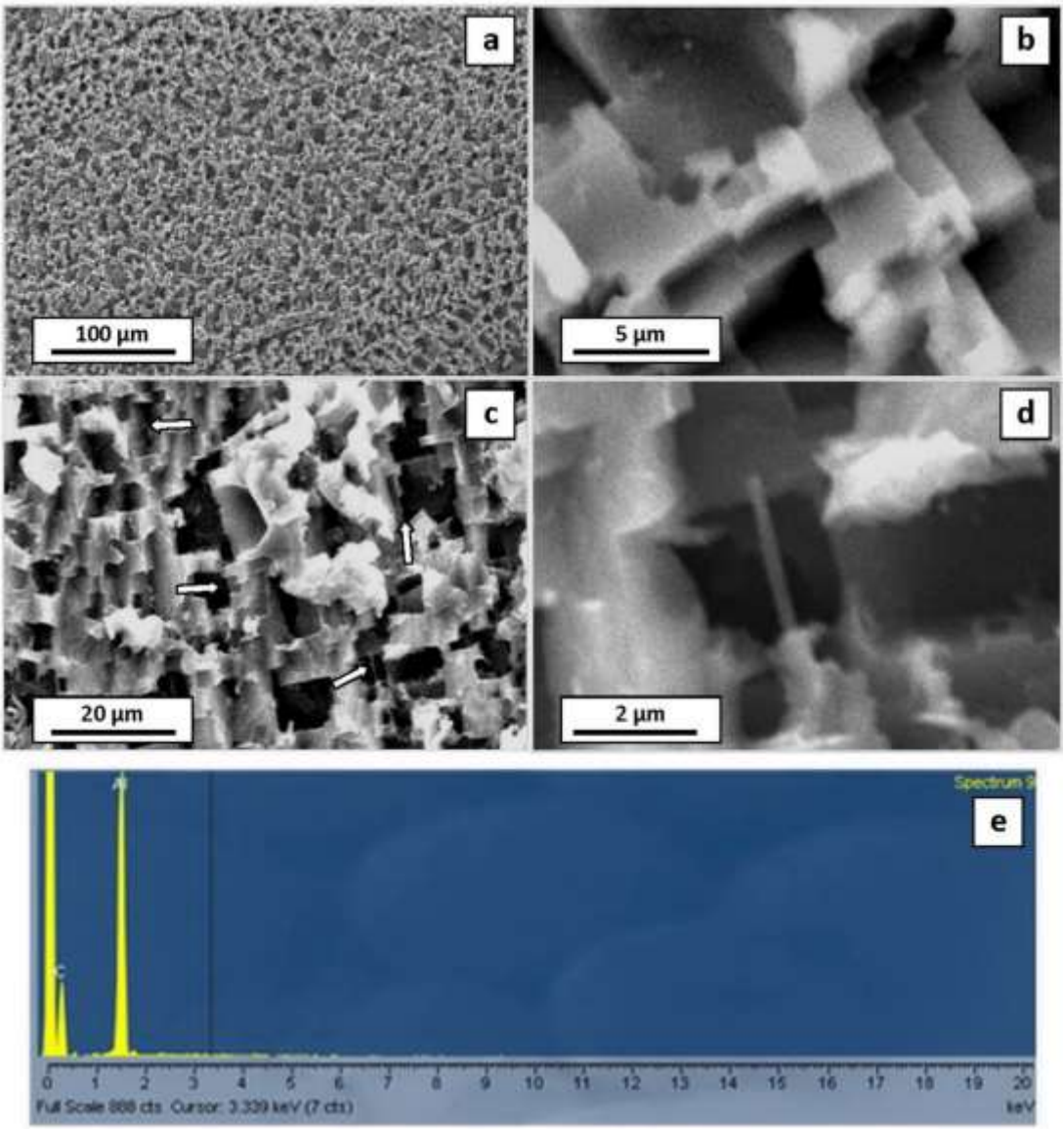

Figure-5.19 SEM micrographs of various specimens in etched condition. a) pure aluminum b) same as a) but at higher magnification, c) Al-0.2 vol. % MWCNTs composite showing dispersed nanotubes in the matrix, d) higher magnification of c) showing an isolated nanotube and e) EDS spectrum of the nanotubes confirming the presence of CNTs in the matrix.

5.3.3 X-ray Diffraction

Figure-5.20 represents XRD scans of aluminum specimens with various concentrations of MWCNTs. The diffraction angles of the peaks were used to identify the structure and the Millers indices, which were found in accordance with PCPDF No: 851327 for pure aluminum. The XRD scans showed no evidence of significant amount of impurities, like potassium, sodium, calcium etc., which had a chance for retention using the processing conditions having large amounts of flux. Although, on the basis of XRD scan, it was difficult to state about non-availability of the impurities in the melt, or their quantity was below the detection limit of XRD i.e. 2% [195].

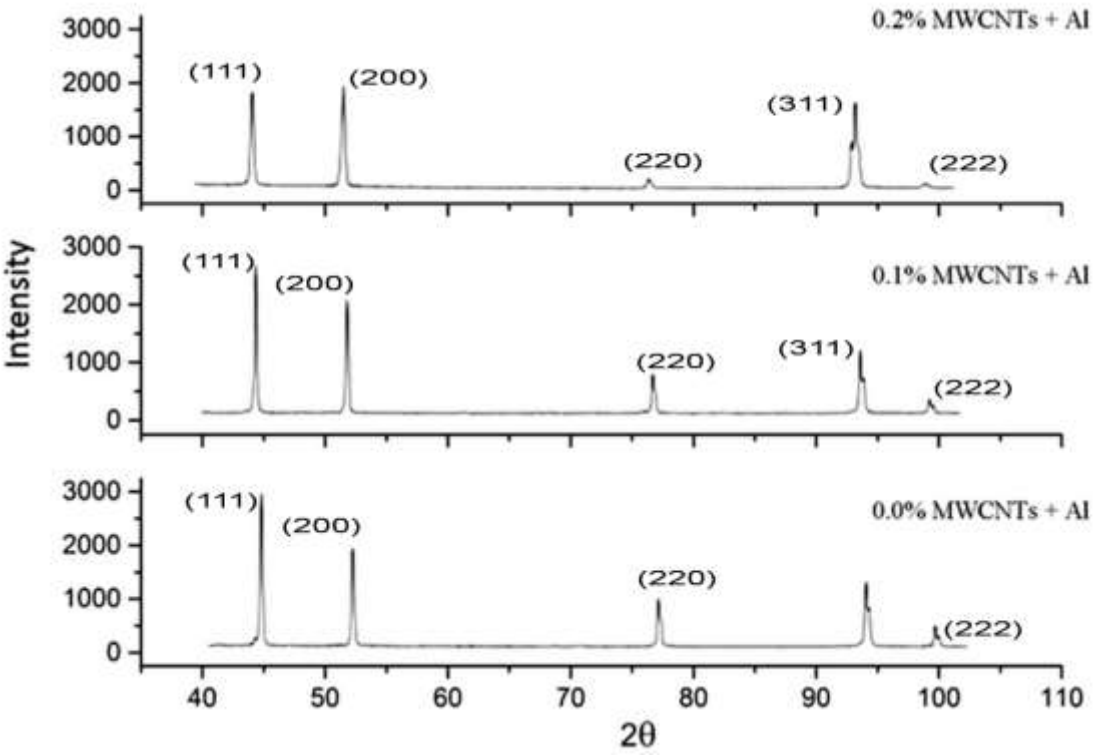

Figure-5.20 XRD scans of aluminum specimens with various concentrations of MWCNTs.

In XRD scans, it was observed that intensity of the peaks and FWHM values varied with the addition of nanotubes. This observation indicated towards some changes in crystallite size and lattice strain associated with the presences of the nanotubes. To find the variations in crystallite size and lattice strain, graphs were plotted between Sinθ and BrCosθ (Figure-5.21). The results obtained from the calculations are given in Table-5.3.

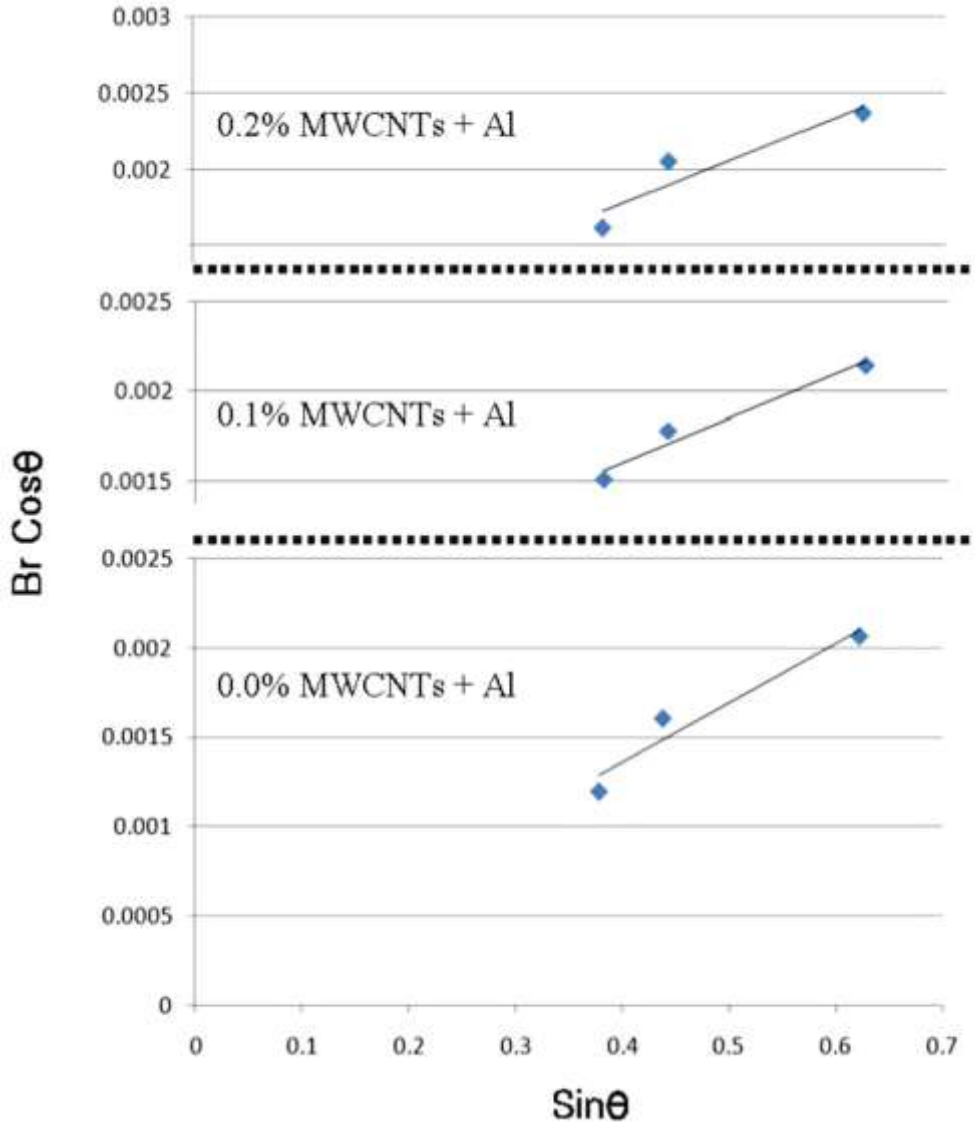

Figure-5.21 Plots of various specimens between Sinθ and BrCosθ to find crystallite size and lattice strain.

Table-5.3 Results of the analyses of XRD scans for various specimens.

Specimen ID	**Crystallite Size (nm)**	**Lattice Strain ($x10^{-3}$)**
0.0% MWCNTs-Al	-	1.62 ± 0.21
0.1% MWCNTs-Al	360 ± 22	2.11 ± 0.17
0.2% MWCNTs-Al	320 ± 24	2.33 ± 0.21

Under the same processing conditions, pure aluminum did not show crystallite size refinement detectable by XRD. However, the specimens having CNTs showed substantial refinement in their crystallite size. Typically, 360 nm and 320 nm crystallite size were observed in 0.1% and 0.2% MWCNTS-Al specimens, respectively. This systematic decrease in crystallite size could be attributed to the addition of CNTs[196]. Besides the reduction in crystallite size, increase in lattice strain was also observed with increasing contents of the nanotubes; the strain could be compressive in nature due to the cold rolling of the composite during fabrication. Change in lattice strain could be a feature of the mismatched coefficients of thermal expansion (CTE) of the two constituent materials (CTE_{Al}~23.6 K^{-1} and CTE_{MWCNTs} ~1K^{-1}). Due to increase in lattice strains, dislocation density also increased, which might had contributed in strengthening of the composite[197].

5.3.4 Mechanical Testing

Stress-strain curves of the tested specimens are shown in Figure-5.22 c. In the results of pure aluminum specimens, deviations of mechanical properties from standard pure aluminum AA1199-H18 were observed. These lower mechanical properties could be attributed to the processing conditions (e.g. usage of excessive flux etc.), which resulted in entrapment of tiny flux particles and/or impurities. However, same processing conditions were used for the preparation of Al-CNT composites. Therefore a justified comparison could be possible for the strengthening effect of the nanotubes in aluminum matrix. A net increase in yield strength, tensile strength and hardness, for the composites having various concentrations of CNTs, was ~77%, ~52% and ~45%, respectively. Corresponding decrease in ductility of the composite specimens was less than 15%. The improvement in mechanical properties seemed to be a synergistic effect of refinement in crystallite size, increased lattice strain and strengthening by the nanotubes. The results of mechanical testing are shown in Table-5.4.

In MM-CNT composites, it was believed that strengthening was influenced by the nanotubes both in elastic and plastic deformation regimes[198]. For simplicity, we consider a single CNT embedded in aluminum matrix in the axial direction of loading, as shown in Figure-5.22b. Applied tensile forces developed gradient of stress along the interface of matrix (aluminum) and reinforcement material (CNT) due to the

difference in their mechanical properties e.g., Young's modulus, yield strength and plasticity. The maximum value of the tensile stress depended upon the length of the reinforcement material (CNT). Under tensile loading conditions, the matrix transfers the load to the CNTs, however, this transfer of load distribution is complex due to the geometry of the fibers, orientation of the fibers and difference between elastic moduli of the matrix and the CNTs. In Figure-5.22 c, tensile curves of pure aluminum and Al-CNT composites are shown, where the composites' curves exhibit four deformation stages. In stage-I, both the aluminum and CNTs undergo elastic deformation, as the stress limit is below the yield strength of aluminum (i.e. <65 MPa). However, when the stress limit exceeds the yield strength of aluminum, the matrix undergoes plastic deformation while CNTs are still elastic. It happens in stage-II and starts anywhere beyond 65 MPa applied stress level. In this stage, the composite behaves in quasi-elastic way; therefore, removal of applied tensile stress will effectuate elastic retention of the CNTs and compression deformation of the matrix. During stage-III, both the matrix and CNTs deform plastically and/or delimitation/fracture of the interphase between matrix and CNT occurs. The stage represents the regions right after the yield points of the stress-strain diagrams in Figure-5.22c. Finally, stage-IV, crack initiation a growth occurs within the composite, which continues until the fracture[199].

Table-5.4 Results of mechanical testing of as rolled composites.

MWCNTs (vol. %)	Yield strength (MPa)	Tensile strength (MPa)	Elongation (%)	Hardness (HV)
0	65 ± 5	82 ± 4	4.14 ± 0.40	27 ± 4
0.1	105 ± 4	112 ± 3	3.85 ± 0.25	34 ± 4
0.2	115 ± 5	125 ± 3	3.56 ± 0.55	39 ± 5
Net change (%)	+77	+52	-14	+45

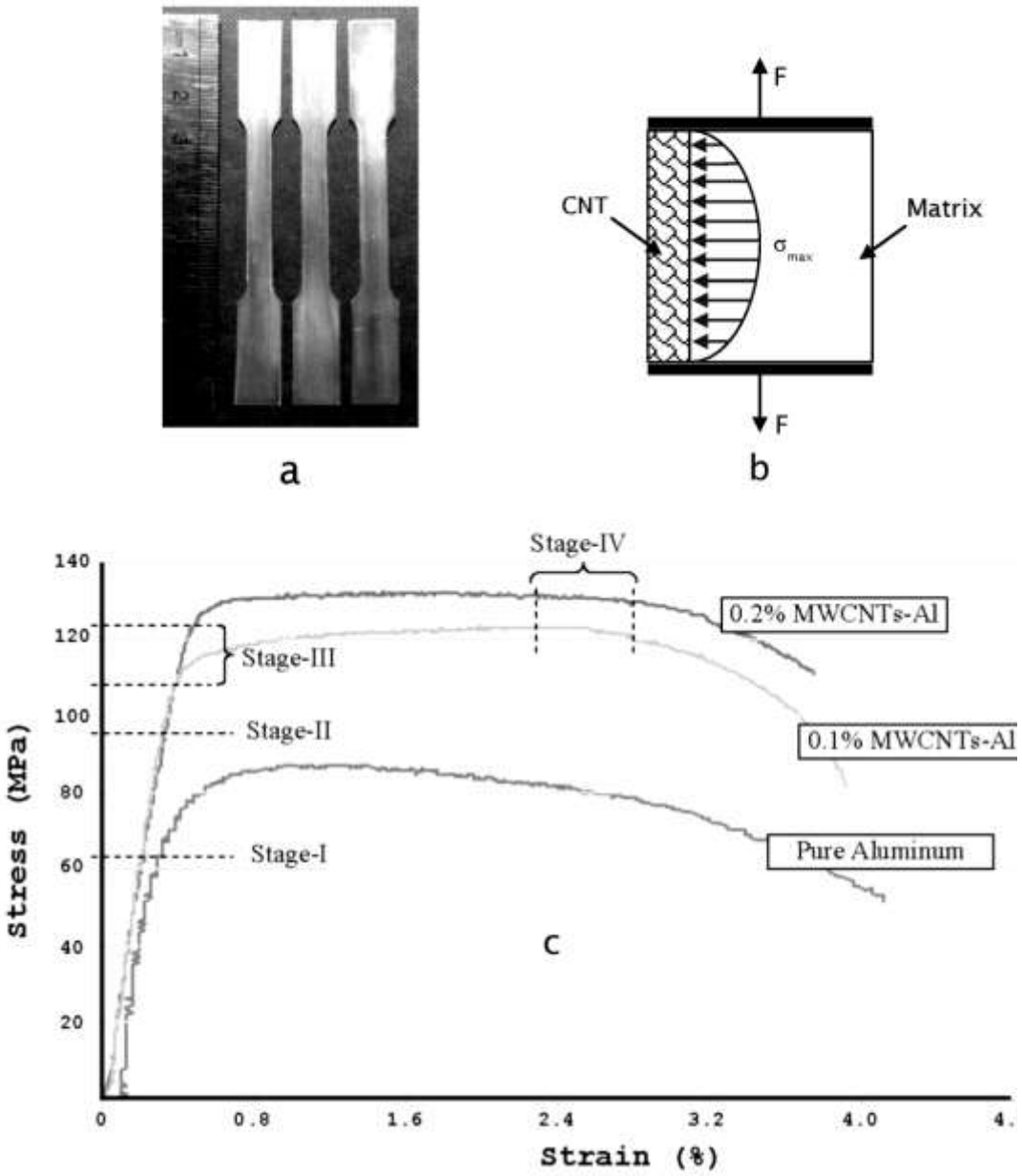

Figure-5.22a) Tensile specimens used for the testing, b) Stress distribution at the interface of CNT-Al under axial loading, and c) Experimental stress-strain curves of various specimens.

5.4 Coating of CNTs with Aluminum

5.4.1 SEM

Figure-5.23 shows a SEM micrograph of the bulk mass obtained after thermal treatment; agglomerates are evident. At relatively higher magnification (Figure-5.24), the agglomerates revealed into Al coated nanotubes (arrows), needle like chemical phases (circle) and clusters of Al and the nanotubes (rectangle). Figures-5.25 shows CNTs (around 100 nm diameter) isolated from the matrix; the increase in diameter occurred due to Al coating. The nanotubes' surfaces were fully covered with Al and demonstrated appreciable wetting. An EDS spectrum is given in Figure-5.26 which reveals elemental analysis of the coated CNTs shown in Figure-5.25.

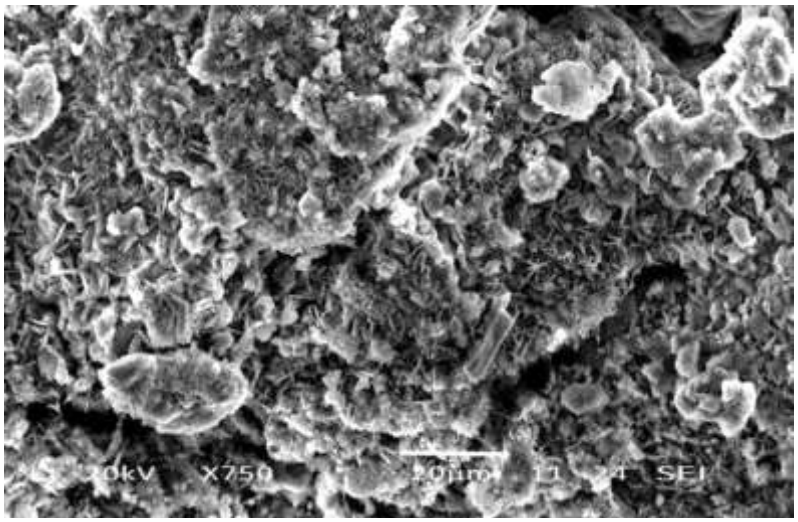

Figure-5.23 Bulk mass of the treated mixture showing agglomeration

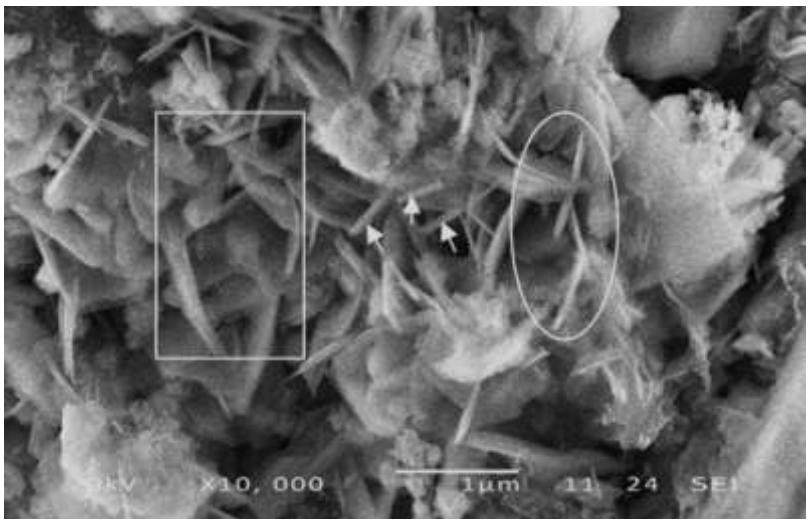

Figure-5.24 A higher magnification SEM micrograph showing Al coated nanotubes (arrows), needle like chemical phases (circle) and clusters of Al and the nanotubes (rectangle).

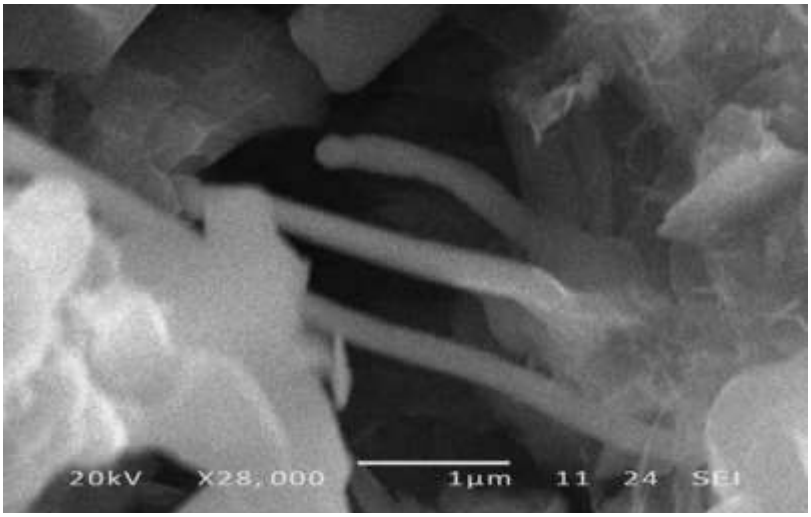

Figure-5.25 At some isolated regions, individual coated CNTs are also observable.

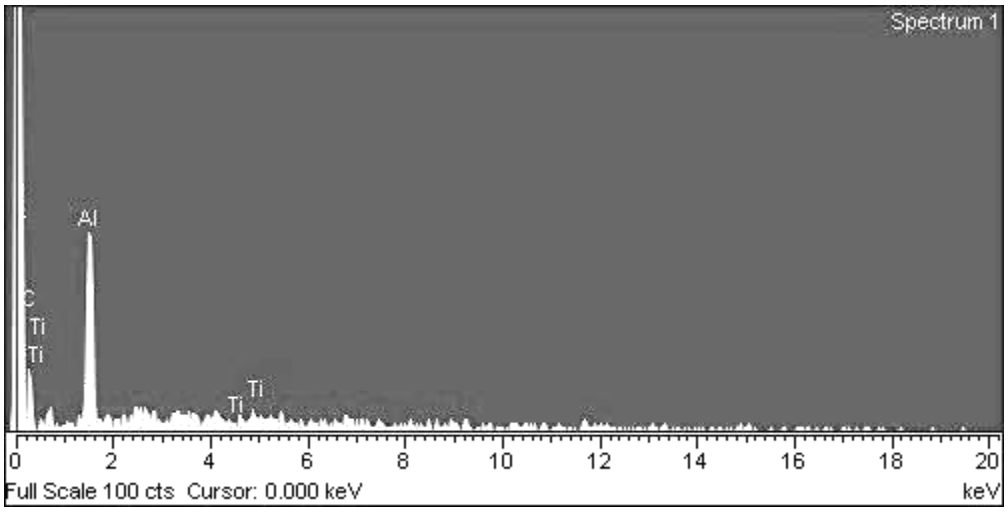

Figure-5.26 EDS spectrum of the coated CNT in Figure-5.25, the coated CNT consisted of small amount of titanium along with aluminum and carbon.

5.4.2 Differential Scanning Calorimetery (DSC)

DSC spectrum, along with a derivative curve, of the mixture is shown in Figure-5.27. There were three endothermic peaks (i.e. 275, 360 and 651 °C) and one exothermic (i.e. 646 °C) peak. The derivative curve elucidated the type of the peak besides the exact temperatures. First peak at 275 °C was endothermic and showed the removal of moisture from potassium hexafluorotitanate. Second peak at 360 °C was also endothermic and probably associated with certain reaction or decomposition of the salt. Third peak (646 °C) was exothermic and could be representative of new phase formation. Fourth peak is at 651 °C (endothermic) represented melting of aluminum. Lowering of the melting point could be an attribute of the salt.

To evaluate the reactions during aluminum coating on the nanotubes, different batches of the mixture were heated at the temperatures identified by DSC studies. To increase the chances for complete reaction, the mixtures were heated to slightly higher temperatures i.e. 280, 370 and 670 °C. Each batch was heated for one hour in argon with a heating rate of 10 °C/min.

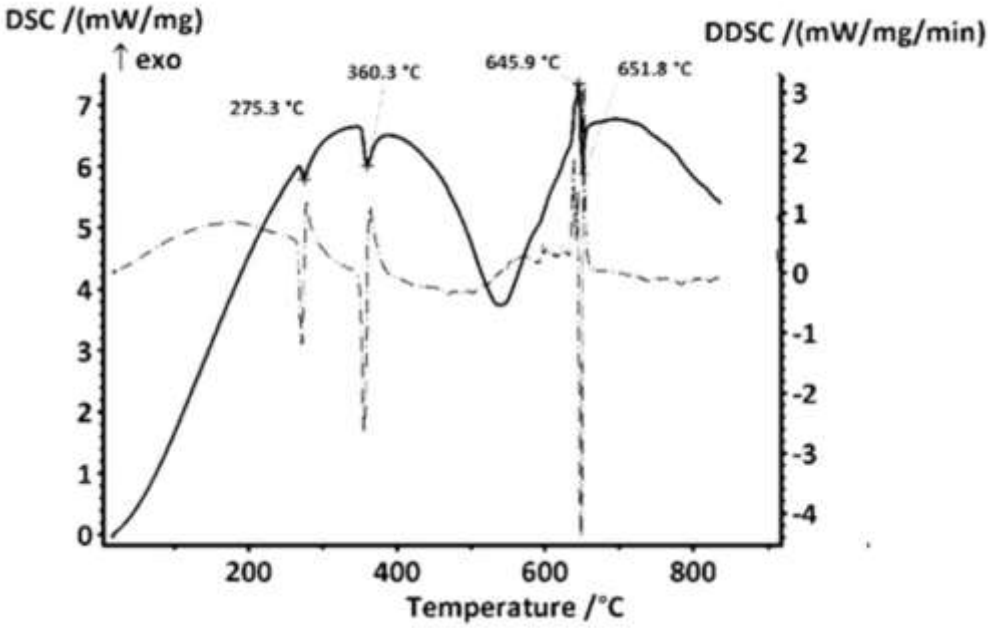

Figure-5.27 DSC spectrum of the mixture along with differential curve, showing occurrence temperatures of various thermal changes

5.4.3 XRD

Figure-5.28 shows the XRD patterns of the treated batches of the mixture at various temperatures. The two scans at the top of the Figure-5.28 represent the as blended untreated and treated at 280 °C batches. No significant change in the structure of the mixture occurred. The intensities of the peaks represented approximate volume fraction of the individual phase present in the mixture.

Third scan represents the mixture heated to 370 °C, where the temperature corresponds to the second endothermic peak in DSC scan. The blend was still in powder form after the treatment. The XRD scan elucidated presence of some new phases along with suppressed quantities of the nanotubes (i.e. carbon phase) and potassium hexafluorotitanate. The new phases formed were identified as titanium carbide (TiC) and potassium fluoroaluminate ($KAlF_4$). Formation of titanium carbide is an exothermic reaction, however no such kind of exothermic peak was found in DSC scan. It could be justified by considering the hold time at 370 °C: in case of DSC it was few minutes while the sample examined by XRD experienced one hour. Therefore, there was sufficient time to effectuate the reaction.

The last scan in Figure-5.28 represents the blend treated at 670 °C for one hour. The blend became dense under the process of liquid phase sintering. Presence of potassium fluoroaluminate in the blend caused the removal of surface oxides of aluminum powder, hence facilitated the sintering[200]. It was found that peaks representing the nanotubes (carbon phase) and the flux were completely diminished, while titanium carbide (TiC) converted into titanium di-carbide (TiC_2). Moreover, potassium fluoroaluminate was disappeared from the spectrum and Al_3Ti phase was formed along with AlF_3. Discernable peaks of aluminum were also present.

5.4.4 Sequence of coating

On basis of the preceding discussion, various stages and sequence of the coating process could be guessed. A schematic of the coating sequence is shown in Figure-5.29. During heating, at 275 °C the mixture experienced a dehydration process in which moisture contents of the salt were removed. Further increasing the temperature, till 360 °C, formation of potassium fluoroaluminate effectuated along with localized nucleation of titanium carbide (TiC) on the walls of the nanotubes. Most probably, presence of surface imperfections (like amorphous carbon, voids, defects, etc.) was the preferred sites for the nucleation of titanium carbide. At 670 °C carbon enriched carbide (TiC_2) was formed, meanwhile presence of potassium fluoroaluminate facilitated to dissolve surface oxides of aluminum particle and melting was effectuated. The molten aluminum was readily available to coat on the titanium carbide decorated nanotubes. Figure-5.26 confirms the fact that coated nanotubes have titanium along with aluminum.

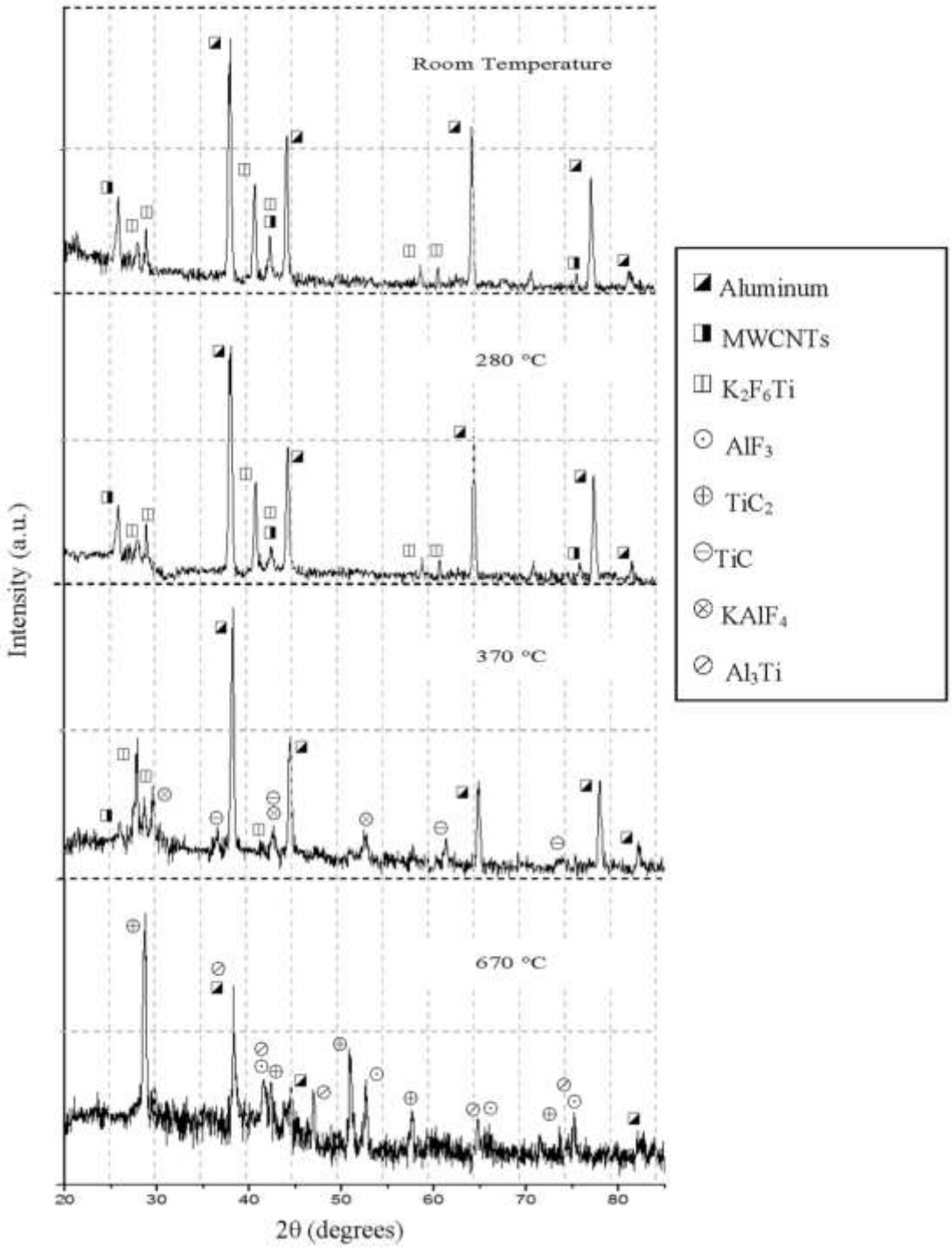

Figure-5.28 A montage of various XRD plots of the treated mixtures at various temperatures.

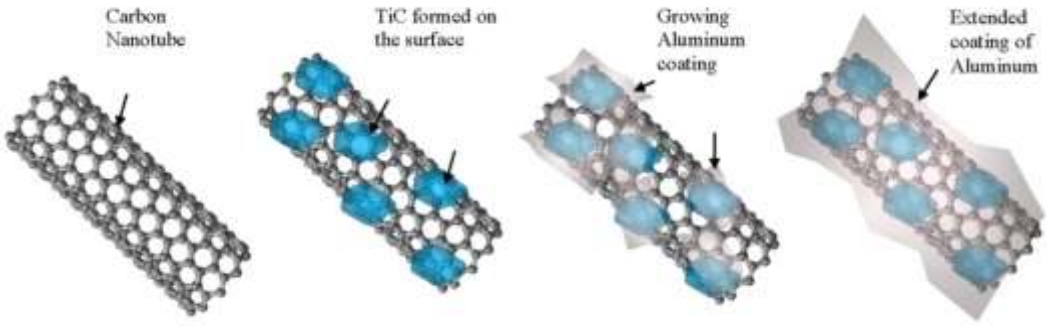

Figure-5.29 Schematic of various stages of aluminum coating on the nanotube: a) carbon nanotube surface exposed to the reactants; b) localized formation of TiC phase on the surface; c) initiation of aluminum coating on the nanotube at the regions where TiC_2 phase was present; and d) extended coating of aluminum covering whole surface of the nanotube.

5.5 Fabrication of Al-CNTs Nanocomposite

5.5.1 Stereoscopy

Figure-5.30 shows as cast image of the composite. Prior to the fabrication of the composites for testing and evaluation; casting parameters were optimized to produce sound cast structures. Figure-5.31 shows radiograph of the cast ingots at 100 and 150 °C mold temperatures, featuring least defects in the castings carried out at 150 °C mold temperature. Specimens were sectioned from the runner of the castings, which were subsequently, mounted, polished and etched for stereoscopy.

A montage of stereographic images of various pure and composite materials is shown in Figure-5.32. Large columnar grains were seen in pure aluminum sample. The casting was carried out in copper mold, yet very large grains were present, whose size was smaller near the mold walls than the ones at the center. The grains were 2 to 5 mm wide and more than 8 mm long. The presence of the large grains is characteristics of solidification of pure metals[201].

In the specimen where the flux (i.e. K_2TiF_6) was added in the aluminum melt, mixed structure consisting of columnar and equiaxed grains were seen. Addition of the flux during melting induced formation of intermetallic compound (Al_3Ti)[202], which acted as second phase particles. Therefore, the melt solidified to an intermediate structure, having a wider mushy zone, consisting both columnar and equiaxed grains[201,203].

In case of Al-CNTs composite specimens, the melt consisted of multi-phase (e.g. aluminum, Al_3Ti, TiC and MWCNTs). Presence of the multiple phases in the melt further widen the mushy zone, hence during solidification very fine equiaxed grains were nucleated at numerous sites within the melt. Excessive nucleation of the grains restricted their successive growth.

The stereographic observations of the composite specimens lead to following facts:

- The average grain size was submicron, as it could not be resolved by optical microscope even at higher magnifications (e.g. 500X to 1000X). In Figure-5.33, an optical micrograph of the etched specimen of Al-1.6 vol. % MWCNTs (T5) is shown, where the structure is too fine to be resolved.

- Uniform distribution (from outer walls to the center of the casting) of the fine equiaxed grains depicted the uniform distribution of the strengthening phase (i.e. MWCNTs etc.) in the matrix.
- No lumps or segregation of the nanotubes were seen at macroscopic level.

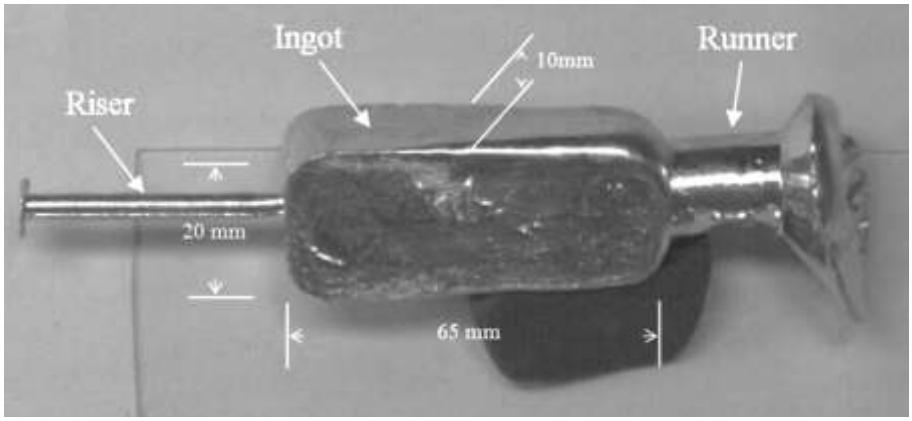

Figure-5.30 The cast ingot of Al-CNT composite.

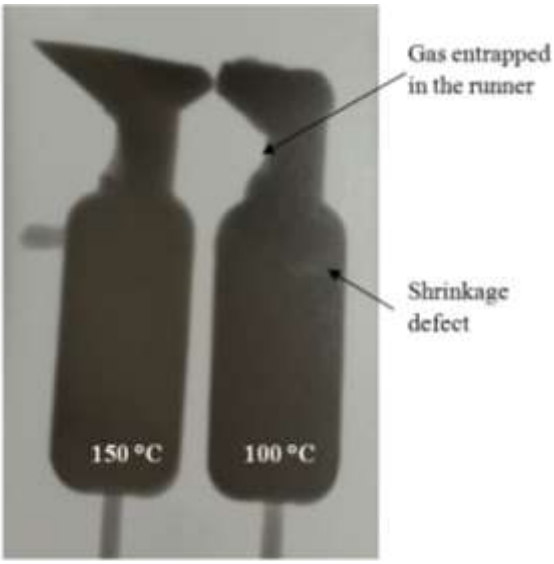

Figure-5.31 Radiographs of the two cast ingot of Al-CNT composite solidified at different mold temperatures.

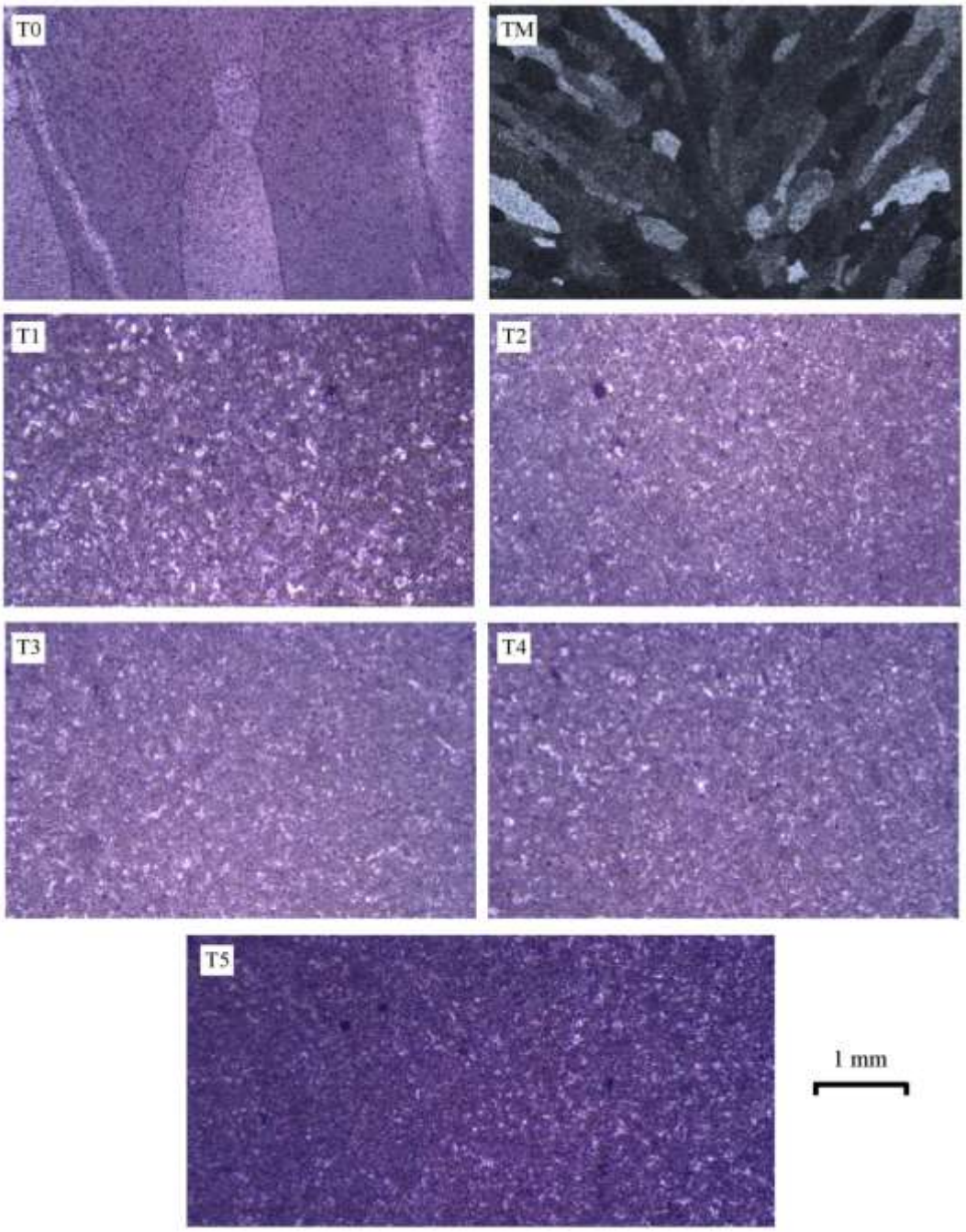

Figure-5.32 Stereographic images of the materials having various fractions (vol. %) of MWCNTs.

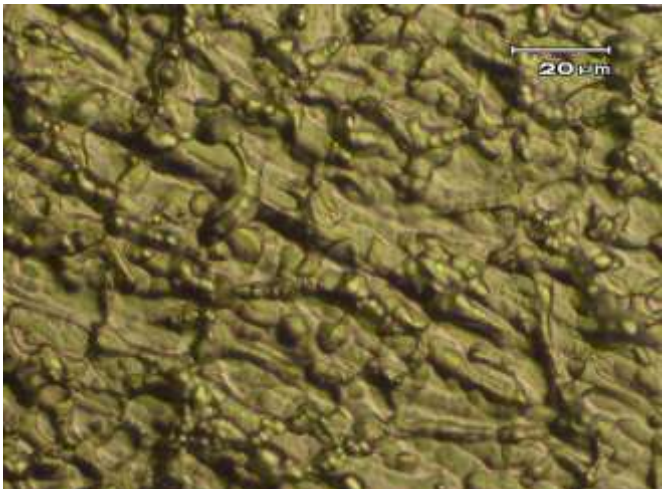

Figure-5.33 An optical micrograph of the etched T5 specimen. The NIC illumination mode was used to reveal the microstructural features.

5.5.2 Scanning Electron Microscopy

5.5.2.1 Cast Specimens

The microstructures of various specimens were studied in cast as well as in rolled conditions. Figure-5.34 shows the microstructures of as cast specimens. In 'T0' (pure aluminum) specimen, etching of the preferred crystallite was seen. It was observed that the etchant had attacked preferentially on the crystallites more rapidly. A similar type of the etchant attack was observed in 'TM' (pure aluminum treated with K_2TiF_6) specimens. However, in the composites' specimens, presence of individual CNTs was noticed at various locations. The frequency of the nanotubes increased as CNTs contents increased in the composites. Almost at all the locations singly dispersed nanotubes were found. There were some exceptions, where couple of the nanotubes was found at few locations. No segregation or clustering of CNTs was found in the cast composite specimens.

The active agent in the etchant was cupric chloride, which attacked crystallites' plains having certain orientation (Figure-5.35a). Addition of K_2TiF_6 in aluminum caused no change in the orientations, therefore no change in the etching was observed in 'T0' and 'TM' specimens. However, when CNTs were added in the melt, the orientation order was altered (section-5.4.4) and etching pattern was affected as well. Therefore, instead of rapid and preferred etching, a uniform and slower etching took place at the

regions of the specimens where crystal orientation was not favorable (Figure-5.35b). In all the cast composite specimens, dispersed nanotubes were seen along the grain boundaries.

5.5.2.2 Rolled Specimens

A montage of SEM micrographs of the rolled specimens is presented in Figures-5.36 and 5.37. A major difference, which was observed between cast and rolled specimens, was morphology and distribution of the etched structures. In contrast to the cast specimens, no defined grains were observed in rolled specimens. However, in pure aluminum (T0) and pure aluminum treated with K_2TiF_6 (TM) specimens elongated grains were seen along with some refinement of the grains. This grain refinement could be attributed to the presence of titanium, which acts as grain refiner for aluminum. In rolled composite specimens, the grain size was quite small and could not be revealed under SEM in present operating conditions. There were two major observations, made during SEM studies of the rolled composite specimens:

i. The microstructural details became finer with the addition of CNTs (Figure-5.37).
ii. The distribution of the nanotubes was uniform and the nanotubes were oriented in the direction of elongated grains (i.e. in the rolling direction). EDS line scan of the various composite specimens proved the presence of CNTs in the matrix along with small quantity of titanium (Figure-5.38 a & b).

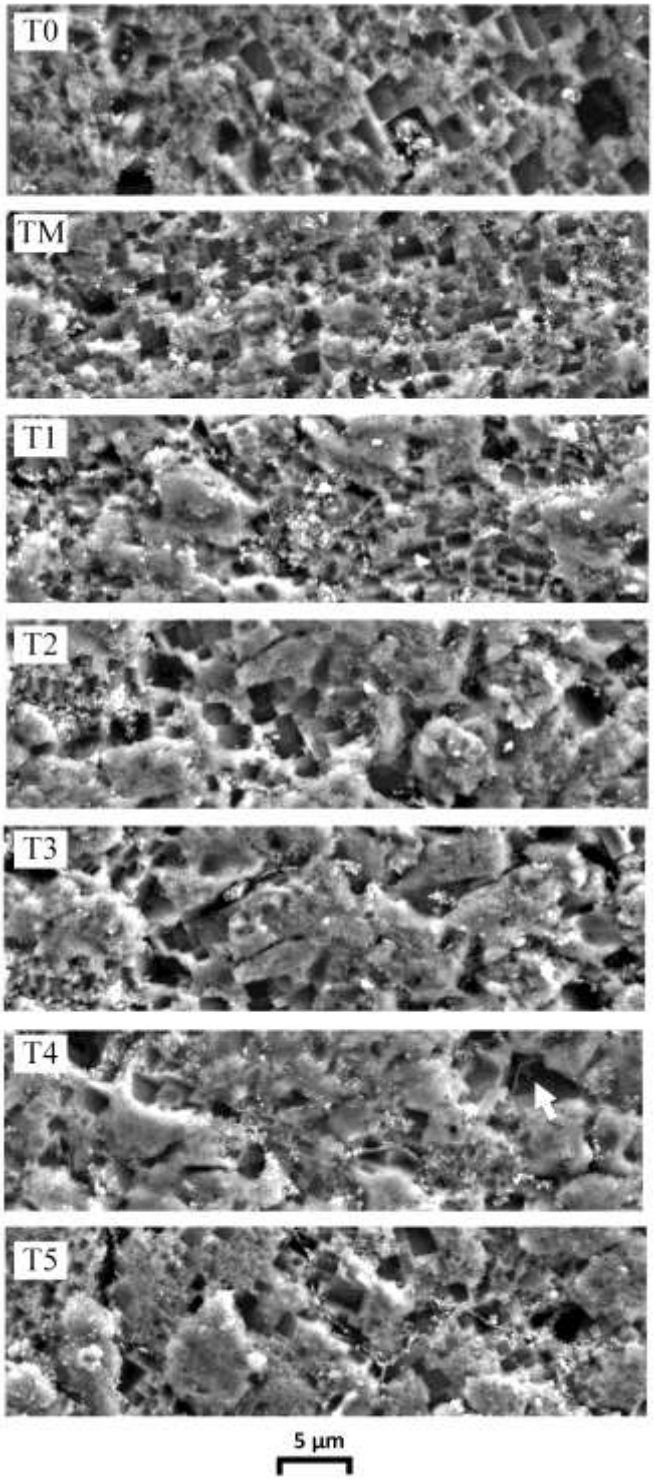

Figure-5.34 SEM micrographs of various specimens in as cast condition.

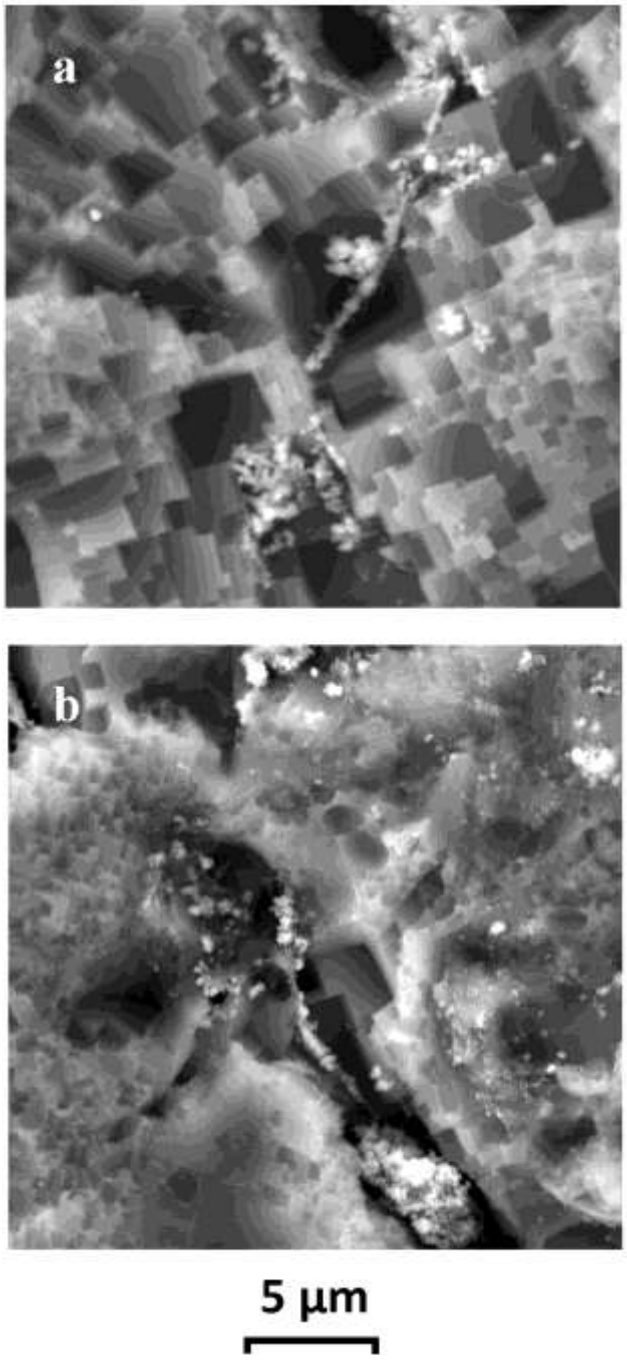

Figure-5.35 SEM micrographs of various specimens in as cast condition, showing a) preferential and b) uniform etchant attack.

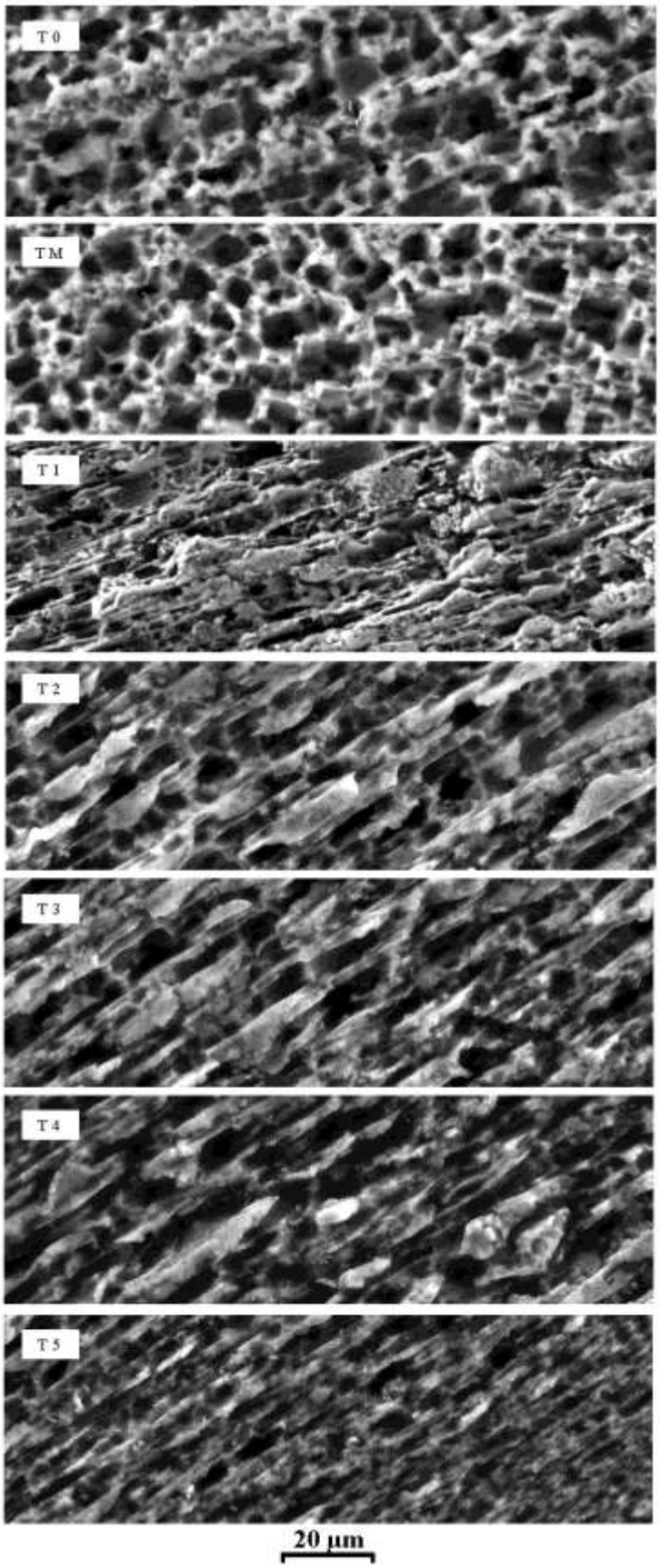

Figure-5.36 Cross sectional SEM micrographs of various specimens in as rolled condition.

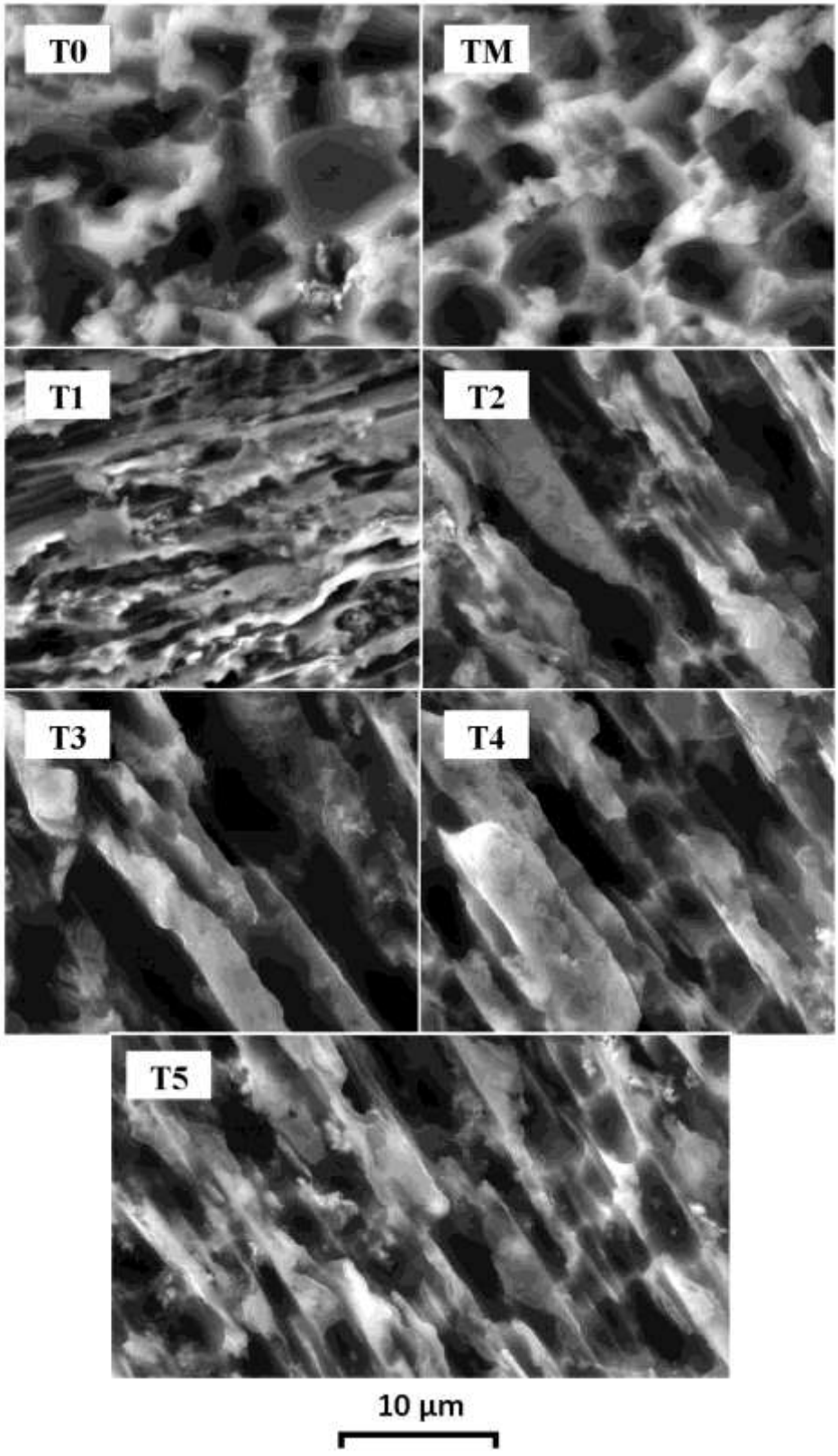

Figure-5.37.Higher magnification views of samples shown in Figure-5.36 showing refinement of microstructural details with increasing contents of the nanotubes.

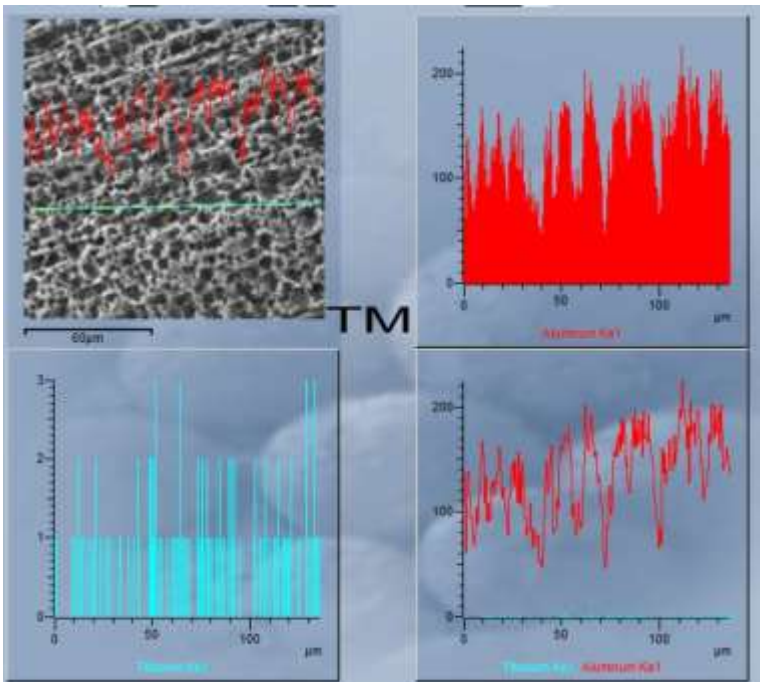

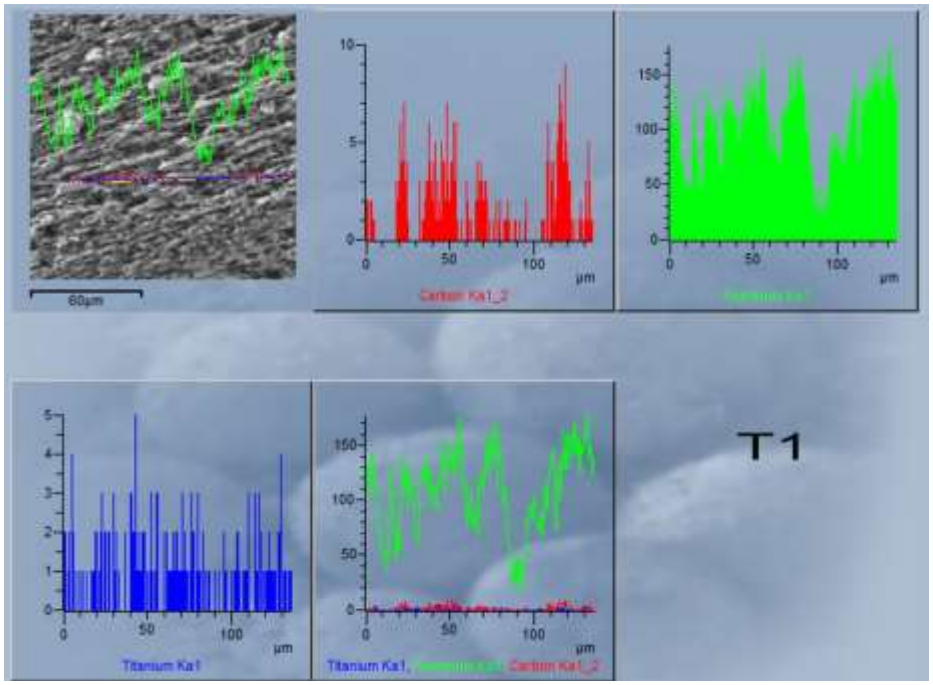

Figure-5.38 a) Microstructure and EDS line spectrum of ‘TM’ specimen, where presence of titanium is evident. In ‘T1’ composite specimen, presence of carbon confirms the presence of CNTs in the matrix, along with titanium.

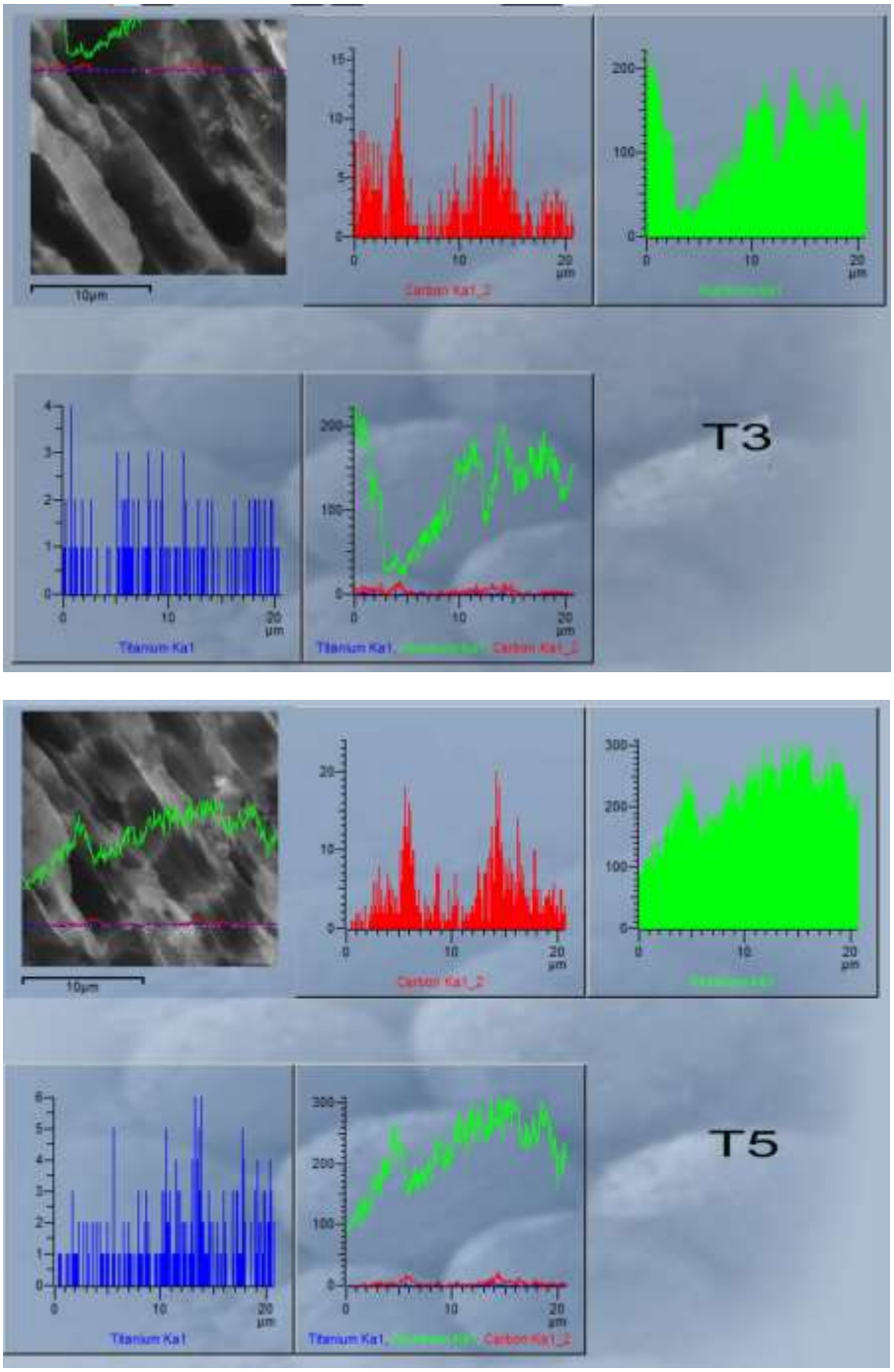

Figure-5.38 b) Microstructure and EDS line spectrum of ‘T3’ and ‘T5’ composite specimens. Carbon in the matrix represents CNTs.

5.5.3 Transmission Electron Microscopy

The thinning of the composite material was quite difficult than pure aluminum specimen due to their higher tendency of pitting, however controlled operating condition (temperature, electrical potential and pumping speed) resulted in substantial uniform thinning at macroscopic level. Even so, the uniform thinning appeared oblique during TEM studies, which contributed in variation of the contrast of the images.

Due to the low diffraction contrast of the nanotubes, it was difficult to observe them in the matrix. The nanotubes were observable only in the regions, where the diffraction contrast of the matrix was lower than the nanotubes. Generally speaking, the high diffraction contrast of the nanotubes would occur in conditions, where less matrix material existed (i.e. thin cross section of the matrix). This means that lower quantity of the matrix's diffraction could not override the contrast of the nanotubes, making them visible during TEM observations. TEM images having low matrix and high CNTs contrast, are shown in Figure-5.39.

In Figure-5.39a (bright field image exposed at 72,000 magnification), a nanotube embedded in the matrix is visible. The matrix around the nanotube was thinned and oriented creating a good contrast. Appreciable wetting of the nanotube with the matrix could be seen at the marked region (arrow) in the micrograph, where the matrix contrast was relatively high.

In Figure-5.39b (bright field image exposed at 120,000 magnification), two distinct nanotubes embedded in the matrix are visible. It is evident that aluminum matrix was fully attached with nanotube depicting substantial wetting between the two. Had the nanotubes not wetted by the matrix, a separation of the matrix from the nanotubes might have been visible.

Additional diffraction contrast was observed (inscribed by a rectangle in the Fig.5.39), which might be due to presence of further phase on the walls of the nanotubes. Formation of titanium carbide on the walls of the nanotubes instigated the wetting of the nanotubes within the matrix. Therefore, the diffraction contrast at the walls of the nanotubes might be due to the presence of titanium carbide. However, due to the size limitations of the diffraction apertures of the microscope used in the present work, it

was not possible to get diffraction patterns of the nanotubes' walls, to prove the presence of titanium carbide phase or else.

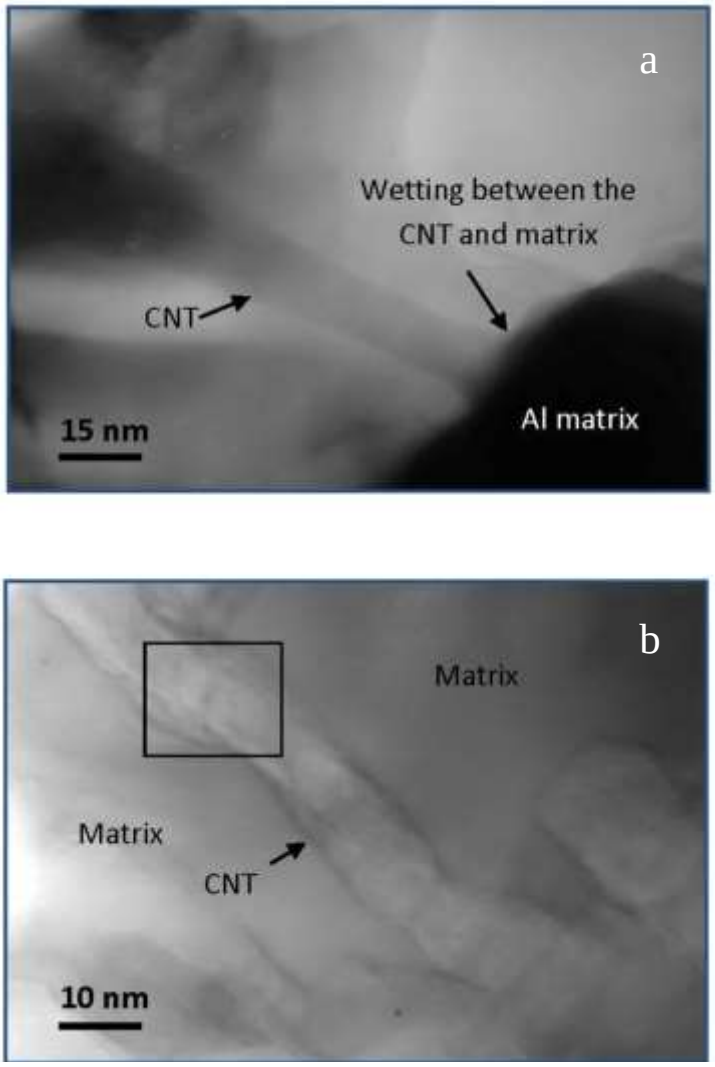

Figure-5.39 TEM micrographs of Al-CNT composite; embedded nanotubes in the matrix are visible. Arrow points the wetting of a nanotube with the matrix and rectangle shows presence of a second phase on the walls of the nanotube.

In Figure-5.40, a nanotube protruded out of the matrix can be seen. The nanotube was exposed at the tip of the protruded region, while rest of its body was embedded in the matrix. The feature revealed the fact about the wetting of the incorporated nanotubes in the composite. As described earlier, addition of potassium hexafluorotitanate made the possibility of the wetting by forming titanium carbides on the nanotubes' surface.

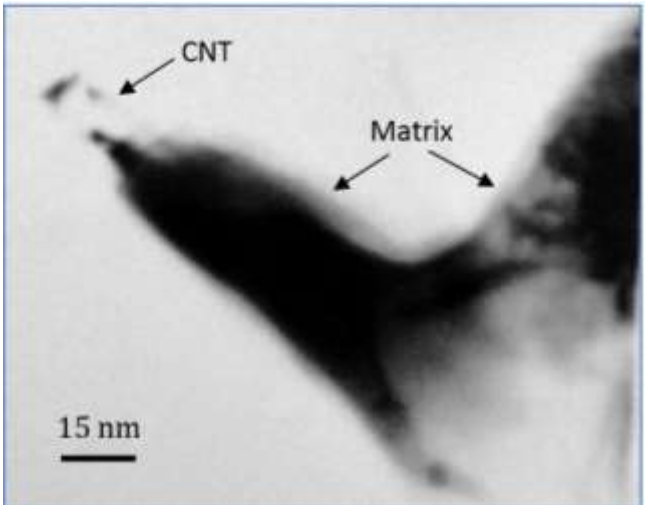

Figure-5.40 TEM micrograph of the composite; an isolated nanotube can be seen protruding out of the matrix.

The refinement of the grain size is shown in Figure-5.41. It is evident that the composite consisted of fine grains. This observation depicted the fact that addition of the nanotubes in aluminum refined the grain size of the matrix, as well.

To find the effect of the nanotubes addition on the grain refinement, three specimens of Al-CNT composite (i.e. 0.1, 0.4 and 1.6 vol. % MWCNTs) were examined using TEM. Figures-5.42 (a-c) show the variation of the grain size with volume fraction of the nanotubes. In these micrographs, presence of the nanotubes could not be seen due to higher diffraction contrast of the matrix material.

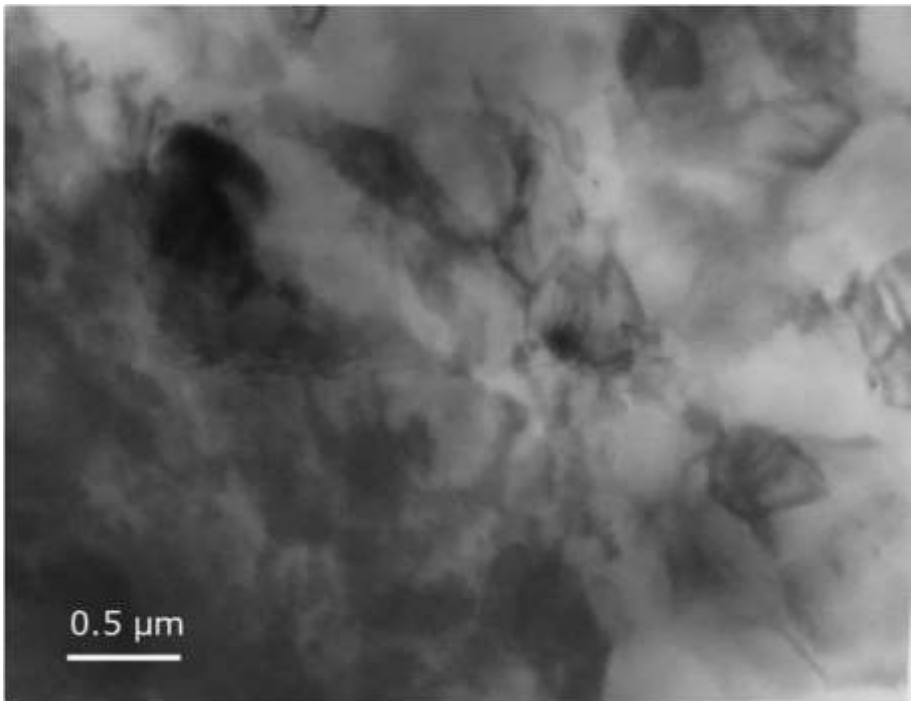

Figure-5.41 TEM micrographs of ‘T1’ composite at low magnification; refined matrix grain size could be seen.

The grain size of the composites appeared to be a function of the nanotubes concentration, i.e. the size of the grains varied from 300 nm to 150 nm with variation of the nanotubes from 0.1 to 1.6 vol. %, respectively. It was apparent according to the TEM investigations that the presence of dispersed nanotubes provided numerous nucleation sites for aluminum, confining their subsequent growth. Therefore, final structure consisted of nano-metric grains. The effect became more pronounced when the nanotubes were wettable with aluminum in the presence of titanium carbide phase on their walls. The measured grain sizes of various Al-CNT specimens are given in Table-5.5.

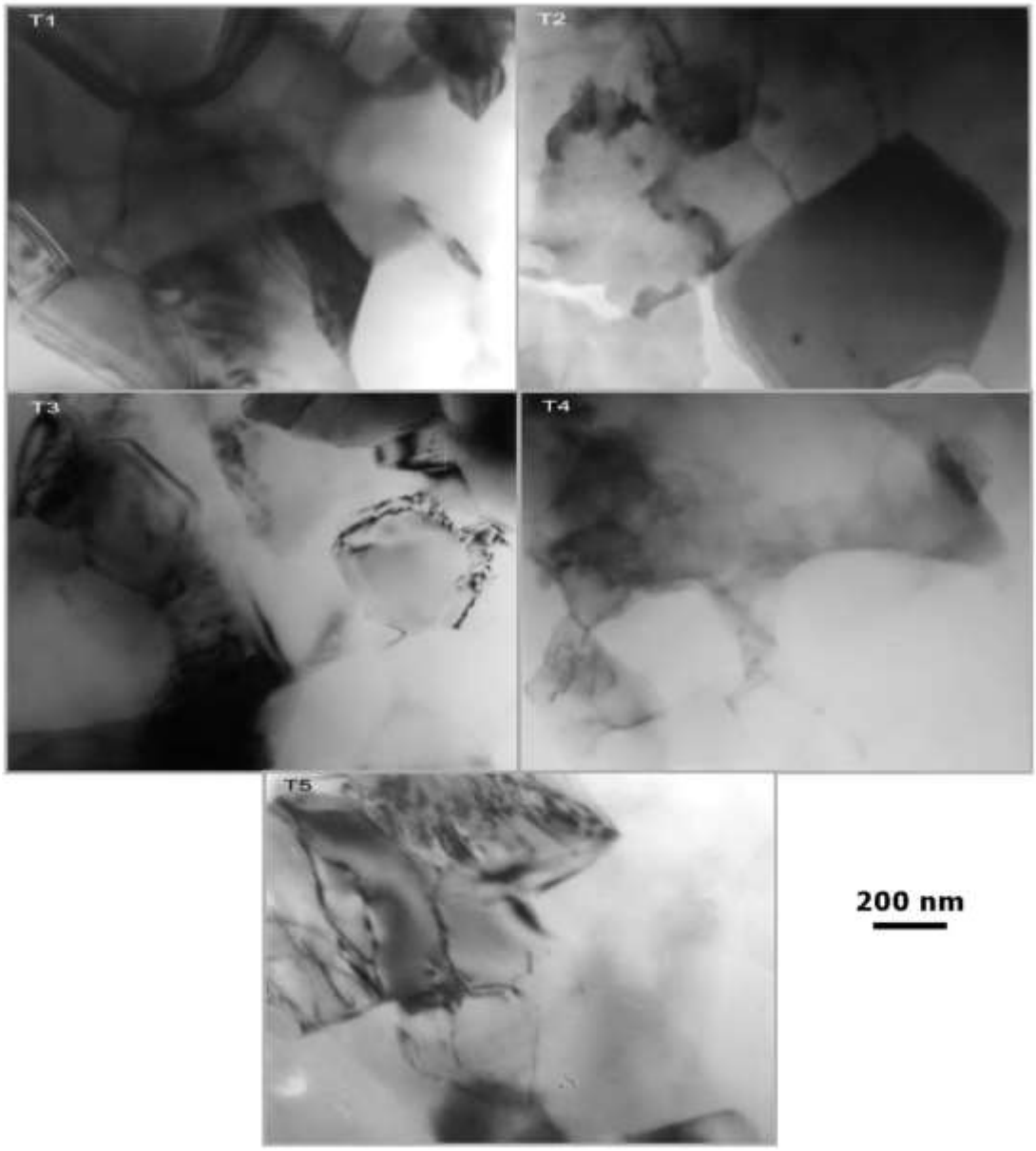

Figure-5.42 TEM micrographs of Al-CNT composite showing the variation in grain size of the matrix with the addition of MWCNTs.

5.5.4 X-ray Diffraction

The XRD scans of pure aluminum and the composites with various concentrations of the nanotubes are shown in Figure-5.43. The diffraction angles and corresponding d-spacing values were in accordance with PCPDF No: 851327 for pure aluminum. Although, during fabrication of the composites heavy quantity of potassium

hexafluorotitanate (10%) was used but no evidence of titanium or its compounds besides compounds of potassium and/or fluoride were detected by XRD. Albeit, on the basis of XRD scan, it was difficult to state about their absence in the melt, alternatively their quantity was below the detection limit of XRD i.e. 2% [195].

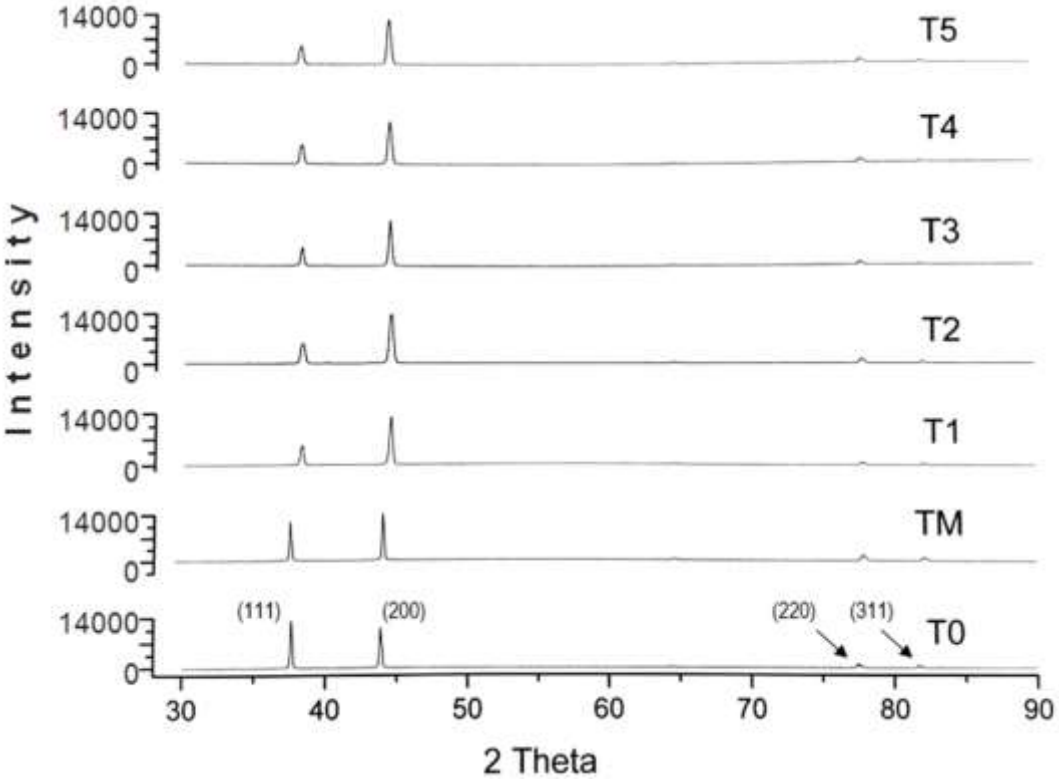

Figure-5.43 XRD scans of aluminum specimens with various concentrations of MWCNTs.

In comparison with pure aluminum, the XRD scans of Al-CNTs composites were affected in three aspects:

- Variation in peak intensities
- Increase in FWHM of the peaks
- Shift in 2Θ values

These observations indicated variations in crystallite size and lattice strain associated with the presence of the nanotubes. The variation in crystallite size and lattice strain in the composites were determined using integral peak broadening method[182]. The

graphs for various specimens were plotted between Sinθ and BrCosθ (Figure-5.44) and crystallite size and lattice strain were measured by intersect and slope of the plots, respectively. Table-5.5 contains the results of crystal size and strain determination. Further, to study the effect of CNTs addition in aluminum on crystallite size and lattice strain, a superimposed graph was plotted (Figure-5.45). It was found that in Al-CNTs composites both the crystallite size and lattice strain were influenced by the addition of CNTs. The changes were rapid and more pronounced for low concentrations of the nanotubes; however these changes became steady at higher concentration of the nanotubes. The observations lead to the fact that addition of CNTs in aluminum matrix have certain limit of their concentration to effect crystallite size and/or lattice strain. In present case, the limiting concentrations of the nanotubes are 0.8 and 0.4 vol. % for crystallite size and lattice strain, respectively.

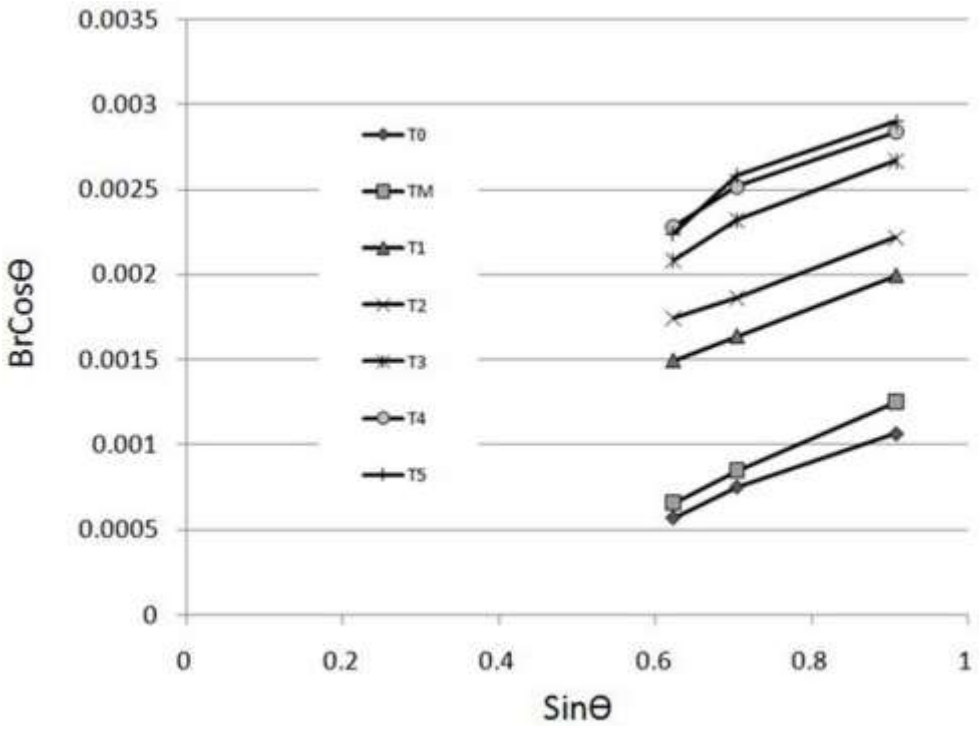

5.44 Plots of various specimens between Sinθ and BrCosθ to find crystallite size and lattice strain.

Table-5.5 Analyses of crystallite size and lattice strain of various specimens in as rolled condition.

Specimen ID	Crystallite Size (nm)		Lattice Strain ($x10^{-3}$)
	TEM	XRD	
T0	22000±800†	-	1.07 ± 0.21
TM	-	-	1.24 ± 0.14
T1	288 ± 95	328 ± 12	2.30 ± 0.12
T2	252 ± 105	295 ± 11	2.61 ± 0.19
T3	240 ± 55	232 ± 16	3.17 ± 0.13
T4	185 ± 56	186 ± 14	3.42 ± 0.11
T5	147 ± 31	172 ± 17	3.46 ± 0.16

†grain size measured by SEM in section 5.3.2,

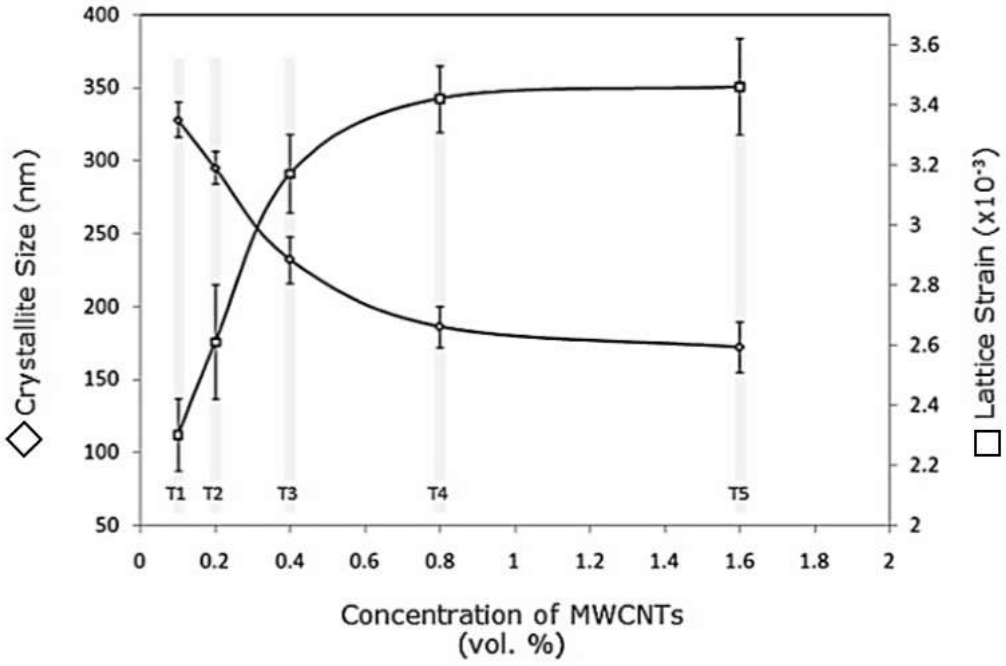

Figure- 5.45 Plots of crystallite size and lattice strain with respect to concentration of MWCNTs in aluminum matrix.

5.5.5 Mechanical Testing

A superimposed montage of the engineering tensile curves of the various specimens in as rolled condition (i.e. pure aluminum, aluminum treated with the flux, and Al-CNTs composites with different fractions of the nanotubes) is shown in Figure-5.46.

The tested specimens of pure aluminum (T0) melted in the induction furnace and solidified in copper mold under standard condition H18 for grade-1199,were strained to more than 90 % by cold rolling. The strength and ductility of the tested pure aluminum specimens were comparable with standard designations[204].

Tensile testing of specimen 'TM', revealed the effect of flux on mechanical properties of pure aluminum. It was observed that the yield and tensile strengths were found to be increased, however ductility was decreased. The variation in the mechanical properties of 'TM' could be attributed to finely dispersed Al_3Ti phase within the matrix, as reported by Birol[202]; formation of fine dispersion of Al_3Ti phase was actuated in aluminum matrix using K_2TiF_6 in molten aluminum. According to Abbasi et al[205], presence of Al_3Ti phase in aluminum matrix increased mechanical strengths of the aluminum, while size of the phase influenced the ductility of the material diversely, therefore in TM specimens a decrease in ductility was observed.

The composites' specimens with varying concentrations of CNTs (0.1 to 1.6 volume percent CNTs) were mechanically tested. The results demonstrated a simultaneous increase in yield and tensile strengths of the composite with increasing nanotubes concentration. There was three fold overall augmentation in yield and tensile strengths, whereas, the ductility was only decreased by less than a quarter compared with pure aluminum. Similarly, there was corresponding rise in the hardness values from 27HV to 55HV. The results of mechanical testing are given in Table-5.6.

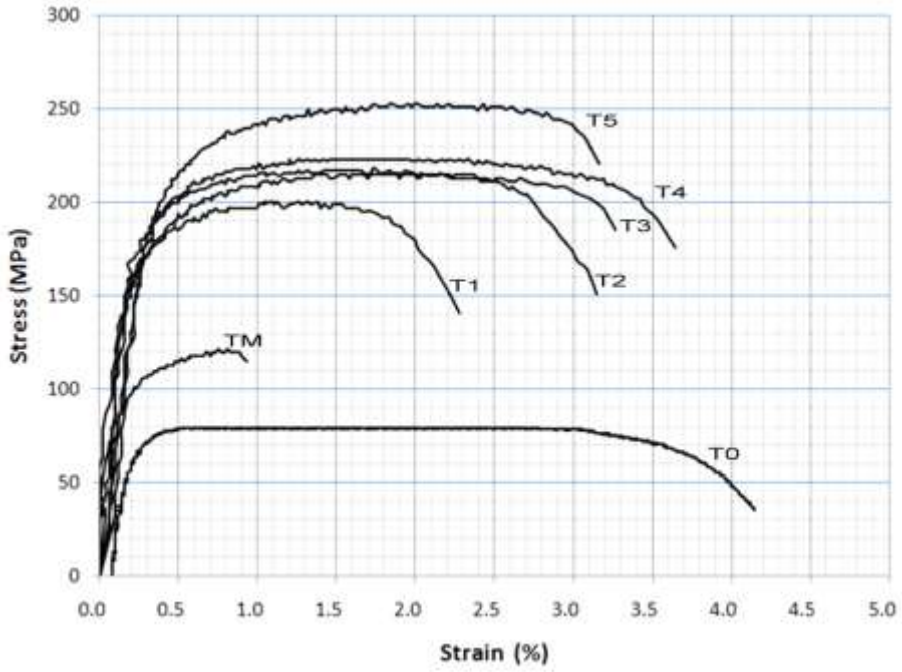

Figure-5.46 Superimposed experimental engineering stress-strain curves of various tested specimens.

Table-5.6 Results of mechanical testing of various specimens in as rolled condition.

Specimen ID	Yield Strength (MPa)	Tensile Strength (MPa)	Elongation (%)	Hardness (Hv)
T0	68 ± 3.5	79 ± 3.0	4.14 ± 0.31	27 ± 2.1
TM	103 ± 5.0	119 ± 4.0	0.93 ± 0.34	32.8 ± 3.2
T1	178 ± 3.2	198 ± 2.6	2.27 ± 0.43	38.3 ± 1.4
T2	180 ± 3.9	214 ± 3.5	3.26 ± 0.28	49.7 ± 4.0
T3	190 ± 4.0	216 ± 3.4	3.14 ± 0.37	52.1 ± 2.2
T4	195 ± 3.8	223 ± 4.0	3.64 ± 0.21	54.7 ± 1.9
T5	210 ± 3.2	252 ± 3.3	3.16 ± 0.44	55.9 ± 1.1
Change	+208 %	+218 %	-23 %	+107 %

5.5.6 Stress Relaxation

5.5.6.1 Tensile test of Annealed Specimens

The tensile curves of annealed specimens of pure aluminum and T4 composite are given in Figure-5.47. The mechanical properties of pure aluminum used were found comparable with that of standard AA1199-O4 alloy, with minor deviations. The deviations could be attributed to the processing conditions and/or purity level. However, the processing conditions for the fabrication of Al-CNT composites were kept constant for consistency. The yield and tensile strengths of pure aluminum and Al-CNT composite (in annealed form) increased from 29 MPa to 97 MPa and 56 MPa to 109 MPa, respectively. However, a decrease in elongation from 22.6 % to 7.4 % was also noticed. It was believed that the amelioration of mechanical strengths is a synergistic effect of the strengthening by the nanotubes, increased lattice strain and refinement in crystallite size[196,197]. Table-5.7 shows the results of tensile testing of annealed specimens along with percent change in various mechanical properties.

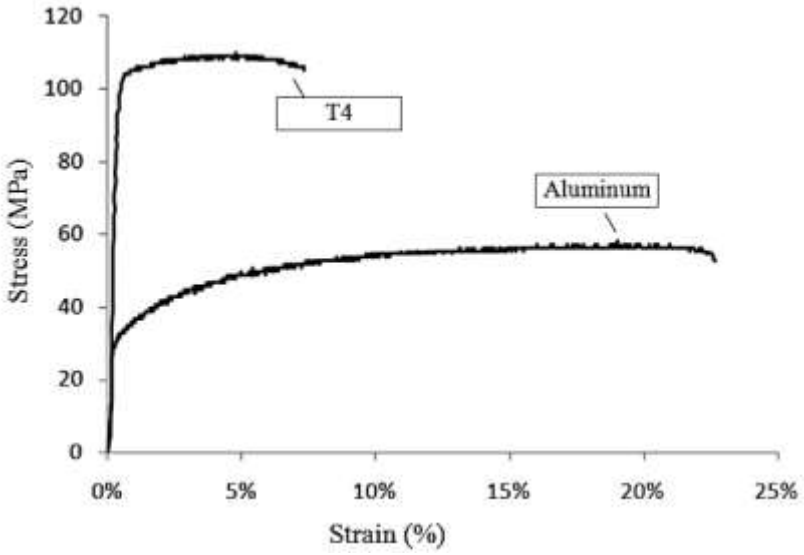

Figure-5.47 Superimposed tensile stress-strain curves of annealed aluminum and Al-CNT (T4) composite.

Table-5.7 Results of mechanical testing of annealed specimens.

Specimens	Yield strength (MPa)	Tensile strength (MPa)	Elongation (%)
Aluminum	29 ± 6	56 ± 5	22.6 ± 1.4
Al-CNT (T4)	97 ± 3	109 ± 3	7.4 ± 0.8
Net change (%)	>230	>90	<65

5.5.6.2 Stress relaxation test

Experimental stress relaxation curves of both the tested materials are presented in Figure-5.48. Inset of the Figure-5.48 is a schematic of the curve's segment where cross-head movement of the testing machine was stopped and the applied stress relaxed for specific time period (i.e. 300 seconds). Point "A" represents the initial stress ($\sigma_\circ$) at t=0, point "B" represents relaxed stress (σ) after t=300 seconds, and point "C" represents the instantaneous rise in the stress (σ') after t=300 seconds when the cross-head movement was re-started.

Stress relaxation and hardening

According to Choudhry et al[206], stress relaxation $\Delta\sigma(t)$ and hardening component $\Delta\sigma'(t)$ can be determined using Eq-5.7 and Eq-5.8, respectively;

$$\Delta\sigma(t) = \sigma_\circ - \sigma(t) \quad (5.7)$$

$$\Delta\sigma'(t) = \sigma' - \sigma_\circ \quad (5.8)$$

The values of $\Delta\sigma(t)$ and $\Delta\sigma'(t)$ were calculated using experimental stress relaxation curves and plotted against corresponding stresses ($\sigma_\circ$) in order to find the trends of stress relaxation and hardening in both the materials under investigation (Figure-5.49). The plots of both the materials showed that the hardening component was initially more than stress relaxation, however as the initial stress increased, a gradual decrease in hardening components occurred. A comparison of stress relaxation and hardening component values of aluminum and Al-CNT composite is given in Table-5.6. It was

observed that the composite exhibited lower values of stress relaxation and higher values of hardening component, as compare to the aluminum.

In case of aluminum, the hardening component ($\Delta\sigma'$) could be attributed to the migration of point defects towards the core of edge dislocations and/or pinning[207]. However, the behavior of composite was different. Under given strain conditions, dislocation loops were generated around the obstacles (i.e. the nanotubes). Continuing strain at point B (inset of Figure-5.48) resulted dislocation multiplication and breakaway, hence dislocation density was increased and hardening component emerged, as manifested by hardening at point C. The hardening component ($\Delta\sigma'$) increased with strain up to a certain tensile stress level ($\sigma_{\circ}$), followed by a decrease in the stress due to stress relaxation ($\Delta\sigma$) which dominated due to limitation of deformation hardening. The limit of deformation hardening indicated that the nanotubes generated effective obstacles dislocations glide until the mentioned strain level; at higher strain levels dislocation to dislocation interaction dominated the deformation mechanism[208,209]. At low strain conditions, the behavior of stress relaxation and deformation hardening of the composite material were similar to aluminum but the amount of the deformation hardening was twice as much of the aluminum. However, at higher stress levels, deformation hardening component decreased rapidly and diminished, as revealed by Figure-5.49. This observation suggested that the strengthening in the composite was induced by deformation hardening (i.e. dislocation-dislocation interactions) at lower stress levels, however at higher stress conditions dislocation interaction based hardening mechanism was replaced by strengthening induced by the interaction of the nanotubes themselves with the matrix, which doubled the mechanical strengths of the material. The phenomenon is known as shear-lag model, where the load is transferred to the nanotubes from the matrix through interfacial shear stress. Hence, the stiffness of the nanotubes was directly involved in strengthening [210].

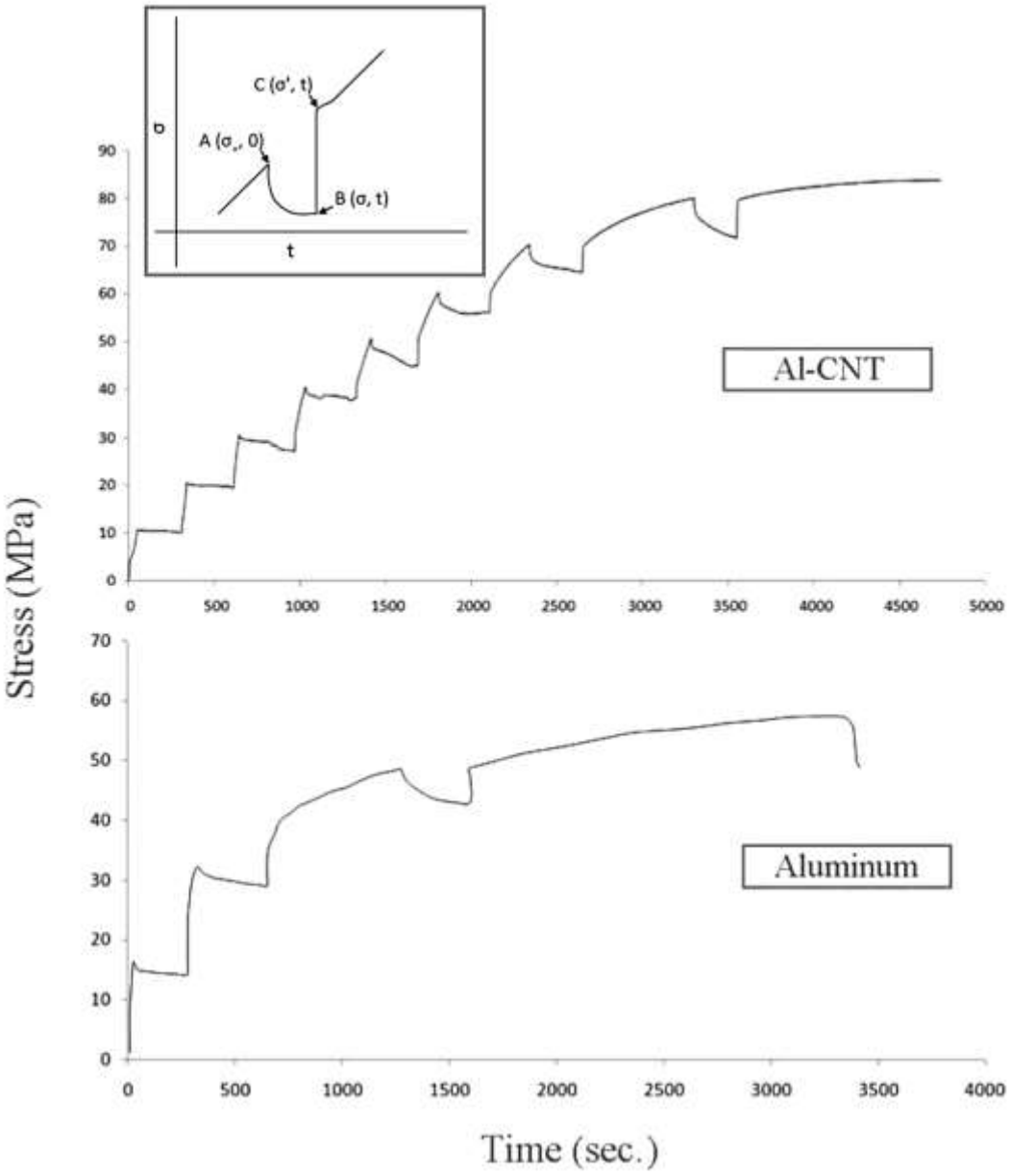

Figure-5.48 Experimental stress relaxation curves of aluminum and Al-CNT composite. Inset is the schematic of the curve segment during relaxation time.

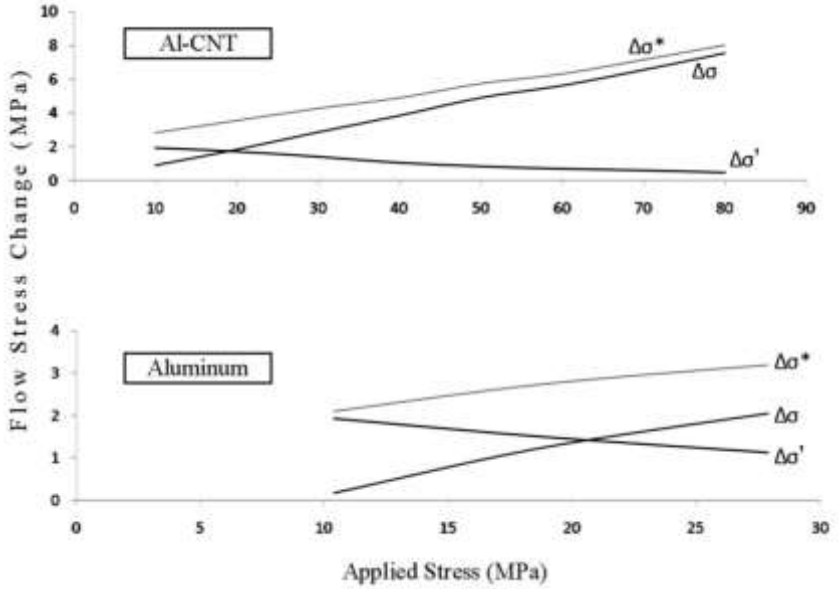

Figure-5.49 Plots of stress relaxation $\Delta\sigma=\sigma_{\circ}-\sigma(t)$, hardening component $\Delta\sigma'=\sigma'(t)-\sigma_{\circ}$ and their sum $\Delta\sigma^*=\Delta\sigma+\Delta\sigma'$ between initial stress $\sigma_{\circ}$, for relaxation time of 300 seconds.

Stress Relaxation Rate and Thermally Activated Barrier

To calculate the strength of thermally activated barrier, graphs of stress relaxation ($\Delta\sigma$) vs. time were plotted at different stress levels ($\sigma_{\circ}$). A logarithmic scale was used at the time axis, which helped to reduce the skewness of the data (Figure-5.50). The slope 'S' of each graph represented the relaxation rate at a particular initial stress level ($\sigma_{\circ}$). It is obvious in Fugure-5.51 that the rate of stress relaxation was lesser for Al-CNT composite than aluminum suggesting that Al-CNT composite presented increased resistance to relaxation in stressed condition, than aluminum. Feltham et al[211] proposed a single barrier model, where height of the thermal activated barrier could be calculated using the relaxation rate (S) and initial stress level ($\sigma_{\circ}$), according to Eq-5.9;

$$U_{\circ} = KT\left[\frac{d\sigma_{\circ}}{dS} + m\right] \qquad (5.9)$$

where, $U_{\circ}$ is intrinsic height of thermally activated barrier, m is a constant (~25), K is Boltzmann constant ($0.8617\text{x}10^{-4}$ eV.K^{-1}), T is room temperature (298K). The values of $d\sigma_{\circ}/dS$ were calculated from Figure-5.51 (i.e. 46 s^{-1} and 102 s^{-1} for aluminum and the composite, respectively). The corresponding values of the strength of the thermally

activated barriers for aluminum and the composite were 1.7 eV and 2.6 eV, respectively. Similar findings were demonstrated by Butt et al[207] and Choudhry et al[206] for aluminum and AA7075, respectively, depicting the magnitude in order for processes like cross-slip, vacancy formation and mutual inhalation of the dislocations. Higher values of the $U_{\circ}$ in case of the composite could be attributed to the impediment of dislocation pile-up due to fine grain size and the nanotubes, seizing the cross slip phenomenon and increasing the dislocation density.

Table-5.8 Change in the rate of stress relaxation and hardening component of aluminum and Al-CNT composite.

	Aluminum	Al-CNT Composite	Change (%)
Stress relaxation	0.13	0.09	<30
Hardening component	-0.05	-0.02	>50

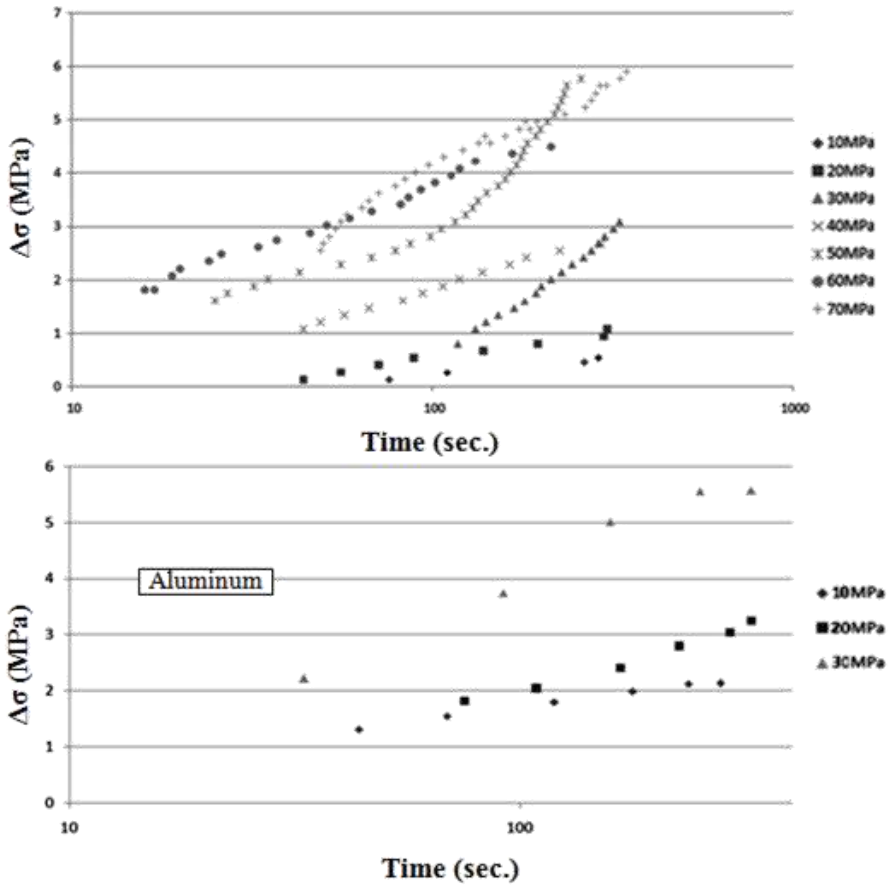

Figure-5.50 Stress relaxation behavior; the time is plotted on logarithmic scale.

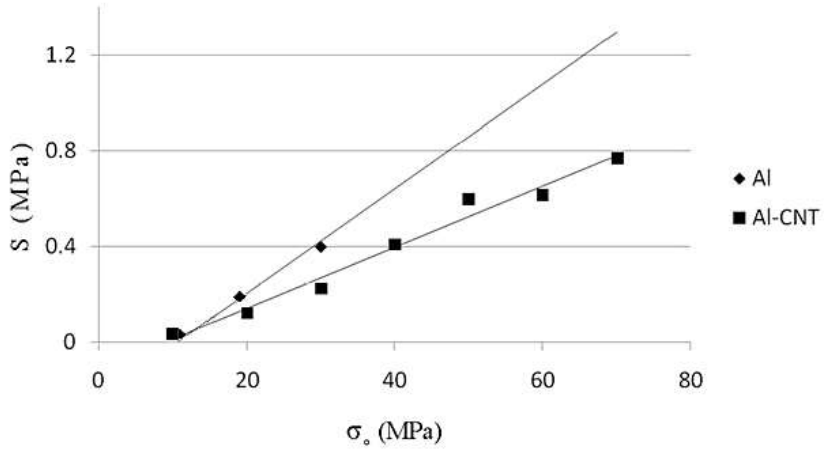

Figure-5.51 Rate of stress relaxation (S) as a function of initial tensile stress ($\sigma_{\circ}$) for aluminum and Al-CNT composite.

5.5.7 Fractography

SEM micrograph in Figure-5.52 shows the fracture surfaces of three materials i.e. pure aluminum (T0), Al-0.4 vol. % MWCNTs (T3) and Al-1.6 vol. % MWCNTs (T5). It was observed that T0 demonstrated almost 100% reduction in area, while the reduction in area reduced gradually with addition of the nanotubes i.e. ~20 % and ~30 % for T3 and T5 composites, respectively. In Figure-5.52 b) and c), the fracture surface consisted of fine dimples and shear lips.

Both the fracture surfaces exhibited ductile fracture, however, their initiation and propagation was different. Fracture surface of pure aluminum (Figure-5.52b) was a typical feature of polycrystalline ductile fracture under tensile loading, where plastic deformation was initiated and propagated by cross-slip. A schematic of ductile failure under cross-slip phenomenon is shown in Figure-5.53a.The deformation initiated necking of the specimen, which increased localized tensile stresses. The increased local stresses effectuated rapid plastic deformation and caused rupture of the material. Nearly 100 % reduction in area is a typical feature of tensile fracture in pure metals, where plastic deformation (under cross-slip) continues even after necking, which finally causes the fracture[212]. Outer surfaces of the pure aluminum specimen near fracture consisted of deformation bands, which were characteristics of cross-slip (Figure-5.53b). The deformation bands became finer near the final fractured region, which was recognized by increased deformation rate with necking[199].

The fracture surface of the composite specimen was accompanied by considerable reduction in area. At the periphery of the fracture region, a discernable shear-lip was also observed (Figure-5.52c). Presence of strengthening material(s) can decrease the toughness of the material (i.e. reduction in area). Under loading conditions, micro cracks or voids were generated at or around the CNTs. Moreover, geometrically necessary dislocations were generated due to the non-compatible strain between the matrix and the strengthening material. There could be three typical conditions in the presence of any strengthening material[212]:

- If the strengthening material deformed only elastically, the geometrically necessary dislocations would be located in the matrix.

- If the plastic strains of the matrix and the strengthening material were compatible, a delay in fracture nucleation would be observed.
- If the strengthening material undergone plastic deformation (but was less ductile than matrix), the geometrically necessary dislocations would be divided.

The formation of geometrically necessary dislocations caused internal tensile stresses (σ_i) which added up in the applied tensile stresses (σ_u) and promoted the formation of micro cracks:

$$\sigma_r = \sigma_i + \sigma_u \qquad (5.10)$$

Micro cracks were formed throughout the volume of the material prior to necking. However, as the matrix was ductile, the tensile strength was lesser than the stress required for the propagation of micro cracks (Euqation-5.10); as a result necking occurred prior to the failure. A schematic is shown in Figure-5.53b for various stages of deformation and failure of the composite specimens. Once necking was initiated, voids link-up occurred in the region because true stress in the necking region was higher than other regions of the specimen. This phenomenon is schematically shown in Figure-5.53b(i). As deformation continued, link-ups of the micro cracks/voids aggravated to a penny shaped crack within the material, Figure-5.53b(ii). The extant of micro cracking depends upon many factors related to the strengthening material along with work hardening characteristics of the matrix material:

- Volume fraction
- Size
- Yield strength

When a big void (penny shaped) was formed, true engineering stress exceeded the tensile strength of the material and final fracture occurred by shearing. Due to the occurrence of shearing fracture, a shear lip surrounded the fracture surface of the composite.

Further feature and characteristics of the dimples in the fracture surface of the composite material were revealed at higher magnifications shown in Figure-5.54 and 5.55 for T3 and T5 composite specimen, respectively. In Figure-5.54, uniform dimples were seen with embedded nanotubes in the matrix. Presence of the nanotubes was confirmed by EDS point analysis, where carbon was detected (Figure-5.54c). It was

also observed that the fracture dimples were hollow and their centers were free of MWCNTs, suggesting that the facture was initiated within the matrix and not from the nanotubes. The Figure-5.55 (fractograph of T5 composite) is almost identical to Figure-5.54; however, it comprised of an additional feature of pulling-out of the nanotubes at the edges of the fracture dimples (Figure-5.55c). It could be inferred that as the fracture propagated under testing conditions, the nanotubes, which were aligned (due to cold rolling) in the fracture direction, were pulled-out by the sliding of the outer shells, contributing towards resistance to the fracture growth[127].

5.4.5.1 Fracture mechanism:

Based on the preceding discussion and experimental findings, the mechanism of fracture initiation and propagation in Al-MWCNTs composite can be understood. It is known that both the constituent materials of the composite are capable of plastic straining, therefore a delayed fracture could be expected. Moreover, the nanotubes are also capable of high elastic straining [213]. Therefore, micro crack or voids were initiated in the matrix instead of at CNT-Al interface under tensile loading. The fact could be observed in Figures-5.54 and 5.55, where the centers of the dimples were free of any second phase (i.e. MWCNTs). Once initiated, the voids grew in the direction of applied load (i.e. tensile axis). The growth of the voids was driven by plastic deformation of the matrix.

Geometrical conditions showed that the strain rate in the voids (ε_v) was more than overall strain rate (ε_u) according to the equation-5.11:

$$\varepsilon_v = C\varepsilon_u \qquad (5.11)$$

where, *C* is a constant (the value is between 1 and 2).

The increased strain rate (ε_v) caused the final fracture of the composite[212]. Equation-5.12 defines the critical strain rate (ε°) at which micro-ruptures can occur:

$$\varepsilon^\circ = [\alpha(\frac{1}{\sqrt{f_v}} - 1)] \qquad (5.12)$$

where, α is an empirical constant and f_v is the volume fraction of the strengthening material. The primary features of the geometrical effects on the ductility of the material are:

- De-coherent or fractured particles cause reduction in ductility.

- Non-deforming particle do not affect ductility of the matrix.

It was observed during fractography that the fracture dimples were not initiated from the nanotubes, which indicated that the CNTs did not contribute towards formation of the micro voids. Hence, no significant decrease in the ductility of the composite was found experimentally in tensile tests. On the other hand, the nanotubes remained active to contribute strengthening to the composite according to the 'shear-lag model', which states, 'in short fiber composites, the load is transferred from matrix to the fibers through an interfacial shear stress[197,214]:

$$\sigma = \sigma_{\mathrm{r}} V_{\mathrm{r}} \left[\frac{l}{l_{\mathrm{e}}}\right] + \sigma^{\circ}(1 - V_{\mathrm{r}}) \qquad (5.13)$$

where; l_e is the critical length of the nanotubes, V_r is the nanotubes volume fraction, l is the average nanotubes length, σ° is matrix strength, σ_r is the nanotubes' strength. A justifiable comportment of the composite was observed during tensile testing where strength of the composite was increased with volume fraction of the nanotubes.

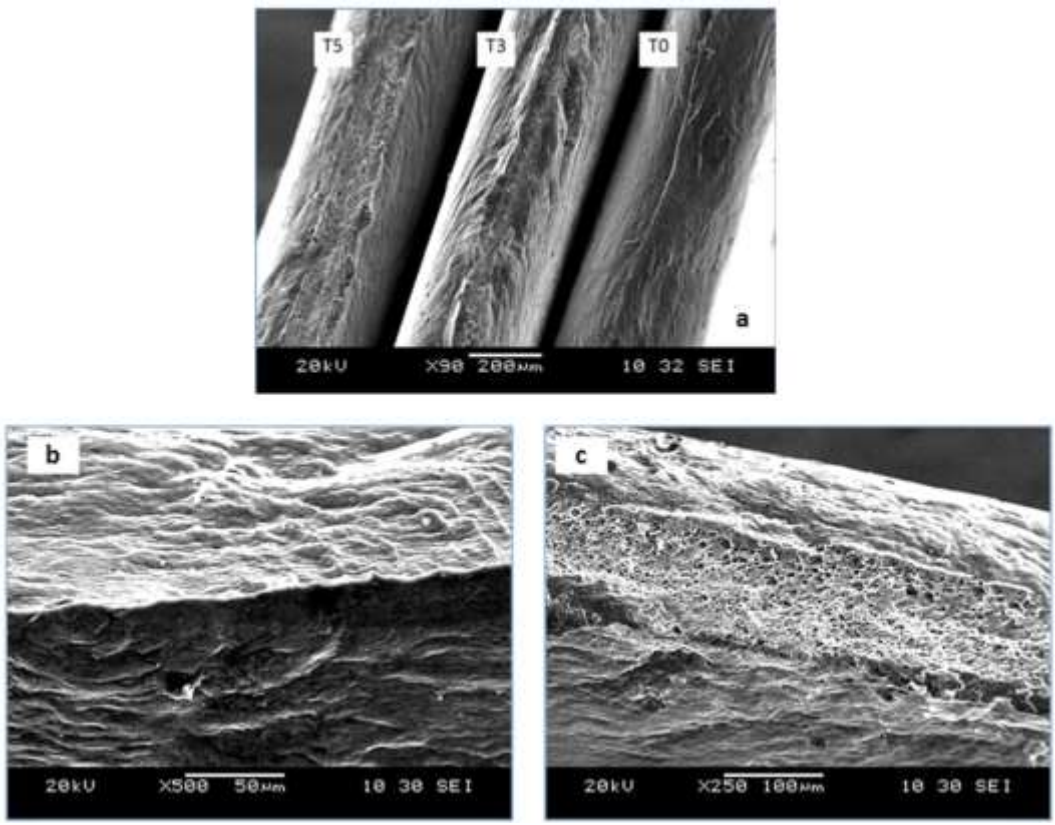

Figure-5.52a) SEM micrograph of the fracture surfaces of the tested materials, b) Fracture surface of pure aluminum (T0) specimen showing nearly 100 % reduction in area and c) Fracture surface of Al-CNTs composite having 1.6 vol. % MWCNTs (T5) showing discernable reduction in area along with fine dimples and shear lip.

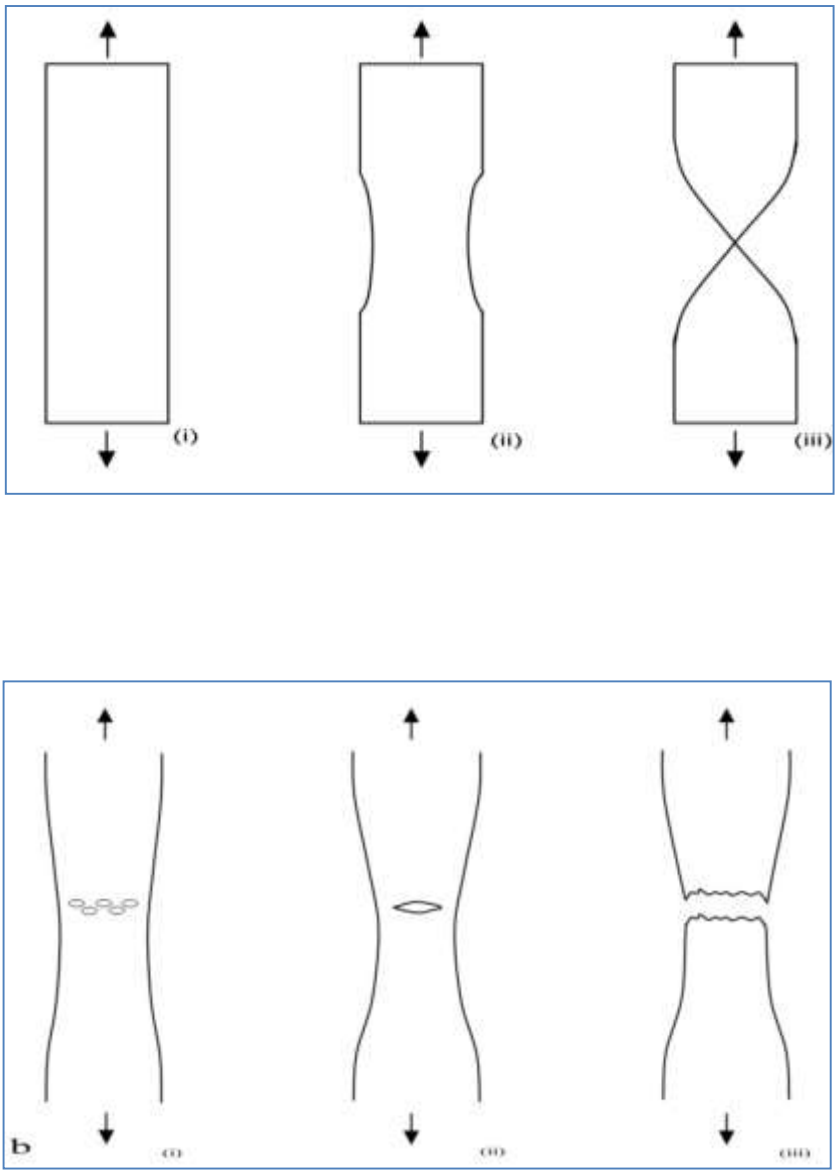

Figure-5.53. Schematics of initiation and propagation of ductile fractures under tensile loading, a) fracture initiation and propagation governed by purely cross-slip, and, b) transaction of fracture initiation and propagation mode due to the presence of strengthening material.

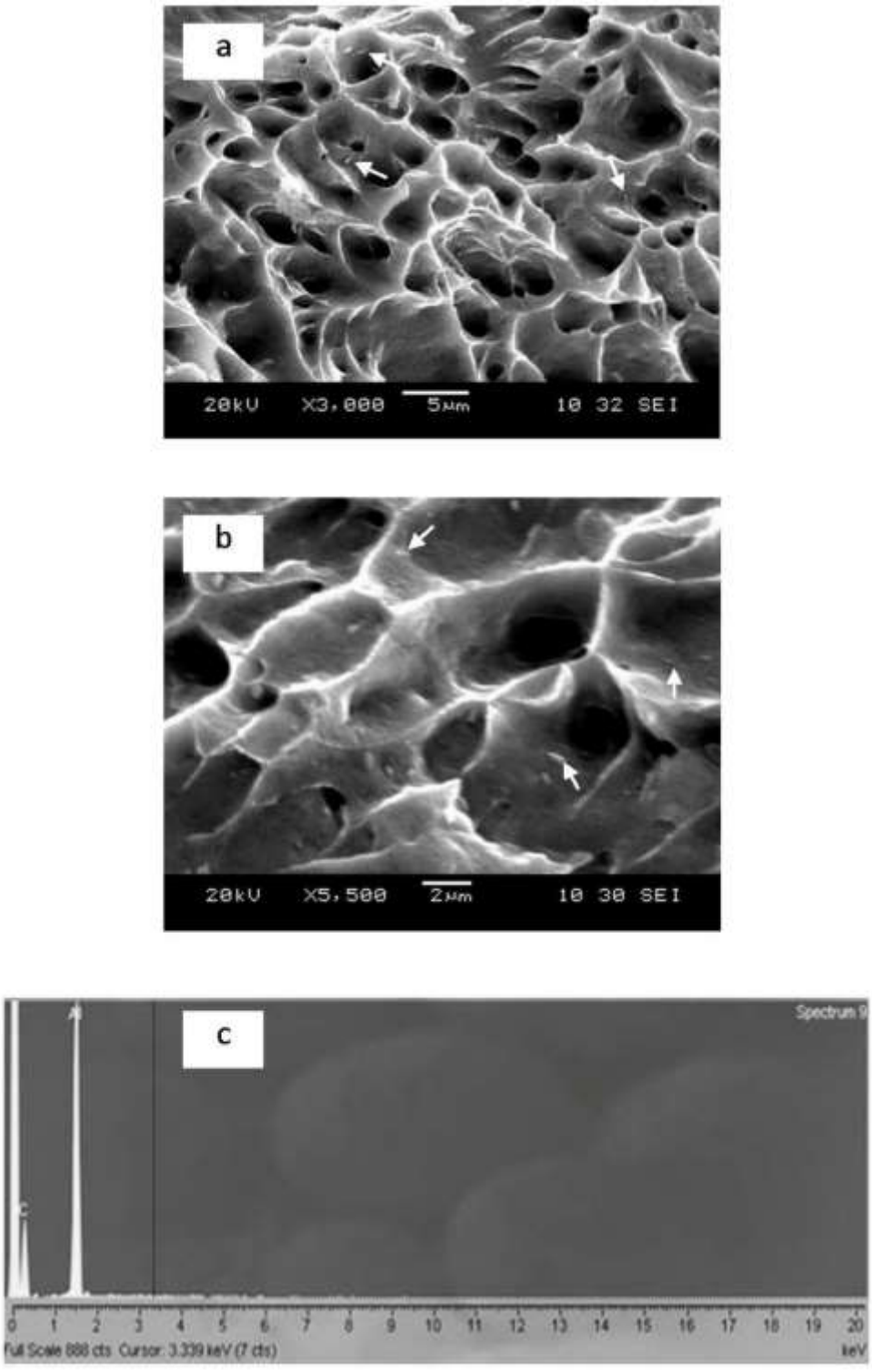

Figure-5.54 Fractographs of Al-0.4 vol. % MWCNTs (T3) composite's fracture surface. In Figures-5.54 'a' and 'b' arrows indicate embedded MWCNTs in the matrix. The EDX spectrum (c) was taken from pointed locations in Figure-5.54c.

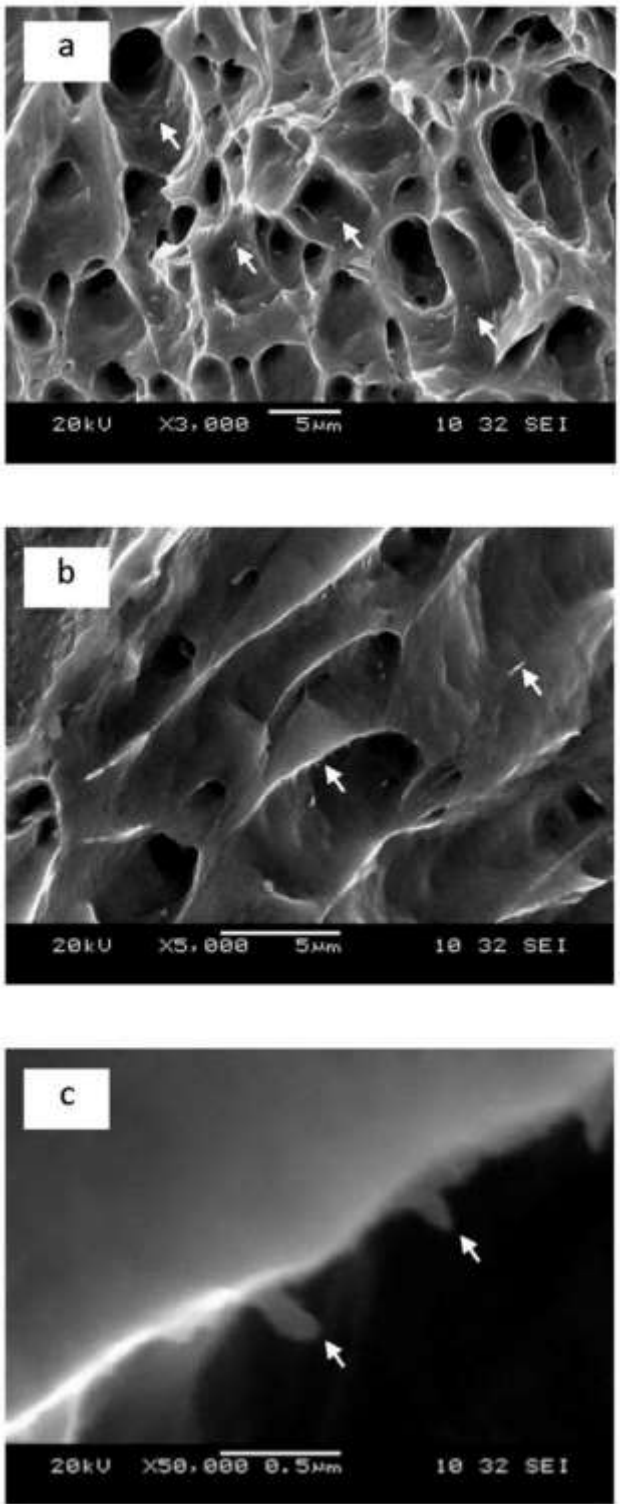

Figure-5.55 Fractographs of T5 composite's fracture surface. In Figure-5.55a and b arrows indicate embedded MWCNTs in the matrix. In Figure-5.55c arrows are indicating pulled-out nanotubes.

Chapter No: 6

Conclusions

6.1 Synthesis of MWCNTs

Ethanol assisted synthesis of MWCNTs was realized in a CVD reactor successfully. Maximum yield of MWCNTs (>80%) was attained by optimizing ethanol flow rate and catalytic activity of nickel particles. An ethanol flow rate of 20-30 sccm with other described operational parameters, proved to be optimum for efficient synthesis of MWCNTs as evident by various characterization techniques, however, nickel particles rendered maximum activity. A variation in ethanol flow rate other than the optimum value (20-30 sccm) caused formation of excessive amorphous carbon and synthesis products along with MWCNTs, resulting in decrease in efficiency of overall process. The structural homogeneity of the CNTs is attributed to the nickel's catalytic activity.

6.2 Dispersion of CNTs in Aluminum

The Al-CNTs composites were successfully fabricated using induction melting. SEM and TEM studies elaborated the homogeneous distribution of the nanotubes and no evidence of their segregation was found, which was further supported by simultaneous increase in strengths and hardness. The improvement in mechanical properties seemed to be a synergistic effect of refinement in crystallite size, increased lattice strain and strengthening by the nanotubes. In our opinion, induction melting holds strong promises for the fabrication of Al-CNTs composites, especially for its scale up capabilities.

6.3 Coating of CNTs with Aluminum

Aluminum coating on MWCNTs was successfully effectuated using potassium hexafluorotitanate at 790 °C. During coating process, initially titanium carbide was formed on the outer walls of the nanotubes, which increased the wetting of the nanotubes towards molten aluminum.

6.4 Fabrication of Al-CNTs Composite

- During optical microcopy and SEM studies of as-cast specimens, it was observed that the nanotubes were dispersed along the grain boundaries, and in the direction of rolling in case of rolled specimens. Presence of CNTs was confirmed by EDS analysis line scans. No clustering or aggregates of the nanotubes were observed.
- A further confirmation of the dispersion and wetting of the nanotubes in aluminum matrix was ascertained by TEM observations, where a second phase (most probably titanium carbide) was formed on the walls of the nanotubes, providing wetting for aluminum.
- TEM and XRD studies elaborated the extent of grain refinement in the composite specimens due to the presence of CNTs. It was evident that the grains were refined from 300 to 150 nm with the addition of CNTs from 0.1 to 1.6 volume percent, respectively. Moreover, XRD evaluations depicted the fact that presence of CNTs increased the lattice strain, besides grain refinement, of the Al-CNTs composites. The strain induced by the nanotubes varied from $2.3x10^{-3}$ to $3.46x10^{-3}$ after addition of 0.1 to 1.6 volume percent CNTs, respectively. The effect of CNTs addition on the grain refinement and lattice strain was more pronounced up to 0.8 %after which it became steady.
- An appreciable increase in mechanical properties of the composite was achieved, which was believed to be assisted by:
  - dispersion of mono-strands of the nanotubes in aluminum matrix assisted by induction stirring action during fabrication of the composites.
  - wetting of the nanotubes with aluminum matrix assisted by the in-situ exchange reaction of potassium hexafluorotitanate with molten aluminum and then CNTs, forming titanium carbide on the surface of the nanotubes providing wetting sites for molten aluminum.

  The experimental results yielded noticeable increase in yield strength, tensile strength and hardness of the composite i.e. ~208, ~218 and ~100 percent, respectively. A reduction in elongation of the composite was observed less than 25 %. Increase in mechanical strengths and hardness, without much

compromise on the ductility of the composite could be an indirect indicator of good dispersion and wetting of the nanotubes in aluminum matrix. Otherwise, in the presence of CNTs' clusters, with negligible wetting, would decrease ductility of the composite drastically.

Future Suggestions

In the present work it was demonstrated that:

i) effective dispersion of the CNTs in molten aluminum is achievable using induction furnace and

ii) wetting of the CNTs with molten aluminum could be ameliorated using potassium hexafluorotitanate.

The combined action of the two (i.e. dispersion and wetting of the CNTs) caused a threefold increase in mechanical strength as compare to the pure aluminum. However, the experimental regime was primarily focused on the development of, above mentioned, the two processes.

In an extended work, optimization of the constituents (CNTs and hexafluorotitanate) could be carried out. The effort can result in even higher mechanical strengths.

Another promising approach could be the type of matrix material; one may use high-strength aluminum alloys as matrix material.

Apart from mechanical strengths, properties like tribology, corrosion, thermal conductivity and electro-magnetic shielding might also be varied due to the presence of CNTs in the matrix. Therefore, any work related to the above mentioned properties may open new venues of industrial applications of the composite.